AD 608185

U. S. ARMY
TRANSPORTATION RESEARCH COMMAND
FORT EUSTIS, VIRGINIA

TRECOM TECHNICAL REPORT 64-48

DOWNWASH IMPINGEMENT DESIGN CRITERIA
FOR VTOL AIRCRAFT

Task 1D121401A14129
Contract DA 44-177-AMC-65(T)

August 1964

prepared by:

DYNASCIENCES CORPORATION
Fort Washington, Pennsylvania

20040702046

4373-64

DISCLAIMER NOTICE

This report has been reviewed by the U. S. Army Transportation Research Command and is considered to be technically sound. The report is published for the exchange of information and the stimulation of ideas.
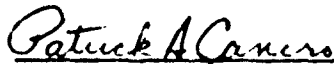
PATRICK A. CANCRO
Project Engineer
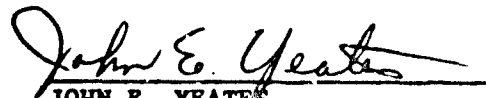
JOHN E. YEATES
Group Leader
Aeromechanics Group

APPROVED.

FOR THE COMMANDER:
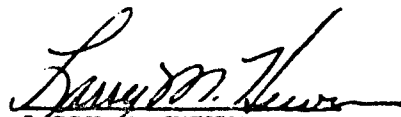
LARRY M. HEWIN
Technical Director

Task 1D121401A14129
CONTRACT DA 44-177-AMC-65(T)
TRECOM TECHNICAL REPORT 64-48
August 1964

DOWNWASH IMPINGEMENT DESIGN
CRITERIA FOR VTOL AIRCRAFT

Dynasciences Report No. DCR-139

Prepared by

DYNASCIENCES CORPORATION

Fort Washington, Pennsylvania

FOR

U. S. ARMY TRANSPORTATION RESEARCH COMMAND

FORT EUSTIS, VIRGINIA

PREFACE

This report presents the results of a study, conducted by Dynasciences Corporation of Fort Washington, Pennsylvania, to determine design guidelines for the purpose of eliminating or minimizing the operational problems associated with downwash impingement. The work was conducted for the U. S. Army Transportation Research Command, under Contract DA 44-177-AMC-65(T), during the period of July 1963 to March 1964.

Mr. Patrick Cancro was the TRECOM Project engineer for this program. Mr. M. M. George, Dr. A. A. Perlmutter, and Mr. L. Butler were the principal investigators for Dynasciences Corporation.

CONTENTS

ILLUSTRATIONS

viii

SYMBOLS

fully developed slipstream area, ft^2

particle frontal area, ft^2

projectile impact area, ft^2

acoustic velocity in target material, ft/sec

particle diameter, inches

drag coefficient based on frontal area and
local dynamic pressure

propeller diameter, ft.

exit diameter of nozzle or ducted fan or
effective diameter of slipstream from free
propeller (0.707 propeller diameter), ft.

projectile energy ft-lb.

acceleration due to gravity, ft/sec^2

height of survey station or particle trap
above the ground, ft.

height of particle cloud above terrain, ft.

height of nozzle exit or propeller plane
above the terrain, ft.

impact factor (Figure 27)

terrain factor (Figure 21)

nozzle efficiency factor (Reference 28)

particle mass, slugs

P	projectile penetration in target, ft.
P_a	ambient atmospheric pressure, lb/ft^2
P_s	absolute static pressure along ground surface, lb/ft^2
Q	particle flow rate, $\dfrac{lb}{ft^2 - min}$
q	local dynamic pressure at any point in the airstream, lb/ft^2
q_N	average dynamic pressure at nozzle exit or propeller slipstream, lb/ft^2 ($q_N = T/A_e$ for propellers and $q_N = T/2A_e$ for ducted fans)
R/L	projectile shape correction factor
R_e	Reynold's number
r	radial distance from nozzle or propeller center, ft.
T	air flow temperature
T	lift device thrust, lb.
T	material thickness, ft.
t	time, sec.
U	inviscid velocity just outside the ground boundary layer, ft/sec
u_o	reference velocity in the ground boundary layer at center of the sphere, ft/sec
V_A	average airstream velocity, ft/sec
V_{AV}	area weighted average of airstream velocity within the limits $0 < \dfrac{x}{d_e} < 3.0$, ft/sec

average velocity at nozzle exit or propeller slipstream, ft/sec

entrained particle velocity, ft/sec

airstream velocity along the ground surface, ft/sec

weight of entrained object, lb.

lateral axis of VTOL aircraft (Figure 7)

radial distance along the ground from the center of jet impingement, ft.

longitudinal axis of VTOL aircraft (Figure 7)

yield stress of target material, lb/ft^2

vertical axis of VTOL aircraft (Figure 7)

distance from nozzle exit or propeller plane survey station, ft (Figure 2)

particle size parameter, $\dfrac{3d_e C_D \rho_A A_F}{m_p}$

boundary layer thickness, ft.

static deflection, ft.

mass density of air at sea level, $slugs/ft^3$

mass density of particle material, $slugs/ft^3$

mass density of terrain, $slugs/ft^3$

mass density of target material, $slugs/ft^3$

static stress due to bending, p.s.i.

impact stress, p.s.i.

ϕ angle between maximum water depression and normal ground surface (Figure 11)

SUBSCRIPTS

amb	ambient
eff	surface dynamic pressure corrected for type of terrain
F	overall field maximum
J	gas temperature at jet exit
max	maximum
P	particle
s	surface
T	target
t	terrain
u	upflow
w	water
x	along X axis
y	along Y axis
z	at station z from exit
τ	terminal

SUMMARY

The objective of this program was to utilize existing data for the preparation of design charts for VTOL aircraft to aid in the establishment of aircraft designs that will alleviate the adverse operational conditions resulting from downwash impingement on terrain. Specific areas of investigation included particle entrainment and ingestion and their effect on pilot vision, aircraft damage, personnel injury, and aircraft signature. Methods to quantitatively predict operational conditions resulting from downwash impingement of a VTOL aircraft are presented.

1

CONCLUSIONS

Using existing data, methods have been formulated
to quantitatively predict operational conditions resulting
from downwash impingement on terrain. Because of the dearth
of existing quantitative data, however, particularly in the
area of entrained particle density, the design charts
utilized in these methods will provide only first-order
estimates. Additional analytical and experimental investi-
gations are recommended to increase the utility and accuracy
of these charts.

RECOMMENDATIONS

T following areas of investigation warrant further
and testing as a result of the information obtained
this program.

1. Practical solutions of velocity and pressure
   distribution for uniform and nonuniform jet
   impinging on a flat surface at various angles
   relative to the jet axis of symmetry.

2. Investigation of the transient operating
   conditions of take-off and landing on the
   downwash on terrain problems.

3. Experimental flow profiles for multilift air-
   craft design, particularly at the planes of
   symmetry, as a function of aircraft geometry.

4. Relationship between particle density and
   visibility as a function of aircraft operating
   conditions and geometry for various terrains.

5. Relationship between velocity of particles or
   debris and aircraft operating conditions and
   geometry.

6. Experimental data on damage resulting from
   impact of low-speed, high-mass objects with
   aircraft structural components.

7. Experimental evaluation of propeller, turbo-
   prop, and turbojet engine limitations as a
   function of particle size and flow rate.

8. Feasibility studies of promising alleviation
   techniques described in Section IV of this
   report, with particular emphasis in the field
   of soil stabilization.

I INTRODUCTION

Experience with existing type vertical take-off and landing aircraft (helicopters, tilt-wing aircraft, etc.) has demonstrated that certain operational problems arise when the high-velocity air generated by these aircraft impinges upon the ground or water surface. The most serious problems encountered are:

1. Obstruction of pilot's vision

2. Injury and adverse environment for ground personnel

3. Aircraft and equipment damage

4. Difficulty in achievement of effective operational concealment

5. Aircraft performance degradation

These problems, for the most part, were experienced with aircraft of relatively low disc loadings and with test-bed simulations of higher disc loading VTOL models. Investigations which have been performed of the downwash impingement problems have led to a qualitative understanding of the operational limitations and also have provided some experimental data.

To aid in the development of future VTOL aircraft, the results of the work performed previously in this field are reviewed and evaluated in this report. These data are then utilized in the formulation of methods for the estimation of the effects of pertinent design parameters on the severity of the operational problems that may be encountered. Because of the dearth of existing quantitative data, however, particularly in the area of entrained particle density, the design charts utilized in these methods will provide only first-order estimates. Additional quantitative data are, therefore, needed to increase the utility and accuracy of these charts.

4

Section II of this report presents a discussion of
the design parameters affecting downwash impingement. The
methods and design charts for estimating the operational
conditions arising from operations of VTOL aircraft in the
proximity of the ground are presented in Section III. A
sample calculation of these conditions for a hypothetical
VTOL aircraft is presented in Appendix I. Appendix II pre-
sents a compilation of additional literature pertaining to
downwash impingement on terrain.

The problems associated with operations of VTOL air-
craft in close proximity to the ground result primarily
from the high-velocity slipstream generated by the aircraft
lift devices. Compared to a helicopter, which also gives
rise to operational problems over soft ground surfaces, the
VTOL aircraft, because of the higher slipstream velocities
involved, will generate more severe conditions. An indica-
tion of the relation between disc loading and slipstream
velocities, as generated by various types of lift devices,
is presented in Figure 1. It may be noted that hurricane
velocity, which is indicated as 65 knots, corresponds to an
average velocity generated by an open propeller having a
disc loading of 16 pounds per square foot. The disc loadings
proposed for future VTOL aircraft are many times this magni-
tude, and therefore the severity of the problem can be
easily appreciated.

For a more basic understanding of the downwash phenom-
enon, a description of the behavior of a jet impinging on the
ground and of the entrainment process is presented herein.
This is aided by extensive utilization of existing theoreti-
cal and experimental data.

CHARACTERISTICS OF AN IMPINGING JET

The notation used throughout the report is presented
in Figures 2.a and 2.b for a jet expanding in free air and
impinging on a flat plate, respectively. The essential
characteristics of impinging jets are:

1.   Viscous decay from jet source to impinging
     surface

2.   The radial expansion of flow along the ground

3.   The aerodynamic forces exerted on the terrain
     particles

A great deal of effort in both theoretical analyses
and experimental studies has been directed towards obtaining
a better understanding of the mechanics of jet impingement.

6

Generally the impingement process has been shown to be a function, in varying degrees, of the following aircraft and terrain parameters:

1. Area loading (disc loading) of lift device, T/A_e

2. Nozzle exit or propeller plane height above the ground, h_e

3. Jet exit configuration

4. Jet temperature

5. Number of lift devices

6. Terrain cohesion

7. Particle size

Jet Decay

A slipstream emanating from either a single nozzle or an open propeller, discharging into free air, expands gradually due to mixing, with a corresponding reduction in the dynamic pressure, q_z , with increasing distance, z/d_e , from the nozzle exit. Typical experimental values of dynamic pressure decay with distance for various lift device configurations discharging into free air are shown in Figure 3, which is reproduced from Reference 1. The maximum dynamic pressure, $(q_z)_{max}$, measured at various distances from the nozzle exit is divided by the average dynamic pressure in the fully developed slipstream. The experimental data are compared with the viscous decay theory of Reference 2. Overall agreement is seen to be good. Unfortunately, in the region of interest from practical design considerations ($z/d_e < 6.0$), the theoretical prediction of dynamic pressures is inadequate. The variation of the maximum dynamic pressure at distances less than three diameters from the nozzle exit, shown in Figure 3, is due to the flow at the jet origin. For propellers the flow is basically triangular whereas the nozzles have uniform flow. This variation, however, as will be shown later, does not materially effect the flow along the ground plane.

7

Jet Impingement on a Flat Surface

An air jet impinging on the ground loses its vertical velocity, and the energy is converted to pressure that accelerates the air flow in all directions away from the impingement area. This results in high-velocity air flowing near and parallel to the ground and a static pressure gradient on the ground surface.

Dynamic Pressure Profiles

Typical profiles of the dynamic pressure along the ground surface, q_s , are presented in Figure 4. The data representing lift device configurations ranging from a 35-foot rotor to a 4-inch nozzle show that q_s is virtually independent of configuration and flow conditions in the slipstream. Near the impingement point of the outer portions of the descending flow, $x_s/d_e = 1$, the height of the lift device is seen to have a marked effect on the thickness and maximum value of the radial flow. This effect, however, diminishes at radial stations greater than two jet diameters from the center of impingement. The distribution of q_s normal to the surface is near triangular with a peak value at a height of about 2 percent of the jet slipstream diameter above the ground.

Peak values of surface dynamic pressure, $(q_s)max$, for a 4-inch nozzle are reproduced from Reference 1, in Figure 3, as a function of nozzle height ratio, h_e/d_e, and radial distance ratio from the jet centerline, x_s/d_e. Maximum values of $(q_s)max$ herein designated as maximum field dynamic pressure, q_F , occur at approximately one diameter from the jet center and decrease rapidly with increasing lift device height. At radial distances beyond two jet diameters, the effect of lift device height is again seen to be small. For $x_s/d_e > 2.0$, an approximate relationship of $(q_s)max$ with x_s/d_e can be established in terms of q_N. This relationship, which is independent of nozzle height, is given as

8

$$\left[\frac{(q_s)_{max}}{q_N} \right] \left[\frac{x_s}{d_e} \right]^2 = 1.40 \qquad (1)$$

(for $x_s/d_e > 2.0$).

Equation (1) is in good agreement with Reference 3, in which ground velocities of many lift device configurations ranging from a 1-inch nozzle to full-scale rotors are compared. Furthermore, as shown in References 3 and 4, Equation (1) also implies that $(q_s)_{max}$ is a function of total lift rather than of disc loading. It should be noted, however, that the majority of entrained particles were observed to originate from locations having a radial distance of less than two jet diameters from the center of impingement. Within the circular area bounded by $x_s/d_e < 2.0$, the surface dynamic pressure and the static pressure on the ground, both primary causes of surface erosion, are significantly dependant upon disc loading and nozzle height. These parameters cannot, therefore, be ignored in any particle entrainment analysis.

The 4-inch nozzle data of Figure 5 are replotted in Figure 6 together with data from several other lift device configurations, all obtained at a height of approximately one jet diameter. The data of Reference 5 represent VTOL aircraft with two lift devices. The dynamic pressures shown are taken along the X-Z plane through the center of the propellers as shown in Figure 7. Although some scatter exists, a consistent pattern of decay with radial distance is evident in Figure 6. The one exception to the general trend is the dynamic pressure measured in the vicinity of an RB108 turbojet engine with afterburner, from Reference 6. It is believed that this variation is primarily due to the underdeveloped jet still existing at the nozzle exit. Although not shown in Figure 6, this difference diminishes for increasing nozzle heights. Generally, therefore, the dynamic pressure data of the 4-inch nozzle can be accepted as representative of lift device configurations presently in existence.

9

As was previously mentioned, the maximum field dynamic pressure, q_F , occurs at approximately one jet diameter from the center of impingement and is a function of the lift device height above the ground. Vidal, in Reference 7, suggests a method of predicting q_F by utilizing the decay data of a jet discharging into free air. This method specifies that for a direct correlation of q_F with q_z the length to be used for the impinging jet should be the sum of the ground separation distance, h_e , and the distance along the ground where the maximum dynamic pressure, q_F , occurs. A comparison of the decay of the jet in free air with that of an impinging jet is made in Figure 8. From this figure it can be seen that the correlation between the free jet and the impinging jet data is quite good.

A survey of existing theories for the prediction of the downwash flow profile is reported in Reference 7. The case of the two-dimensional impinging jet has been solved analytically, but solution of the three-dimensional or axisymmetric jet are limited to approximate or numerical methods. A typical comparison of axisymmetric inviscid flow theory and experimental data is shown in Figure 9, which is reproduced from Reference 7. The experimental data are corrected for viscosity effects for direct comparison with theory. It can be seen that this theory is inadequate for values of $x_s/d_e > 0.6$. This inadequacy results mainly from the representation of the free streamline bounding the jet. A more recent iterative method is reported in Reference 8. Formulation of the inviscid jet flow has been derived in terms of vortex sheet representation for the jet boundaries. As yet, conclusive final results have not been obtained.

Static Pressure Due to Impinging Jet

Along with the radial flow, an impinging jet generates a static pressure gradient along the ground surface. Figure 10 represents the static pressure at the ground, as a function of x_s/d_e . The model rotor data show a region of negative pressure at the center of impingement; and, for the case of the 15-foot propeller data, a region of negative pressure occurs at approximately one jet diameter.

ie uniform jet data show similar gradients of static pressure
th radial distance. These abrupt changes in pressure may
itiate the erosion process by subjecting particles to
fferential pressures. The static pressure also results
i a depression in the terrain. When the terrain is water,
ie depression is directly proportional to the static
essure. For soils, particularly the loose granular type,
milar depressions occur. The cohesive qualities of the
il, however, will reduce the overall depression; but as
re and more of the particles are eroded under sustained
erations, a large depression is formed. At an h_e/d_e of
5, a depression with a diameter equal to four jet dia-
ters was reported in Reference 9 for tests over dry sand.
e diameter of the depression increases with increasing
$/d_e$, with an accompanying reduction in the depth of the
pression.

Since the high-velocity radial flow is parallel to,
i very close to, the ground (see Figure 4), the forces
insmitted by this airstream to the particles could not be
> sole mechanism for obtaining the particle heights in-
:ated by experiments (Reference 9). Additional contri-
:ions to the particle upward motion are:

a) chance collisions, which will cause
   particles to bounce higher than the
   region of the radial flow

b) the transportation of disturbed aeorosol
   particles by relatively low surface winds,
   or by the upward-directed induced flow
   field surrounding a typical lifting
   system (see Reference 20)

c) the projection of particles upward along the
   crater slopes created by an impinging jet

d) size of lift device

An indication of how craters affect particle heights
l be obtained by observing the water depression result-
from static pressure along the ground surface, shown in
ire 11.

11

The data shown in Figure 11 are obtained from Reference 9. Since the majority of particles originate within the depressed area, they will be initially propelled at an angle, ϕ, that is a function of the slope of the lip surrounding the depression. For surfaces other than water, the initial depression will be augmented by the erosion of additional particles, forming a deeper hole. Reference 9 reports that during operations over sand, the initial particle flow was relatively parallel to the ground. As the test progressed, the flow of particles was observed to change from horizontal to vertical in the immediate vicinity of the lift device.

Lift device size also affects the height of entrained particles. This is indicated by the fact that stagnation pressures are a function of the area loading of the lift device and act upon the ground surface in a region with an area that is proportional to the lift device diameter. Furthermore, the depth of the eroded hole, particularly in the case of water terrain, is directly proportional to the static pressure acting upon it, which, in turn, determines the slope of the lip surrounding the terrain depression. As a first-order approximation, the particles are assumed to be projected upwards as a function of the angle, ϕ, defined in Figure 11 as

$$\phi \approx \tan^{-1}\left[\frac{h_w}{d_e/2}\right] \quad . \tag{2}$$

The water depth can be expressed as

$$h_w = \left[\frac{P_s - P_{amb}}{\rho_w g}\right] \quad . \tag{3}$$

Equation (2) can then be expressed as

$$\phi \approx \tan^{-1}\left[\frac{2(P_s - P_{amb})}{\rho_w g}\right] \quad . \tag{4}$$

12

The height of entrained particles is related to an increase of the magnitude of angle, ϕ . This relationship, however, is relatively complex, since it is a function of the mechanics of turning air flow as well as the entrainment process. However, as can be seen from Equation (4), at constant static pressure, the slope, and hence the particle height, will increase with a decrease in jet diameter. Also, at constant jet diameter, an increase in disc loading, and hence static pressure, results in an increase in particle height. Substantiating experimental results on the effect of lift device size and disc loading, expressed in terms of field dynamic pressure, q_F , on particle cloud height are shown in Figure 12. As seen from Figure 12, a decrease in lift device diameter, for constant q_F , or an increase of q_F for constant d_e , results in an increase of particle cloud height. Caution must be exercized, therefore, in the extrapolation of small-scale particle entrainment data to full-scale VTOL aircraft.

Multilift Device Interaction

When two or more slipstreams in proximity to each other impinge on a flat surface, a flow pattern results which is different from that of the single jet discussed before. The multilift device interaction will be illustrated by considering the dual propeller VTOL aircraft shown schematically in Figure 7. The dynamic pressure profiles outboard of the propellers in the X-Z plane are very similar to the single jet case. However, in the plane of symmetry, where the slipstreams meet, there is an upward flow of air with a velocity which is vertical at the intersection with the X-Z plane, and which tilts increasingly toward the horizontal with increasing distance along the Y axis (see Figure 13). Furthermore, because the two slipstreams reinforce each other at the plane of symmetry (Y-Z plane), the decay of q_s in this plane is appreciably slower than at the plane through the propeller axis (X-Z plane).

The dynamic pressure profiles along the X and Y axes at two radial stations are presented in Figure 14. It may be noted that in the Y-Z plane, q_s persists as high as 80

percent of the jet diameter and is approximately twice the dynamic pressure measured along the X-Z plane. Another point of interest resulting from jet interaction is the large variations in dynamic pressure experienced in the plane of symmetry as represented by the shaded area in Figure 14. These variations are of low frequency and arise from the mixing and eddying of the two slipstreams.

Figure 15 is a survey of $(q_s)_{max}$ along the X-Z and Y-Z planes, also showing the consistently higher values of dynamic pressure along the plane of symmetry. The maximum dynamic pressure contours of a two-propeller VTOL model aircraft are shown in Figure 16. It is noted that the high dynamic pressures occur only within a very small region on either side of the plane of symmetry. In areas other than this region, the magnitude of radial dynamic pressure is very similar to that of a single lift device configuration.

It can be concluded, therefore, that for multiple impinging jets the downwash impingement problem will be most severe along the planes of symmetry, this severity resulting from the increased magnitude of both radial and upward flow at these planes.

The flow intensity at the plane of symmetry is, of course, also dependent upon the distance between the lift devices. The closer the lift devices are located to each other, the higher q_s will be at the plane of interaction, thus resulting in more intense flow along these planes. Experiments indicate, however, that the trend indicated above is reversed when the lift devices are very close together. When this occurs, the slipstreams mix prior to impingement, thus resulting in a minimum of interaction along the ground. The crossover point where this occurs is not presently known. Generally, however, when the lift device centers are one diameter apart or less, the resulting slipstream can be considered as that originating from a single lift device.

At radial planes other than the plane of symmetry, problems resulting from particle entrainment can be expected to be similar to those reported for single lift device configurations.

14

Jet Temperature Effects

For the turbojet lifting type of aircraft, the characteristics of the jet are somewhat altered by the hot temperatures. As may be recalled from Figure 6, the surface dynamic pressure decay with increasing radial distance was not as rapid for the hot jet as that for the cold jet data. Furthermore, the hot exhaust gas from turboject engines impinging on the ground result in hot-air recirculation and a breakdown of the cohesive qualities of terrain. Materials such as sod or asphalt, able to withstand dynamic pressures on the order of 2000 pounds per square foot at ambient temperatures, break down quickly when subjected to the hot exhaust gases of a turbojet engine.

Quantitative hot gas data presently available provide suface material limitations and temperature profiles on the impinging surface. Typical ground level temperature contours are shown in Figure 17. Two sources of data are represented: a) a steady-state value of the gas temperature at the ground as generated by a 2.5-inch-diameter turbojet model reported in Reference 11, and b) ground temperatures after 10 seconds of operations of an RB-108 turbojet engine reported in Reference 6. The differences between the two curves shown in Figure 17 are believed to be due to scale effects and the methods of measurements utilized in obtaining the data.

The effect of nozzle height on the maximum surface temperature is presented in Figure 18. It may be noted again that the small-scale data of Reference 11 are not in agreement with the full-scale data of Reference 12. Whereas the model data show no significant reduction in temperature at nozzle heights of five jet diameters, the J-85 turbojet engine data indicate a 20 percent reduction in maximum surface temperature at a nozzle height of four diameters.

EROSION CHARACTERISTICS

The discussion thus far has been concerned with the basic air flow characteristics of a vertical jet impinging on a flat surface. It has been shown that the surface dynamic

15

pressure and temperature vary with nozzle height, radial location, disc loading and initial jet temperature. Variations in other geometric parameters such as lift device configuration or flow uniformity were shown to have very little effect on the surface dynamic pressure profiles.

Aerodynamic Forces on Terrain Particles

The aerodynamic forces on ground particles are of fundamental importance in the downwash impingement problem, since a quantitative understanding of these forces will explain the mechanism of the initial entrainment process.

A method of defining approximate entrainment criteria for particles initially immersed in nonuniform flow has been proposed by Vidal in Reference 7. Drag forces on particles were estimated by assuming the particles to be spheres in nonuniform flow and with a velocity that is acting at the center of the spheres.

Using a coefficient of static friction of $\sqrt{2}/2$, the drag criterion for entrainment of particles in contact with the ground plane is obtained by Reference 7 as

$$\frac{\rho_p g \delta}{1/2 \; \rho_A U^2} \leq \frac{3 C_D \delta}{2 \sqrt{2} \; a} \left[\frac{u_o}{U}\right]^2 . \qquad (5)$$

where $\rho_p g$ = weight density of particle, lb/ft^3

δ = boundary layer thickness, ft.

U = inviscid velocity just outside the ground boundary layer, ft/sec

u_o = reference velocity in the ground boundary layer at the center of the sphere, ft/sec

Lift forces were estimated by using the analysis of a sphere near a wall acted upon by uniform flow. Under

16

those conditions, the wall constraint deforms the flow about the sphere, producing a lift force. With the assumption that the effect of ground proximity is the same in both uniform and nonuniform flow and accounting for the effects of shear flow by strip integration, the criterion for lift equal to or greater than the particle weight is

$$\frac{\rho_p g \delta}{1/2 \; \rho_A U^2} \leq \frac{u_o}{U} \left[\frac{9 \delta}{32a} \; \frac{u_o}{U} + 0.672 \; \frac{\delta}{U} \frac{du_o}{dy} \right] \; . \quad (6)$$

Equations (5) and (6) were used to calculate entrainment criteria for ground particles using the laminar-boundary-layer solution for axisymmetric stagnation flow. The data shown in Figure 19 should apply to ground stations from the stagnation point to the point where peak radial velocities are observed ($x_s/d_e \approx 1$). The abscissa of Figure 19 is essentially the ratio of particle weight to dynamic pressure outside the boundary layer. Entrainment will occur if this loading parameter is equal to or less than the value indicated by the curves. It should be noted that either mechanism can dominate depending on particle size. For particle sizes such that $a/\delta < 0.6$, the lift mechanism will predominate. For larger particles, the drag mechanism should produce entrainment.

Once particles are lifted into the mainstream, whether by lift or drag forces, they will be subjected to the maximum velocities existing in the radial flow. Under these conditions, a theory based on the terminal velocity in free fall has been suggested by Kuhn, Reference 1, to provide an indication of the particle size that can be transported by the airstream.

The terminal velocity of the particle or, conversely, the air velocity required to support the particle is defined as

$$V_T = V_A = \sqrt{\frac{\text{Particle Weight}}{1/2\, \rho_A C_D\, \pi/4 \left[a/12\right]^2}} \quad . \quad (7)$$

(for $V_T > 10$ ft/sec).

Assuming spherical particles and including the density of the particle material, the diameter of a particle supported by a given dynamic pressure may be expressed as

$$a = \frac{18\, q_s C_D}{\rho_p g} \quad , \text{ inches } \quad . \quad (8)$$

Equation (8) and experimental data of Reference 1 were used to obtain the curves of Figure 20. The maximum size of water, sand and gravel particles that can be supported by an airstream of arbitrary velocity can be obtained from this Figure. This method is compared in Figure 21 with experimental data from Reference 9. The maximum sizes of particles collected at three radial locations about the impingement area, at a height of approximately 0.10 jet diameter above the ground, were compared with the sizes predicted by use of Equation (8). In the process of arriving at this comparison, the particle sizes were originally calculated using the dynamic pressures at the points of collection, $(q_s)_{max}$. This, however, resulted in predicting particle sizes smaller than those collected. Next the use of the maximum field dynamic pressure, q_F, resulted in an overestimation of particle sizes. Subsequently, the values of q_F and $(q_s)_{max}$ at each point of collection were averaged, and the results, as indicated in Figure 21, were in fair agreement with theoretical predictions. The use of an average velocity appears to be reasonable, since particles originating from an area within one jet diameter of the stagnation point will be initially subjected to the

18

field maximum dynamic pressures. At increasing radial distances, the entrained particles will therefore possess energies greater than the local airstream.

In addition to the particle size, Reference 9 presented data on particle flow for various terrains. The flow rate, Q , defined as the quantity of particles impacting a unit area per minute, is plotted in Figure 22 as a function of the average of $(q_s)_{max}$ and q_F . The data within the expected experimental scatter indicate the general trend of increased particle flow at increasing surface dynamic pressures and decreasing heights. Unfortunately, because of the lack of air flow data at the collection points and the inefficiency of the collection traps, the data can be used to obtain only general trends of particle recirculation.

Terrain Limitations

Experimental work in the entrainment mechanism have defined the limiting dynamic pressure or temperature which will initiate the entrainment process. Ground surfaces can be divided into two categories: (1) terrains that are primarily susceptible to surface dynamic pressure and (2) those that can withstand pressure but are susceptible to temperature. Figure 23a presents those surfaces that are affected by dynamic pressure. Sand starts to erode at 3 pounds per square foot, whereas sod may withstand pressures up to 2000 pounds per square foot (depending on the grass root structure). Figure 23b presents the limitations of materials that are primarily temperature limited. Materials such as phenolic-covered glass cloth or aluminum sheets are also included in this chart as possible ground covers.

It must be emphasized, however, that incipient erosion signifies the initial disturbance of particles at the ground level. Experience has shown that, particularly for the case of loose granular terrain, dynamic pressures on the order of two to three times the incipient erosion value will entrain particles in sufficient quantities and to heights that will present operational problem to VTOL aircraft.

19

III DESIGN CRITERIA

The operational problems associated with downwash impingement depend on the physical characteristics of the entrained particles and on their velocity and space distribution. These parameters, in turn, depend on the following:

1. Jet dynamic pressure, q_N

2. Height of jet nozzle, or propeller, above the terrain, h_e

3. Jet diameter, d_e

4. Radial distance from jet centerline, x_s

5. Height of object to be viewed, or aircraft component that is subject to damage

6. Terrain characteristics

7. Jet temperature

8. Aircraft material characteristics

In the formulation of practical downwash impingement design criteria, it is necessary to devise methods by which these parameters can be logically grouped.

The utility of these methods is, of course, dependent on the accuracy with which the severity of the operational problems can be predicted. Previous investigations have been largely concerned, however, with the qualitative rather than the quantitative aspects of these problems.

In this section, methods are formulated to provide the designer with quantitative information on the severity of the operational problems resulting from downwash impingement. Because of the dearth of available experimental data,

these methods will provide, at present, first-order informa-
tion only. The accuracy of these methods will be increased,
however, as more quantitative data is acquired. The methods
described in this section pertain to the following opera-
tional problems:

      1. Visibility
      2. Concealment
      3. Aircraft damage
      4. Personnel injury

      An example of the use of the methods for predicting
the environmental conditions resulting from downwash im-
pingement on terrain is presented for a typical VTOL air-
craft in Appendix I.

VISIBILITY

      Visibility is defined herein as the ability to
identify visually an object of known size at a specified
distance from the observer. This ability is affected by the
number and the physical characteristics of the entrained
particles in the "cone of vision" between the observer and
the object. In the preparation of the design charts for
estimating visibility, it is assumed that the number of
entrained particles is a function of the dynamic pressure
along the surface that is exposed to the jet flow. The
maximum surface dynamic pressure, $(q_s)_{max}$, is obtained
from Figure 5 as a function of jet dynamic pressure, q_N ;
nozzle or propeller height, h_e ; jet diameter, d_e ; and
radial distance along the ground, x_s . For radial dis-
tances greater than four nozzle diameters, Equation (1),
repeated below, can be used to obtain $(q_s)_{max}$:

$$\left[\frac{(q_s)_{max}}{q_N} \right] \left[\frac{x_s}{d_e} \right]^2 = 1.40.$$

In addition to the surface dynamic pressure, the natural
cohesive quality of terrain particles and the particle size
and weight are also important factors in the determination

21

of the number and physical characteristics of the particles
entrained in the downwash.

These factors as well as the jet temperature effects
are incorporated in the design charts by defining an effective
dynamic pressure,

$$(q_s)_{eff} = f\left[\frac{1}{k_t} \frac{T_j}{T_{amb}}\right]\left[(q_s)_{max}\right] . \tag{9}$$

where

$f\left[\frac{1}{k_t} \frac{T_j}{T_{amb}}\right]$ denotes a function of the

terrain factor, k_t , the jet temperature, T_j , and the
ambient temperature, T_{amb} . The terrain factor, k_t ,
accounts for the particle diameter as well as its density
and is defined in Figure 24. For the case in which the
terrain particle sizes are effectively increased (for example,
the case of wet sand), the values of k_t were selected to
coincide with terrain for which incipient erosion occurred
at approximately the same value of surface dynamic pressure.
From Figure 24 it is noted that, in agreement with experi-
ments, a decrease of k_t corresponds to ground materials
that, at constant jet dynamic pressure, will result in an
increased loss of visibility.

The visibility is a function of the relative loca-
tion of the observer and the object. In order to determine
this function, there is introduced the concept of local
visibility, which is defined as the visibility when observer
and object are separated by a unit distance, say, 1 foot.
If the target is completely obliterated, the local visibility
is zero. Conversely, if there are no particles between the
observer and the object, the local visibility is said to be
unity. The percent visibility between these extremes is
related to the physical characteristics of the entrained
particles and is not known at this time. The zero and
unity values of visibility have been estimated, however,
from films and personal observation of downwash tests. Such
estimation was utilized in the preparation of the chart shown

22

in Figure 25, which presents local visibility vs. $(q_s)_{eff}$ for several values of object height. This figure is believed to give a first-order estimation of local visibility for water terrain where the values of $1/k_t$ and T_j/T_{amb} are unity. In agreement with experimental data, Figure 24 shows that, at constant object height, local visibility decreases with an increase in $(q_s)_{eff}$, or equivalently with increase of radial distance from the jet center.

The ability to identify an object an arbitrary distance from the observer, denoted here as relative visbility, is a function of the variation of the local visibility along the line of vision. This function is not known at present. It cannot be a simple summation of local visibility, since zero local visibility at any point along the line results in zero relative visibility. By plotting the local visibility conditions surrounding the lift device, however, as illustrated in Appendix I, the overall relative visibility conditions can be estimated.

For terrain other than water, the use of $\sqrt{k_t}$ in Equation (9) has resulted in good correlation with visibility conditions as observed from model tests.

The case of a multilift-device aircraft can be treated as a single lift device but only by including the effects of the intensified flow along the plane of symmetry. Recalling the dynamic pressure flow along the X-Z and Y-Z planes from Figure 15, the value of $(q_s)_{max}$ along the plane of symmetry is seen to range from 1 to 2 times greater than the dynamic pressure along the X-Z plane. These ratios have been plotted in Figure 26 as a function of x_s/d_e or y_s/d_e and can be used to obtain the increase in dynamic pressure resulting from multilift interaction. The high-intensity particle flow is limited along a narrow arc of $10°$ to $20°$ to the right or left of the plane of symmetry. This arc may be used as a guide in plotting the visibility curves as indicated in Appendix I.

CONCEALMENT

As with all other problem areas resulting from down-

23

wash impingement on terrain, the aircraft concealment prob-
lem is a complex one and is affected by a great number of
variables. The principal parameters affecting concealment
include:

1. Cloud height
2. Cloud width
3. Cloud density
4. Cloud color
5. Background color
6. Relative position of observer and aircraft
7. Height and location of obstacles between observer and aircraft
8. Atmospheric conditions (i.e., visual range, wind, lighting).

Geometric Parameters

Certain of the above-mentioned parameters, such as
cloud size and density, are functions of the aircraft
geometry. The effect of design variables such as propeller
disc loading and height above the ground on entrainment has
been previously discussed in detail in the visibility
section. It is sufficient to note, however, that cloud size
rather than particle density is of primary concern in the
area of concealment. This is evident by considering the
fact that once the particle cloud is of sufficient density
to be noticed, which will occur at a relatively low particle
density, the aircraft position has been revealed; any in-
crease from this minimum density will not materially alter
this situation.

Physical Parameters

In addition to the geometric parameters, factors
such as terrain and background color, atmospheric conditions,
and location of the observer will also affect concealment
conditions. These parametric variations, however, can not
be controlled by the designer. Consequently, there is
little that he can do to control their effect on the prob-
lem. Once the cloud height has been minimized by design

compromises, operational techniques must be developed to improve concealment further by the judicious use of surrounding obstacles, background color, wind, and existing visibility condition.

Method for Determining Particle Cloud Height

For reasons given above, effort in predicting loss of concealment will be centered on the particle cloud size generated by the VTOL aircraft.

The method described in the visibility section can be used to obtain a full picture of the overall size of the cloud pattern.

For a quick indication of maximum cloud height, however, the following method can be used:

From Figure 5, determine q_F , which corresponds to the maximum value of q_s , as a function of h_e , d_e , and q_N. Determine $(q_F)_{eff}$ by correcting for terrain using the appropriate value of k_t from Figure 24. When two or more lift devices are used, a value of $(q_F)_{eff}$ twice that developed for a single lift device should be used. Maximum cloud height can now be read from Figure 25 at 100 percent visibility and for $(q_s)_{eff} = (q_F)_{eff}$.

AIRCRAFT DAMAGE

Two distinct areas will be considered in the development of damage criteria. These are (1) damage to airframe and (2) damage to rotating aircraft components. The damage that an aircraft will sustain from particle impacts is dependent both upon the aerodynamic parameters previously described in the section on visibility and upon certain physical properties of both the aircraft materials and the entrained particles. A brief discussion of available data on the particle-target impact phenomenon will be presented next, prior to defining methods of predicting aircraft damage.

25

Particle Impacts

There exists a wealth of hypervelocity particle impact information in the literature (References 13 through 17). Unfortunately, the majority of work is derived from particles having velocities greater than 1000 feet/second. Furthermore, limited comparisons of data from one source with those from another, and of experimental data with theory, have shown some discrepancies. These discrepancies have resulted in several more or less contradictory empirical expressions developed by investigators to fit their own data.

For example, the experimental work of Collins from Reference 14 has indicated that penetration depends on the momentum per unit area of the impacting projectile. Also, crater volumes resulting from impacts were found to be directly related to the projectile kinetic energy and a strength parameter, k_I , such that

$$\text{Crater Volume} = 19 \times 10^{-6} k_I \left[\frac{m_p V_p^2}{2} - C \right], \text{IN}^3 . \qquad (11)$$

where C is a minimum value of energy required for permanent deformation in a given material. The impact factor, k_I, represents the resistance of various materials to penetration. It is defined as the ratio of crater volume resulting from the impact of a projectile on a target, both of arbitrary material, divided by the crater volume resulting from a steel projectile impacting on a steel target. This factor is constant, for a given material, within the kinetic energies tested, i.e., 10 to 10,000 foot-pounds. The data plotted in Figure 27 indicate that crater volume is a function of the acoustic velocity of the target material as well as of the density and acoustic velocity of the projectile materials. An increase in projectile density results in larger craters in a given target. Conversely, a decrease in acoustic velocity of a target results in a reduction of crater size for a given projectile. It must be

26

noted, however, that the variables in the acoustic velocity
of any material, i.e., Young's modulus, shear modulus, and
density, do not compensate for the varying hardness conditions
achieved in a given material by heat treatment or other
similar means. Neglecting these hardness variations, the
acoustic velocity relationship was used to extrapolate im-
pact factors of solids for which no experimental data were
available, as shown in Figure 27.

Another penetration relationship was empirically
derived by Charters and Lock in Reference 15. The particle
penetration was found to be a function of the velocity and
density of the projectile and the acoustic velocity and
density of the target in the following manner:

$$P/a = (2.28)(\rho_p/\rho_T)^{2/3} (V_P/A_T)^{2/3} . \tag{12}$$

Although the above relationship was developed for quasi-
infinite targets, it is in agreement with limited thin-
plate experimental data from Reference 16 as indicated in
Figure 28.

A theoretical treatment of impacts, expressly for
thin-plate penetrations based on ballistics research, was
developed by Taylor in Reference 17. Taylor defined the
energy, E, required by a projectile for penetration through
a material of thickness, T, as

$$E = T A_I \left[Y_T/2 + \rho_T/4 \left\{ (\pi/2)(R/L) \, v \right\}^2 \right] \text{ft-lb} \tag{13}$$

where R/L ~ 1 for spheres.

The first term of Equation (13) represents the work required
to expand a hole statically in a target. The second term
is a correction for the plastic flow region in the target
material. This term becomes progressively more important as
the projectile velocities increase. Using the experimental

27

data of Reference 16, the energy generated by a 0.093-inch-diameter steel sphere to perforate targets of various thicknesses was calculated. The results plotted in Figure 28 again indicate fair agreement at the low target thickness. Although many other theoretical and empirical methods for predicting the results of impacts are availabe, the three methods represented by Equations (11), (12), and (13) will be used to develop the design criteria for aircraft damage. Unfortunately, there is a dearth of available impact data in the particle speed regimes anticipated in the VTOL environment, i.e., 0 to 500 feet/second. The application, therefore, of the penetration equations, originally derived from hypervelocity impacts, to entrained particle speeds must be utilized with caution until substantiating data are provided.

Airframe Damage Criterion

Discussed in this section is the airframe damage criterion, which is defined as the minimum thickness of aircraft skin required to withstand impacts from entrained objects. Also presented here is a simplified approach to landing gear impact loads from rolling debris.

Full-scale experimental investigations with simulated or actual VTOL aircraft operating over sand terrain with disc loadings as high as 50 pounds per square foot have reported only superficial damage to the airframe. This is substantiated by Reference 13, which reports that projectile energies of 50 foot-pounds are required to create permanent deformation in quasi-infinite targets of aluminum or steel. Energy levels of this magnitude would apply to relatively solid structures such as landing gear, etc. For thin plates, as in the case of aircraft skin, the energy level required for complete penetration is greatly reduced. As indicated from Figure 28, a 0.093-inch-diameter steel sphere having an energy of approximately 4 foot-pounds will penetrate a 0.062-inch aluminum plate. As a comparison, the energy level of a 0.25-inch pebble with a velocity of 300 feet/second (far above any speed that a particle of this size is expected to attain in the downwash environment)

28

will only be 0.67 foot-pound. Consequently, no extensive
damage, other than pitting of plastic windshields or paint
erosion, can be expected on the airframe from small particles
entrained by propeller-type VTOL aircraft. It has been
determined, however, that even at the disc loadings repre-
sentative of propeller-type VTOL aircraft, debris having
large frontal area to weight ratios, such as broken tree
limbs, flat rocks, etc., can be entrained in the flow along
the ground. Moreover, in the case of multiple-lift devices,
this debris can be lifted at the planes of symmetry to heights
which would present a hazard to the aircraft. In addition,
as disc loadings are increased with the use of turbojets,
lift fans, etc., the maximum size and hence the energy
level of particles that can be entrained increases, with a
corresponding increase in airframe damage.

The discussion thus far has presented some qualita-
tive information on airframe damage gained from operational
experience. For a quantitative evaluation of design limits,
Equation (13) defines the minimum energy required to pene-
trate a material of given thickness in terms of impact area,
A_I, material yield strength, and particle velocity. By
equating this to the energy of an entrained particle, the
minimum thickness of aircraft skin can be obtained. To
determine the energy of a particle at impact, both the size
and the velocity of the particle must be known. Unfortunate-
ly, no data are presently available which can be used to
predict sizes or velocity of particles at any location in
the immediate vicinity of the VTOL aircraft. Although it
is known that size, velocity, and particle concentration
are functions of disc loading, lift device size and height,
number of lift devices, and flow temperature, the degree
to which each of the above parameters contributes to the
particle energy is presently unknown. As a first-order
approximation, however, a technique will be indicated herein
which will provide first-order estimates of particle size
and velocity to be used in conjunction with Equation (13).

Particle Size

The size of particles will be estimated by using
the terminal velocity relationship obtained from Reference 1

and shown in Figure 21. This assumption is based on the
fact that the airstream can support particles whose terminal
velocity is equal to or less than that of the local airstream
velocity. As may be recalled in the discussion accompanying
Figure 21, if an average of the maximum field velocity and
the local velocity at the point in question is used, the
particle size can be closely approximated. The average
velocity of the airstream, V_A , is obtained as follows:

From Figure 5 obtain q_F and $(q_s)_{max}$ as a function

of q_N, d_e, h_e, and x_s. V_A is then equal to

$$V_A = \sqrt{\frac{2}{\rho_A} \frac{\left[q_F + (q_s)_{max}\right]}{2}} \quad , \text{ ft/sec .} \quad (14)$$

By assuming spherical particles, Figure 20 can then be
used to obtain the maximum size of sand or gravel particles,
at any point within the area $0 < x/d_e < 6$, which can be
supported by the average airstream velocity, V_A. The
particle mass is then equal to

$$m_p = \pi/6 \ (a/12)^3 \rho_p \ , \quad \text{slugs.}$$

A limiting condition to particle size is, of course, the
size of particles available in the terrain. If, for ex-
ample, the terrain is sand having particle sizes not greater
than 0.25 inch, the maximum size of particles will be the
maximum size available no matter how large the surface
velocity.

Another limiting condition is the height that
large-size particles will attain. Since $(q_s)_{max}$ occurs at
$h/d_e = 0.02$, the maximum size of particles that can be
supported will decrease with increasing height above the
terrain. From the surface erosion tests of Reference 9,
the maximum size of particles at one diameter above the
terrain generally ranged between one-half and one-third

30

the maximum size of particles at $h_e/d_e = 0.10$. Since the method previously defined will give the overall maximum size of particles, its use will provide conservative damage criteria.

For large objects, such as broken tree limbs, barrels, and other debris, the maximum size-to-weight ratios that can be supported can be written as

$$(W/A_F)_{max} = 1/2 \; \rho_A V_A^2 C_D K_1 \; , \quad \text{lb/ft}^2 \quad (16)$$

where K_1 is a function of the ratio a/d_e and the object shape. No quantitative data are available at present to determine this function. Where two lift devices are used, entrained objects can be lifted at the planes of symmetry to heights far above those attained from a single lift device. In this case the supporting upflow velocity, V_u , that should be used can be approximated by

$$V_u = \sqrt{q_N/\rho_A} \; , \text{ft/sec.} \quad (17)$$

The upflow is expected to decay rapidly with increasing height. The only source of data available, however, is at $h/d_e = 0.30$, from which this relationship was derived. (See Figure 13.)

Particle Velocity

The particle velocity at impact consists of the vector sum of the particle velocity and the velocity of the aircraft component. For airframe damage, only the particle velocity will be considered.

The prediction of particle velocity as a function of time and place becomes a monumental task if the effects of all variables are to be included. Furthermore, even if such an exact solution were developed, there presently

exist no experimental data which could be used for comparison.

With a number of simplifying assumptions, however, a solution can be derived which will provide a first-order approximation of the particle velocity. In obtaining this solution, it will be assumed that the particle velocity of interest is the velocity which the particle will attain three jet diameters from the impingement center. Additional assumptions made are as follows:

1. The particle is acted upon by the radial airstream starting at the center of impingement.

2. The airstream velocity acting on the particle is a constant, which is obtained by an area-weighted average value of $(q_s)_{max}$ within the limits $0 < x/d_e < 3.0$. This average value, V_{AV}, is equal to $\sqrt{q_F/\rho_A}$. The airstream velocity is zero for $x/d_e > 3.0$.

3. Particle rotation is neglected.

4. Particle chance impacts with other particles are neglected.

5. Effects of temperature are neglected.

The resulting equation of motion of a particle becomes

$$d^2x/dt^2 = dV_p/dt = K(V_{AV}-V_p)2 \qquad (18)$$

where

$$K = \frac{C_D \rho_A A_F}{2m_p}$$

Assuming $V_P = 0$ for $t = 0$, Equation (18) when integrated becomes

$$t = \frac{1}{K} \left[\frac{1}{V_{AV}V_P} - \frac{1}{V_{AV}} \right] \quad . \tag{19}$$

Since $V_P = dx/dt$, Equation (19) can be written as

$$dx/dt = \frac{V_{AV}^2 \, Kt}{1 + V_{AV} Kt} \quad . \tag{20}$$

Integrating Equation (20) and setting $x = 0$ at $t = 0$,

$$t = \frac{1}{V_{AV}} \sqrt{\frac{2x}{K}} \quad . \tag{21}$$

The time required for the particle to reach three-jet diameters from the jet center is

$$t = \sqrt{\frac{6 \, d_e \, \rho_A}{q_F \, K}} \quad , \text{ second.} \tag{22}$$

The corresponding particle velocity at three-jet-diameters is

$$V_P = \sqrt{\frac{q_F}{\rho_A}} - \frac{1}{Kt + \dfrac{1}{\sqrt{q_F / \rho_A}}} \quad , \text{ ft/sec} \tag{23}$$

or, in nondimensional form,

$$\frac{V_P}{\sqrt{\dfrac{q_F}{\rho_A}}} = 1 - \frac{1}{\sqrt{6 \, K \, d_e} + 1} \quad . \tag{24}$$

33

As indicated above, the simplifying assumptions made in the solution for particle velocities imply that the value obtained from Equation (24) is an approximation of the maximum particle velocity, which is assumed to occur at three-jet-diameters from the center of impingement. Bearing this in mind, the values of particle velocity thus obtained, along with maximum size of particles to be transported, can be used to determine the energy of an entrained object. Subsequent use of Equation (13) in conjunction with handbook values of allowable yield stress for the aircraft component in question will provide first-order design limits as to thickness and/or material selection. To facilitate the use of this method, the data have been combined into two design charts shown in Figures 29 and 30. Figure 29 provides the ratio of particle velocity to average field velocity in terms of a size parameter, β , where

$$\beta = \frac{3 \, d_e \, C_D \, \rho_A \, A_F}{m_P} .$$

Having the particle velocity from Figure 29 and the particle mass from Equations (15) or (16), the designer can determine the particle kinetic energy from

$$E_P = 1/2 \, m_P \, V_P^2 \quad , \text{ft-lb.} \tag{25}$$

The minimum skin thickness, T, for a given material yield strength, Y_T , required by the aircraft skin to resist penetration, from particle energy found above, can then be obtained from Figure 30. The values of TY_T shown in the figure do not include the second term of Equation (13), which corrects for compressibility effects. Numerical evaluations show that the contribution of this term in the low particle speed regimes is negligible. To compensate for rotation of irregular objects, where by chance the impact area may be less than the frontal area, several ratios of A_I/A_F also are included in Figure 30.

34

In addition to the airframe skin, landing struts or other appendages exposed to rolling debris will be subjected to impact loads which must also be considered in VTOL design. A simplified analysis of impact loading on beams based on Reference 18 follows.

It is assumed that an entrained object with weight W is moving horizontally with a velocity V_p and strikes a vertically suspended beam (landing gear) fixed at one end against horizontal motion. The resultant maximum stress due to impact, σ_I , divided by the maximum stress due to static loading of weight, W, is

$$\frac{\sigma_I}{\sigma} = \sqrt{\frac{V_p^2}{g\epsilon}} \qquad \qquad (26)$$

where

ϵ =   maximum static deflection of cantilever beam subjected to load W, feet.

σ maximum static stress of cantilever beam subjected to load W, pounds per square inch.

As was pointed out in Reference 18, the impact stress thus determined is greater than that observed in tests. Furthermore, the method applies only within the proportional limit of the material in question. With these limitations, the impact stresses determined above will provide conservative design limits for landing struts and other appendages subjected to the VTOL environment.

Damage to Rotating Aircraft Components

From the full-scale experimental investigations previously mentioned, the most severe damage reported was sustained by propellers and turbine engines. The high

rotational velocities of these components result in relatively high energy impacts and consequently extensive damage when these components come in contact with entrained particles. Particle velocities become insignificant when compared to the rotational speed of propellers or turbine blades and will therefore be neglected for this analysis. The quantity of particles ingested by a turbine or propeller now becomes of paramount importance in the prediction of damage to these components.

The quantity of particles ingested is dependent upon the density of entrained particles in the vicinity of the intakes and the mass flow of the lift device.

The presently available particle density data shown in Figure 31 are limited to low-disc-loading helicopters from References 19 and 20 for sand and water terrain, respectively. Reference 21 also provides some indication of particle density for wet sand particles passing through an 8-foot duct.

There is an obvious need, therefore, of particle density information in the vicinity of the lift device as a function of all the pertinent particle entrainment parameters.

With the limited data available, propeller and turbine engine endurance limits are indicated in Figure 32. The limits are based on full-scale tests over wet sand, reported in Reference 21, and a test cell report by a turbine engine manufacturer, Reference 22. The full-scale tests consisted of a tandem ducted configuration tested at $q_N \approx 25$ pounds per square foot. After 8 minutes at an ingestion rate of 29 grams/second, of particles ranging in size from 200 to 5000 microns, the first-stage compressor blades of the T53 turboprop engines used in this test rig were extensively damaged and had to be replaced. The test cell data indicated extensive power loss and erosion after 3.25 hours at an ingestion rate of 1.36 grams/second, with particle sizes from 105 to 210 microns. Although criteria cannot be based on just two instances, the information pro-

36

vides an indication of the limitations of turboprop engines when operating over sand terrain. Furthermore, these limitations apply only within the size of particles ingested. Larger size particles are expected to increase blade erosion, particularly of the first-stage compressor blades. Particles are generally pulverized as they progress past the first-stage compressor blades.

Aluminum propellers subjected to the sand environment conditions reported in Reference 21 also sustained critical damage to their leading edges and the downstream surfaces. The extent of damage to the propellers as reported in Reference 21 indicates crater sizes above the allowable tolerance limitation as defined by propeller maintenance specifications. Based on the above information, the propeller endurance limitations are also shown in Figure 32. The increased capacity of the propeller over that of the turboprop engines is primarily due to the high percentage of open area for the particles to flow through without impacting the blades.

Quantitative evaluations of propeller or turbine blade damage can be obtained by using Equations (11) and (12) in terms of crater volumes and penetrations, respectively. The particle size previously determined from Equation (15) and the appropriate impact factor k_I from Figure 26 used in conjunction with the rotational velocity of the aircraft components will indicate the resulting crater sizes or penetrations on the impacting surfaces. The quantity of particles flowing through the lift device will provide the endurance limit of these components. By using the density of particles in the air and the volume flow of the lift device, the quantity of particles ingested can be found. From this, an indication of the endurance limit for the lift device can be obtained from Figure 32.

Particle density, in addition to the VTOL parameters affecting the entrainment, is also a function of location on the aircraft. Items such as wings, tail surfaces, and fuselage shape will also affect the local air flow conditions and hence the local particle density. No general rule of thumb can, therefore, be applied to determine the optimum location for engine intakes. Inlet screens, particle separators, and deflectors have been tested as means of

37

minimizing particle ingestion. These items will be discussed in detail in the section on downwash alleviation techniques.

In addition to the damage that gas-turbine engines will sustain when operating over sand or other hard, granular terrain, another operational problem reported, is the experience of degradation in performance due to water ingestion.

Although this aspect of the problem will not be dealt with extensively herein, it is obviously again the result of high particle density. The sources and the information available on this subject will be briefly discussed below. Data reported in Reference 20 and shown in Figure 33 present a qualitative indication of how salt deposits from brine-water ingestion will reduce the available horsepower of a hovering helicopter during anti-submarine-warfare missions. The 15-foot altitude hover, because of the resulting higher ingestion rate, shows a more rapid initial performance deterioration rate than that occurring at the 30-foot hover. Fresh water, when ingested at high rates, will also result in power loss, as indicated by Figure 34. The data reproduced from Reference 21 indicate the reduction in power loading that occurs when a VTOL aircraft is operating over water.

The possibility of flame-out also exists when an excessive amount of water is ingested. Test conducted on a J-79 turbojet (Reference 23) showed that flame-outs occurred at water-to-air ratios as low as 0.018. For comparison, the weight-to-air ratio of sand ingested in the T-53 engine previously mentioned is 0.0064. An increase in dynamic pressures over the 25 pounds per square foot reported in Reference 20 and the accompanying increase in circulation when the aircraft is operating over water may result in weight-to-air ratios large enough to present flame-out conditions.

PERSONNEL INJURY

The extent of personnel injury primarily depends

38

upon the velocity, mass and quantity of entrained particles as well as the location on the body where the particles will strike. The variables affecting the velocity, mass and quantity of particles are the same as were previously discussed in detail in the section on damage criteria. For the sake of brevity, the methods used in obtaining these parameters will be omitted in the present discussion.

Data defining criteria of personnel injury, in terms of particle mass and velocity have been published. Figure 35 presents typical data, reproduced from Reference 24 depicting the maximum velocity and weight of steel particles striking on a rabbit's eye that can be tolerated without cornea penetration. The effectiveness of plastic eye shields is also included in Figure 35. Although direct correlation between human and rabbit eyes cannot be drawn from these experiments, medical authorities suggest that the results presented may be used as a good indication of human eye tolerance. It is obvious, therefore, from Figure 35 that eye protection is a _must_ for ground personnel in VTOL operations.

Original German work on ballistics, Reference 25, defined a minimum energy for incapacitation by a small fragment as 58 foot-pounds. Of course, certain areas of the body are more susceptible to injury than others. As suggested by Reference 26, fragments possessing energies far less than 58 foot-pounds have resulted in incapacitating injuries when impacting critical areas of the body. More exact information on casualty criteria for wounding by fragments are available in Reference 27. In any case, however, the energy level expected from small particles entrained in the downwash is far below any of the values indicated in ballistics literature. It can be concluded, therefore, that all parts of the body, when properly protected, as with battle dress, will absorb small-particle impacts without serious injury.

This is not the case, however, where large debris are concerned. When debris are available in the terrain and the VTOL aircraft can generate dynamic pressures capable

of entraining them, the energy level that will be generated
will exceed the minimum values defined in References 25
and 26. Even though the energy levels of Reference 25 are
rived for small impact areas, large debris may by chance st
the body at a sharp corner, thus resulting in the same im-
pacting condition.

The energy levels that debris will attain when sub-
jected to VTOL environment can be obtained by using the
method described in the section on damage criteria.

IV DOWNWASH ALLEVIATION TECHNIQUES

The devices and systems which have been considered for alleviation of the problems caused by the impingement of downwash upon terrain can be categorized as follows:

1. Reduction of nozzle jet velocity
2. Ground protection
3. Flow diversion
4. Particle entrapment

A discussion of the potential of these systems is presented below.

REDUCTION OF NOZZLE JET VELOCITY

It has been shown in Section II that surface erosion is a function of the surface dynamic pressure resulting from the high-velocity air of the VTOL aircraft lift devices

An exploratory investigation of the effectiveness of diffusors in reducing this maximum ground surface velocity is reported in Reference 28. Results indicate that velocity reductions as high as 50 percent were obtained by expansion of the main jet with auxiliary nozzle exit air jets flowing at varying angles to the main jet flow. The quantity of air required to effectively reduce the velocity at the ground increases the total power requirement by 35 percent. Typical results obtained with diffusors are shown in Figure 36. The maximum ground velocity is seen to be effectively reduced, particularly at height to jet diameter ratios greater than 1.0. The shaded areas within the curves represent the range of various auxiliary nozzle to main nozzle mass flow ratios tested. Generally an increase in auxiliary nozzle mass flow resulted in a decrease in maximum surface velocity, with an accompanying increase in the power required.

Another solution may be to increase the number of lift engines for the same total thrust. In this manner both the jet velocity and/or ground separation distance ratios

will be increased. This application will, however, be
limited by the maximum number of engines that can be practi-
cally designed in a VTOL configuration and by the penalty
in weight, complexity of installation, and loss of engine
efficiency resulting from multiengine aircraft design.

The reduction of surface dynamic pressure may also
be accomplished by the use of retractable, circular, fine-mesh
screen fences suspended from the lift device as shown in
Figure 37. With this configuration, the flow of vertical
air will encounter minimum resistance and, hence, minimum
lift losses. However, in turning, the surface dynamic
pressure will be subjected to high pressure losses in
passing through the screen, hence significantly reducing
the surface velocity. Furthermore, the majority of particles
entrained within the screen area will be contained within
this area, thus minimizing the problem of vision, concealment,
engine ingestion, personnel injury, etc. The practical
limitations of such a device are (1) the size of the lift
device that can be encircled by a screen and (2) the extent
of damage to lift device components such as propellers,etc.,
caused by increased particle concentration within the en-
circled area. Preliminary investigations with this type of
device, conducted by the contractor, indicated favorable
results in containing the entrained particles within the
screen area.

GROUND PROTECTION

Ground protection techniques which have been proposed
to prevent surface erosion fall into two major categories:

        1.   Stabilization of the soil through chemicals,
           and

        2.   Protection of the ground through the use of
           prefabricated lightweight covers.

These methods are discussed herein.

Chemical Stabilization

In the past, chemical stabilization of the soil to prevent erosion due to surface winds, as reported in Reference 29, was successfully accomplished. Recently, exploratory investigations in the field of soil stabilization to prevent erosion due to downwash have been initiated by the Air Force Systems Command.

A chemical soil stabilization system to be used in conjunction with VTOL aircraft should possess certain requirements, as suggested in Reference 21. These include:

1. Ability to stabilize effectively various types of soil under the action of the VTOL downwash, including operation under high temperatures for pure jets.

2. Ability to become effective in a short period of time.

3. Efficient area coverage to chemical weight ratios.

4. Application procedure of chemical to terrain should require a minimum of manpower effort.

5. If possible, dispersing of chemical should be from a system within the VTOL.

Based on these requirements, there appear to be two types of chemicals that have merit. The low-density urethane foaming compounds when applied to terrain have excellent bonding qualities. The chemical is fast acting and could possibly be applied to the ground with a self-contained dispersing system. The foam is of low density (0.2 to 0.3 lb/ft^3) and expands to cover large areas when dispersed. Although the chemical itself appears to fulfill the requirements adequately, an effecient dispersing technique must be developed before the system can be fully evaluated. In con-

trast to the foaming chemicals, which provide a surface coating, other chemicals exist which bond the terrain particles to form a hard surface. These chemicals have excellent terrain-bonding qualities and actually increase the bearing strength of the soil.

Ground Covers

Ground-cover systems can be evaluated through consideration of the following requirements:

1. The cover should have the capability of being deployed from the aircraft.

2. Since the cover is to be deployed from an aircraft, the system should be lightweight and reliable (mechanically simple).

3. The cover should be tough enough to resist abrasion and loads imposed by landing troops and equipment.

4. Since the cover is a disposable unit, the cost should be a minimum.

Investigation of ground covers was performed to determine types of materials, size of covers, and deployment techniques, such as in References 6, 11, 12, 21, 37, and 38. The types of materials considered were fabrics, plastic films, metallized films, phenolic and aluminum sheets, and portable airfield landing mats.

An evaluation of the suitability of prefabricated ground covers, for dust proofing VTOL landing areas, has been recently completed by the U.S. Army Engineer Waterways Experimental Station, at Vicksburg, Mississippi. Results of this investigation have not yet been published. Reference 38, however, reports of successful tests conducted in 1958-1959 by the Waterways Experimental Station to provide temporary airfield surfacing using elastomer-coated fabrics.

Experimental work in the determination of minimum ground-cover area required to prevent erosion is reported in Reference 21. The quantity of sand collected on the top of a simulated dual tandem ducted-propeller VTOL aircraft fuselage is shown in Figure 38 as a function of the ground-cover-protected area. These results indicate that an area of approximately twice the duct exit area will reduce particle entrainment to a satisfactory level. However, other sources (Reference 30) report that cover areas as large as 10 times the nozzle area may be required to prevent surface erosion. Reference 6, reporting the results of an experimental investigation to develop alleviation techniques for turbojet engines, indicates that aluminum plates four times the nozzle area were successful in preventing erosion of sod terrain. The aluminum plates were formed with a small lip around the circumference, thus effectively separating the flow from the ground for some distance outside the protection cover. For more permanent sites for jet VTOL operations, bilevel platforms have been used by Bell, reported in Reference 31, with great success. These platforms consist of two metal surfaces 6 to 8 inches apart with perforations on the top plate in the vicinity of the jet exits. The jet exhaust passes through the top plate and discharges around the periphery of the platform. This device also eliminates the recirculation of hot gas into the jet inlets.

FLOW DIVERSION

Flow diversion devices (1) direct or channel the downwash flow from a region in which the downwash creates a problem to an area in which the problem is less severe, (2) reduce the downwash energy, or (3) utilize boundary layer separation to lower the velocities acting on ground particles. When diverters are evaluated, the following requirements should be considered:

> 1. If the diverter is to be placed on the aircraft, it should be lightweight.

45

2. The diverter should be able to be deployed from the aircraft if it is of the ground type.

3. A diverter used on the aircraft should not adversely affect the performance of the aircraft.

Airborne deflectors showed promise in controlling particle flow in a localized area such as at engine inlets. Protection for inlets by using particle separators or inlet screens, as indicated in References 21 and 32, has also been suggested. The tilting of lift-device thrust axis has also been found to be effective in controlling local particle flow conditions. The inclinations must, however, be in the order of 30 degrees for any effective control of particle flow. The loss in vertical lift resulting from inclinations of this magnitude may be greater than can be tolerated.

PARTICLE ENTRAPMENT

The downwash energy along the ground could be dissipated by the use of particle traps. The requirements for this type of alleviation device are:

1. Ground traps should be air droppable.

2. The system should be lightweight and have a small volume when packaged.

3. Since the ground trap system cannot completely eliminate the terrain erosion problem, this type of system should be capable of reducing downwash problems to a point considered satisfactory for VTOL operations.

Some of the ground flow diverters suggested are shown in Figure 39. These include particle traps, annular boundary fences and ground channels.

Operational techniques in landing and takeoff may also provide solutions that are acceptable for certain operating conditions. For example, a taxiing speed as low as 10 knots will prevent sod from eroding when subjected to turbojet exhausts.

Generally, all alleviation methods are dependent on the operational requirements set forth by the VTOL aircraft mission. For instance, the time element for in-ground operations is a major factor in the particle entrainment process.

V   REFERENCES

1.   Kuhn, R. E., "An Investigation to Determine Conditions Under Which Downwash From VTOL Aircraft Will Start Surface Erosion From Various Types of Terrain", NASA TND-56, September, 1959.

2.   Squire, H. B., Trouncer, J., "Round Jets in a General Stream", ARC Technical Report R & M 1974, January 1944.

3.   Hess, P. J., "Downwash From Lifting Devices", General Electric Flight Propulsion Laboratory Department, Evendale, Ohio.

4.   Morse, A., "VTOL Downwash Impingement Study - Summary Report", TRECOM Technical Report TCREC 61-37, August 1961.

5.   O'Bryan, T. C., "An Investigation of the Effect of Downwash From a VTOL Aircraft and a Helicopter in the Ground Environment", NASA TND-977, October 1961.

6.   Fearon, J. R., and Norman, D. H., "VTOL and STOL: Simple Solutions to Some of the Operation Problems During Take-Off and Landing", Journal Royal Aeronautical Society, February 1962.

7.   Vidal, R. J., "Aerodynamic Processes in the Downwash Impingement Problem", Journal Aerospace Sciences, Volume 29, September 1962.

8.   Ludwig, G. R., Brady, W. G., "Theoretical and Experimental Studies of Impinging Uniform Jets", TRECOM Technical Report 63-11, April 1963.

9.   Morse, A., Newhouse, H., "VTOL Downwash Impingement Study-Surface Erosion Tests", TREC Technical Report 60-67, October 1960.

10.   O'Bryan, T. C., "An Experimental Study of the Effect of Downwash From a Twin Propeller VTOL Aircraft on Several Types of Ground Surfaces", NASA TND-1239, May 1962.

11. Grotz, C. A., "Simulated VTOL Exhaust Impingement on Ground Surfaces", SAE Preprint #428 D, October 1961.

12. Mitchell, W., Wherry, J., "Hot Gas Surface Erosion Studies", WADD Technical Note 60-183, August 1960, (ASTIA AD 241779).

13. Herman, N., Jones, A., "Survey of Hypervelocity Impact Information", Massachusetts Institute of Technology, ASRL Report No. 899-1, September 1961 (ASTIA AD 267 289).

14. Collins, Jr., R. D., and Kinard W., "The Dependency of Penetration on the Momentum per Unit Area of the Impacting Projectile and the Resistance of Materials to Penetration", NASA TN D-238, May 1960.

15. Charters, A. C., and Locke, Jr., G. S., "A Preliminary Investigation of High-Speed Impact: The Penetration of Small Spheres into Thick Copper Targets", NACA-RM A58B26, May 1958.

16. Partridge, W., et al, "Perforation and Penetration Effects of Thin Targets", Third Symposium on Hypervelocity Impact, Volume 1, February 1959.

17. Taylor, G. E., "The Formation and Enlargement of a Circular Hold in a Thin Plastic Plate", Quarterly Journal Mechanics and Applied Mathematics, Volume 1, 1948.

18. Carmichael, C., "Kents Mechanical Engineers' Handbook, Twelfth Edition, Willey Handbook Series.

19. Watzen, E., "Amount of Dust Recirculated by a Hovering Helicopter", Kaman Aircraft Corporation Report No. R-169, December 1956.

20. Stirgwolt, T., "Salt Water Ingestion by Gas Turbine Engines", Proceedings of the 17th Annual National Forum.

21.   George, M., Pruyn, R., "Effects of Airframe Geometry on Downwash Problems of a Tandem Ducted Propeller VTOL Aircraft", Kellett Aircraft Corporation, 179 T 80-6 (to be published).

22.   Anon., "Lycoming Sand and Dust Program for the T-53 Gas Turbine Engine", Lycoming Corporation, October 1958.

23.   Warwick, W., "Effect of Water Ingestion on J79-GE-8 Altitude Performance", Proceedings of the Third Annual Conference on Environmental Effects on Aircraft and Propulsion Systems, U. S. Air Turbine Test Station, Trenton, N. J., September 1963.

24.   Stewart, G. M., "Eye Protection Against High-Speed Missiles", U. S. Army Chemical Research and Development Laboratories, Army Chemical Center, No. CRDLR 3007, July 1960 (ASTIA AD No. 241 873).

25.   Rohne, H., "Schiesslehre fur Inanterie", 1906.

26.   McMillen, J., Greg, J., "The Energy, Mass and Velocity Which Is Required of Small Missiles in Order to Produce Casualty", Missile Casualties Report No. 12, Princeton, 1945.

27.   Allen, F., Sperrazza, J., "New Casualty Design Criteria for Wounding by Fragments (U)", Ballistics Research Laboratories Report No. 996, October 1956.

28.   Anon., "Exploratory Investigation of the Usefulness of some Diffusor Systems in Alleviating Ground Erosion Problems From the Downwash Impingement of VTOL Lifting Systems", National Luchtvaartlaboratorium, Report A 1547, October 1961 (ASTIA AD 272 020).

29.   Rostler, F., Kunkel, W., Jr., "Soil Stabilization", Industrial and Engineering Chemistry, Volume 56, April 1964.

30. Colin, P. W., "Ground Proximity and the VTOL Aircraft",
North Atlantic Treaty Organization AGARD Report No.
409, 1962.

31. O'Malley, J. A., Jr., et al, "Flow Phenomena Experienced
With VTOL Aircraft in Ground Proximity", Bell Aircraft
Corporation paper presented at AGARD V/STOL Symposium,
Paris, France, June 1960.

32. Mund, M., Wright, T., "Design, Development and Appli-
cation of Air Cleaners for Gas Turbines", SAE pre-
print No. 538B, June 1962.

33. Fradenburgh, E. A., "Flow Field Measurements for a
Hovering Rotor Near the Ground", paper presented be-
fore the AHS 5th Annual Western Forum, Los Angeles,
California, September 1958.

34. Morse, A., "VTOL Downwash Impingement Study, Velocity
Survey", TREC Technical Report 60-58, August 1960.

35. Newsom, W. A., Jr., and Tosti, L. P., "Slipstream
Flow Around Several Tilt-Wing VTOL Aircraft Models
Operating Near the Ground", NASA TND-1382, September
1962.

36. Pruyn, R., and Goland, L., "An Investigation of VTOL
Operational Problems Due to Downwash Effects",
Kellett Aircraft Corporation Report No. 179T80-2,
June 1961.

37. Tucker, S. G., "Portable Surfacing for Army Airfields",
Army Aviation Volume 10, April 1961.

38. Anon., "Downwash Blast Effects Study", U. S. Army
Engineer Waterways Experimental Station, Technical
Report (to be published).
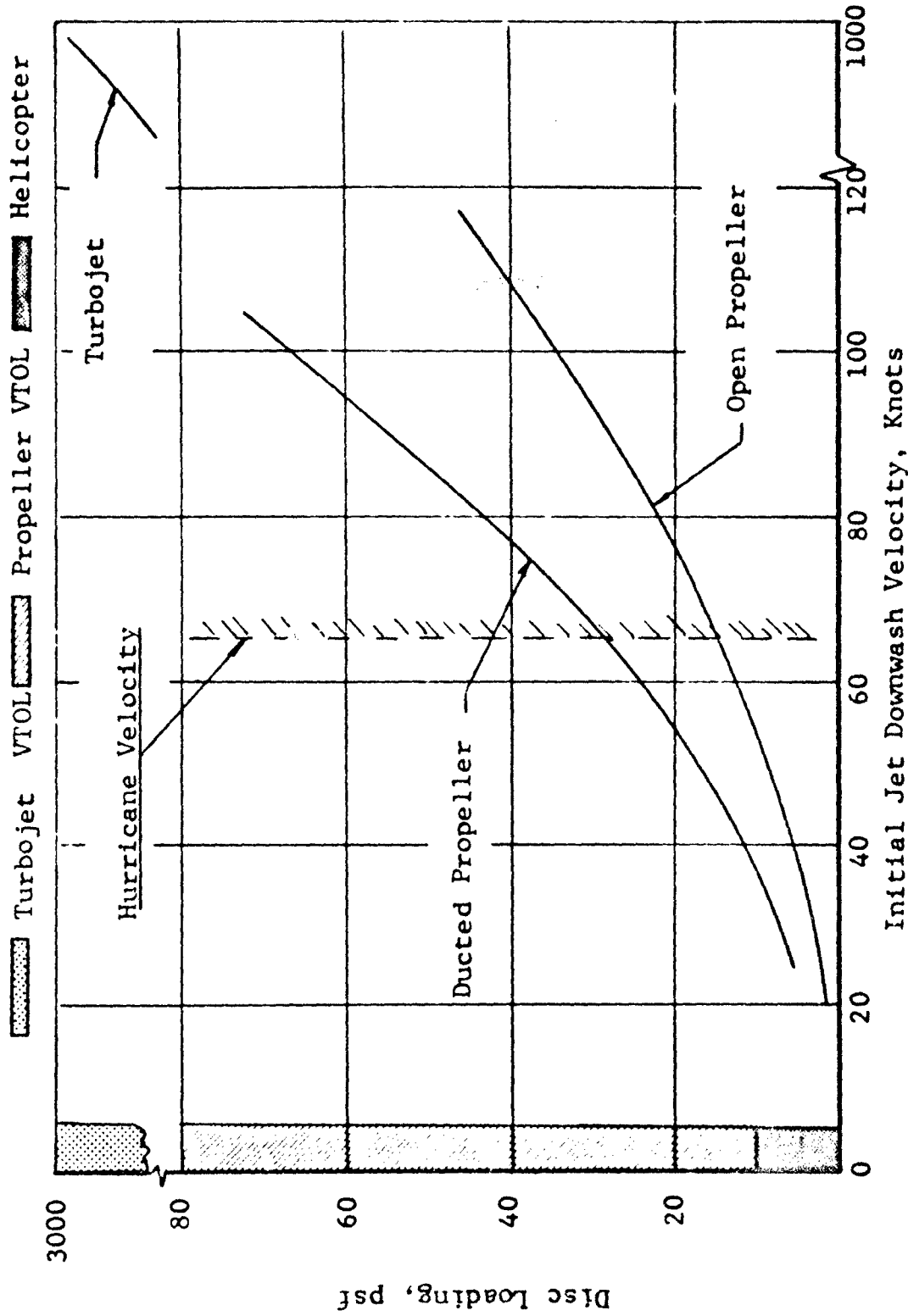
FIGURE 1: DISC LOADINGS vs AVERAGE DOWNWASH VELOCITY FOR VARIOUS LIFT DEVICE CONFIGURATIONS

52
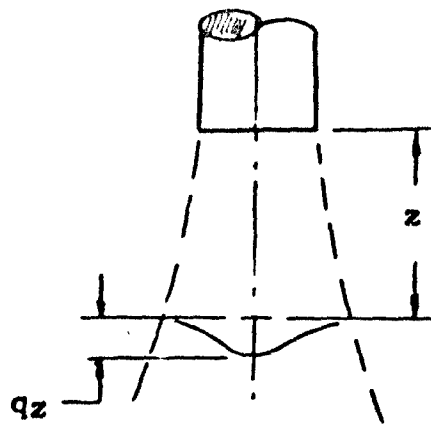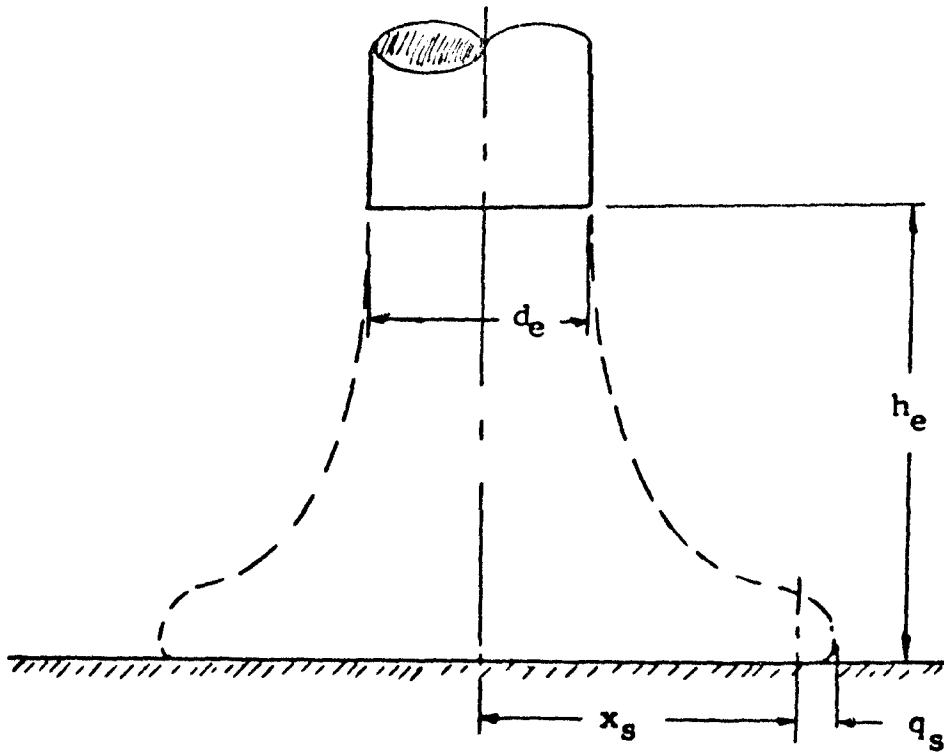
a. Jet in Free Air

b. Jet Impinging on Flat Plate

IGURE 2: JET SLIPSTREAM IN FREE AIR AND IN GROUND EFFECT;
SYMBOL NOTATION
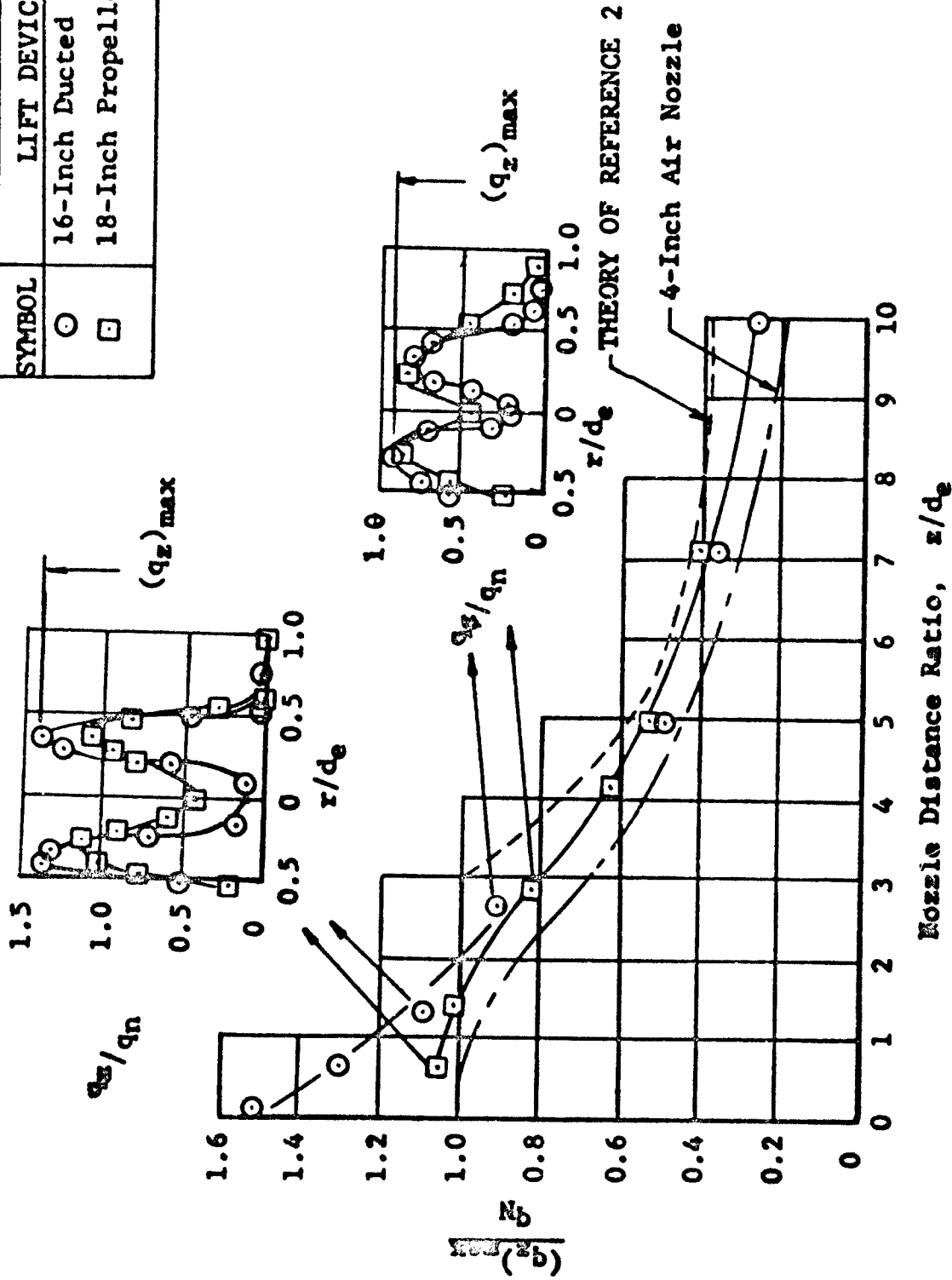
**FIGURE 3: DECAY OF DYNAMIC PRESSURE WITH DISTANCE FROM ROTOR PLANE OR NOZZLE EXIT (Reference 1)**
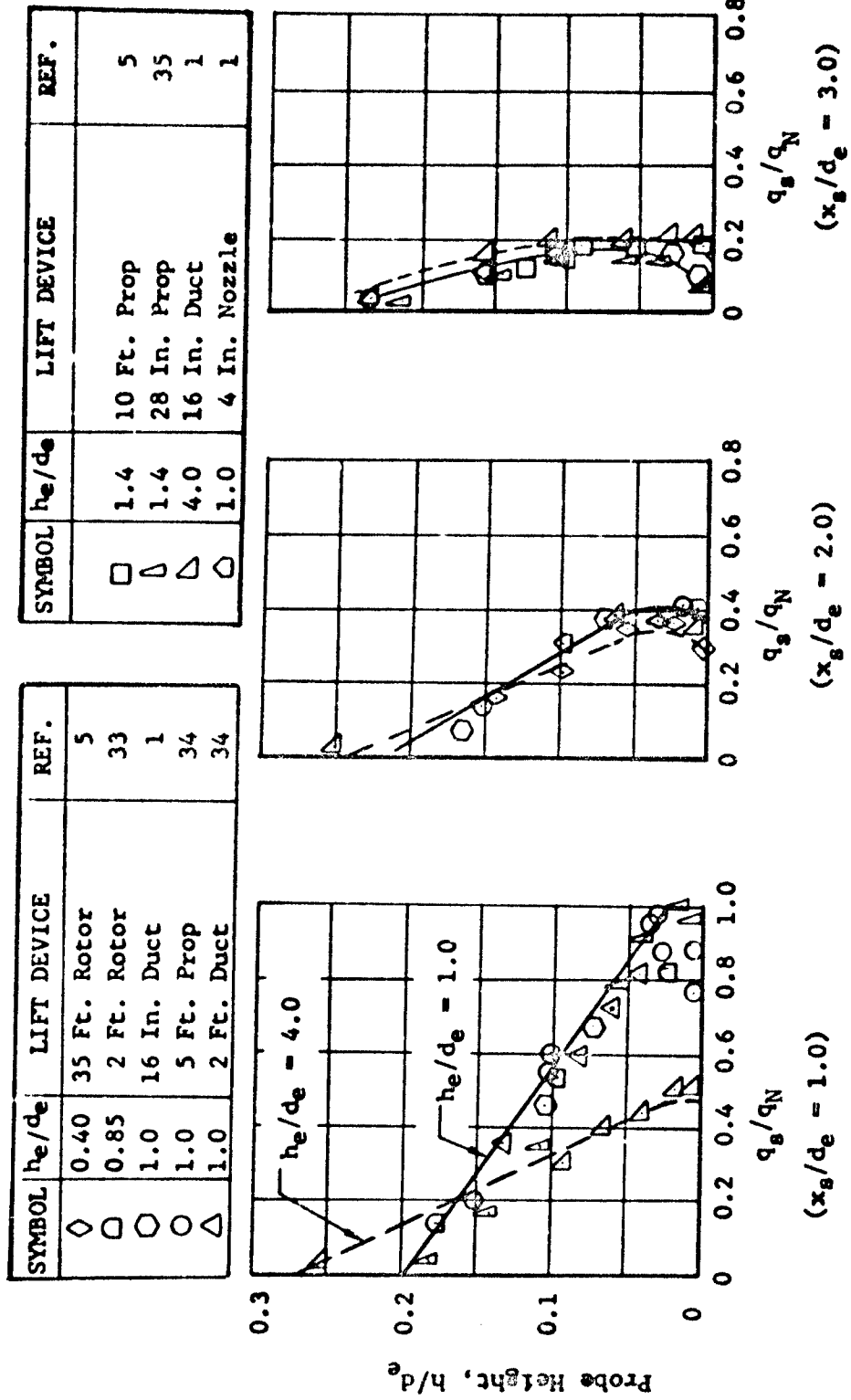
FIGURE 4: TYPICAL DYNAMIC PRESSURE PROFILES OF OUTWARD FLOW OF AIR ALONG GROUND SURFACE

55
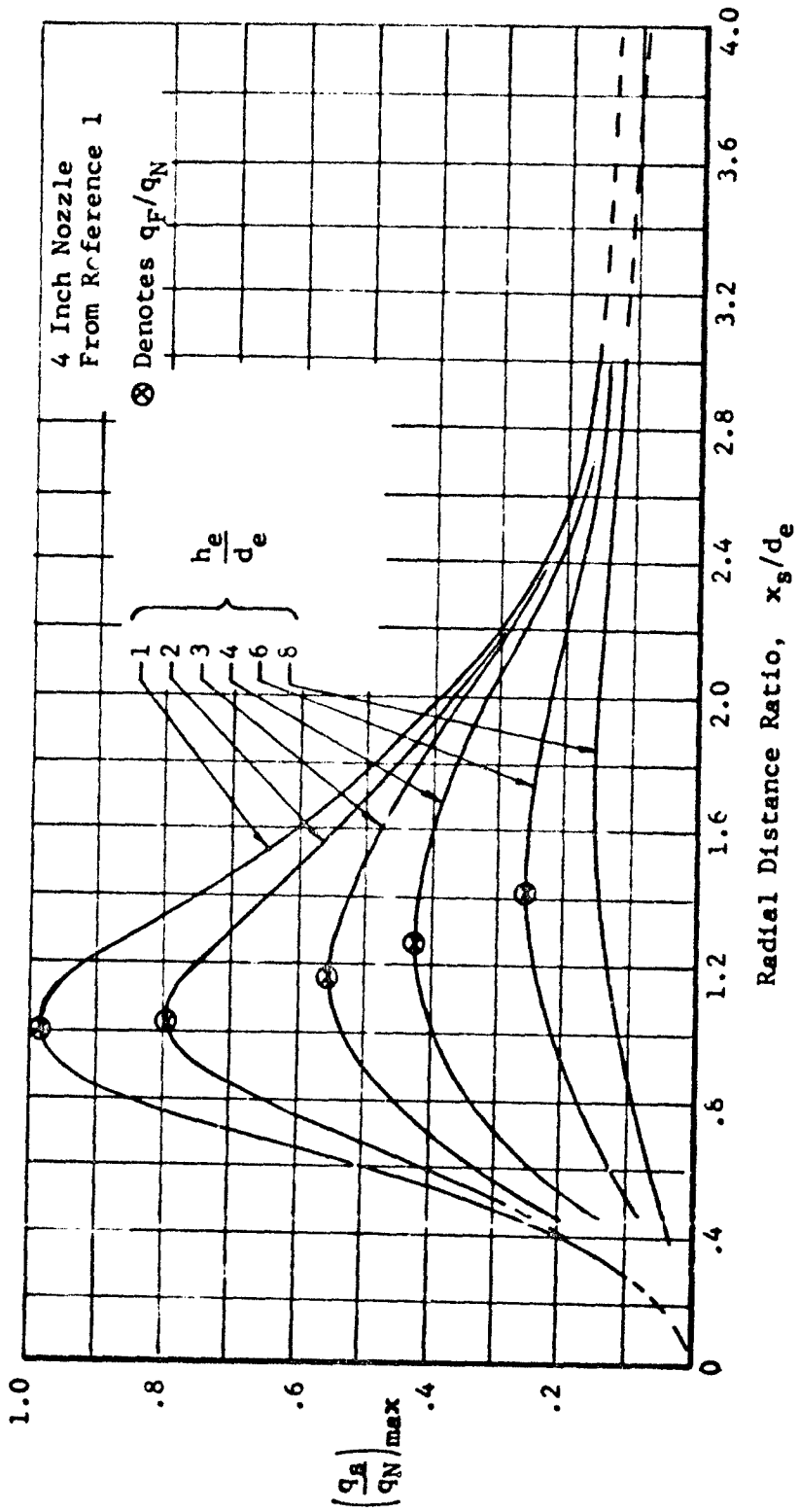
FIGURE 5: MAXIMUM SURFACE DYNAMIC PRESSURE AS A FUNCTION OF NOZZLE HEIGHT AND RADIAL DISTANCE ALONG THE GROUND

56

SYMBOL	h_e/d_e	LIFT DEVICE	REF.
◁	1.0	2 Ft. Duct	34
◯	1.0	16 In. Duct	1
▢	1.0	4 In. Nozzle	1
◺	1.0	1 Ft. Nozzle	8
◿	1.0	2.5 In. Turbo-Jet Model	11
◹	1.0	RB-108 Turbo-Jet	6
◇	1.4	9.5 Ft. Prop (VZ-2 VTOL)	5
◁	1.4	10 Ft. Prop (Curtiss Wright VTOL)	5

Radial Distance Ratio, x_s/d_e

$\dfrac{(q_s)_{max}}{q_N}$
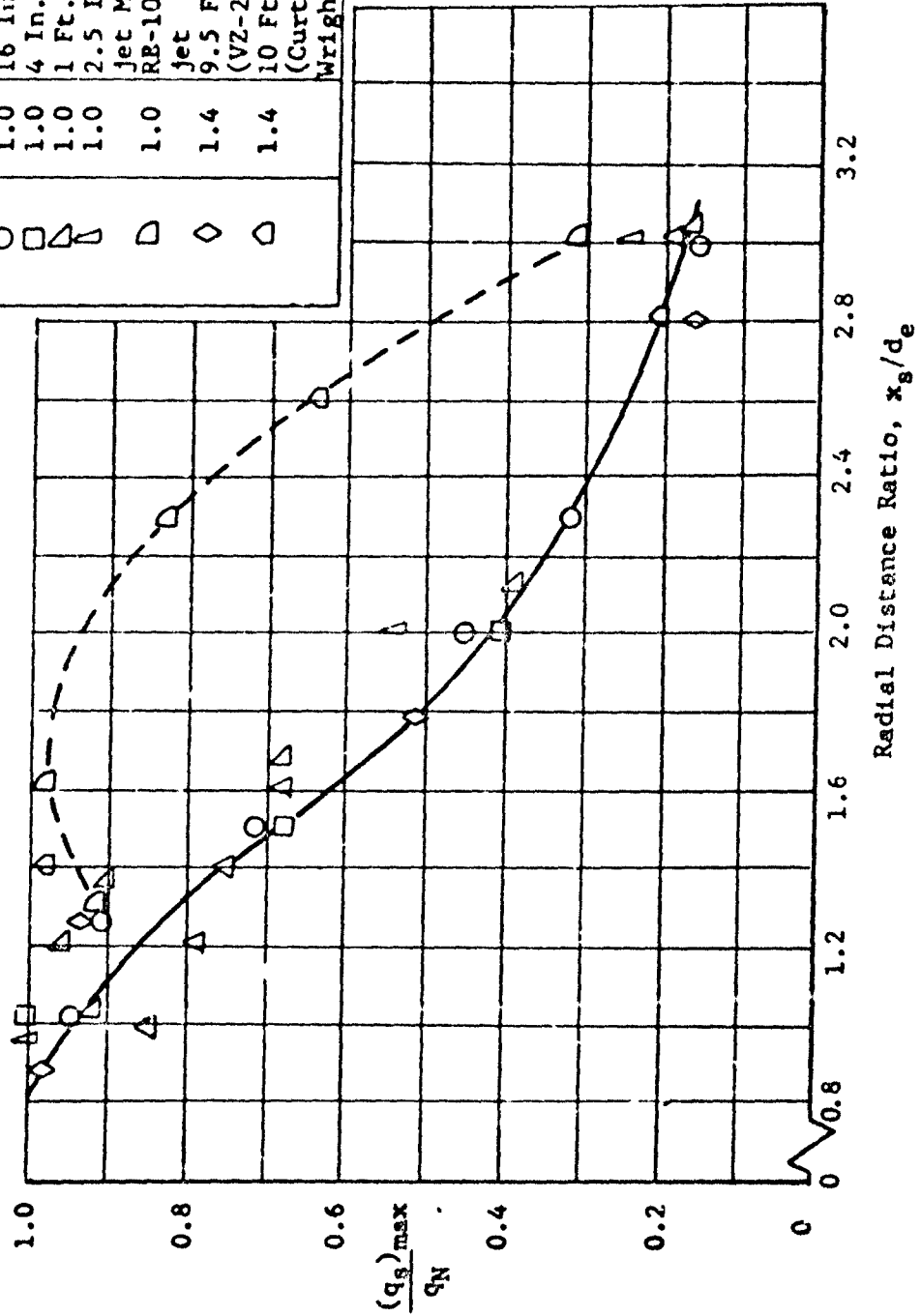
FIGURE 6: EFFECT OF LIFT DEVICE CONFIGURATIONS ON MAXIMUM SURFACE DYNAMIC PRESSURE
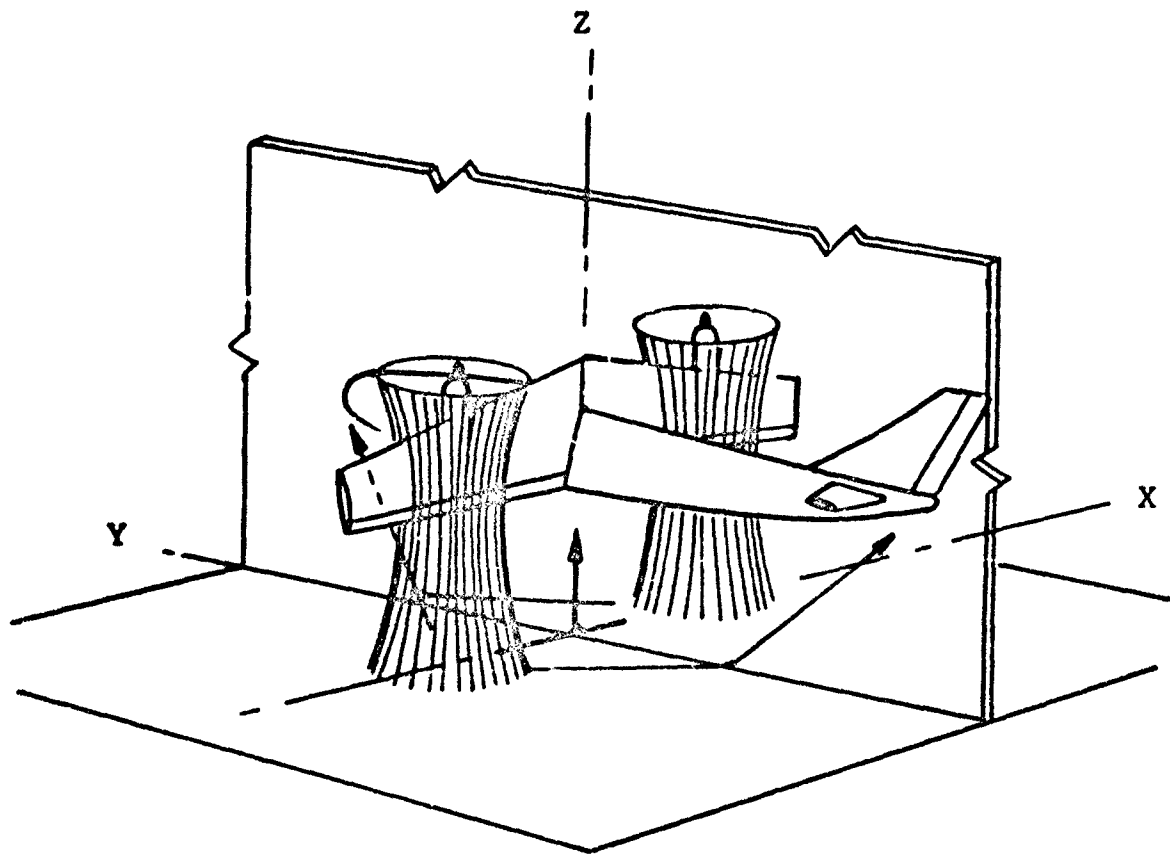
FIGURE 7:   SCHEMATIC OF FLOW FIELD FOR DUAL
PROPELLER VTOL AIRCRAFT

SYMBOL	LIFT DEVICE	REF.
O	4-Inch Air Nozzle	1
□	16-Inch Ducted Fan	1
— —	Decay in Free Air	1

Distance Ratio $\dfrac{z}{d_e}$ or $\left[\dfrac{h_e}{d_e} + \left(\dfrac{x_g}{d_e} \right) q_F \right]$

$\dfrac{q_N}{q_F}$ or $\dfrac{q_N}{q_z}$, or
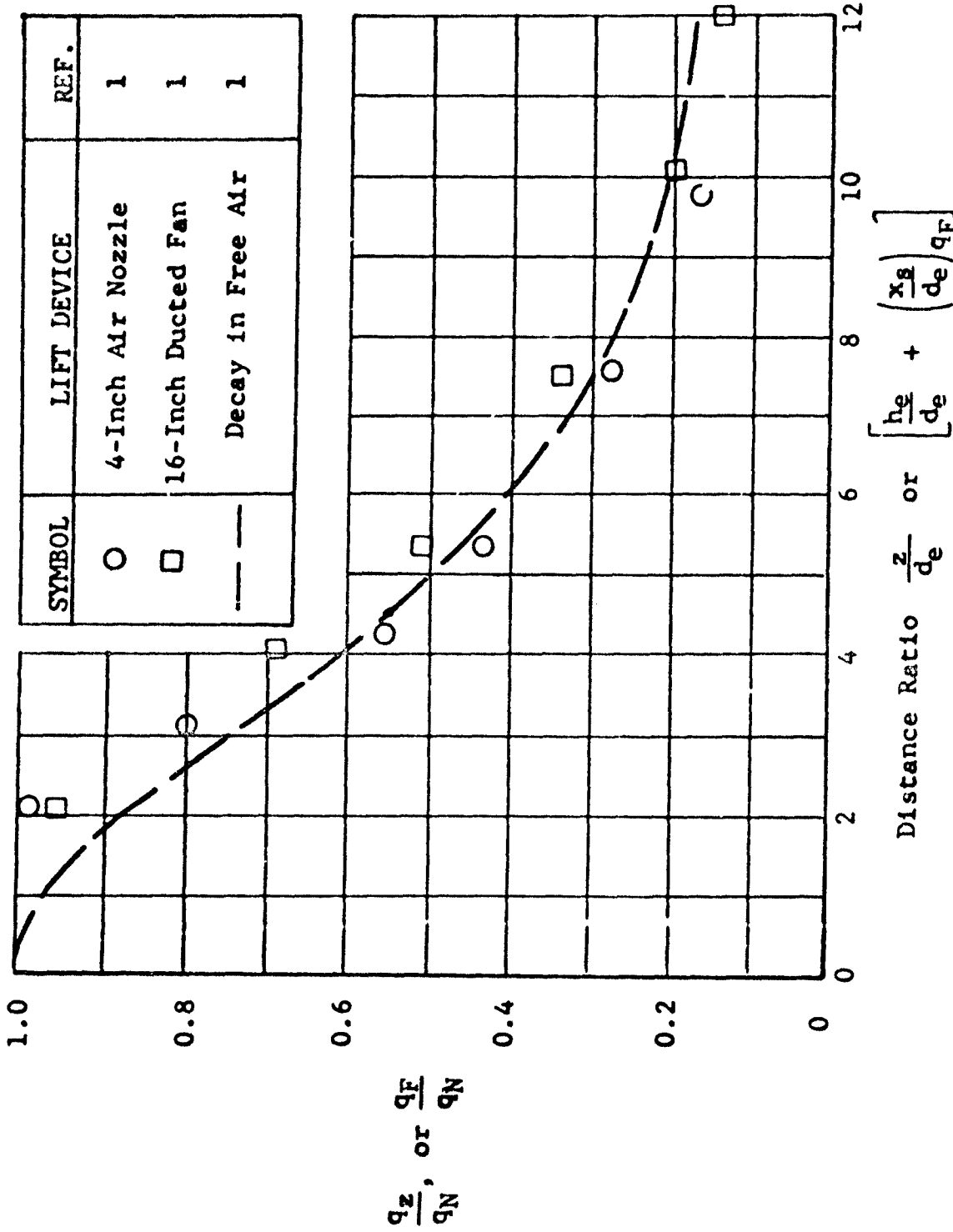
FIGURE 8: MAXIMUM DYNAMIC PRESSURE NEAR THE SURFACE AS A FUNCTION OF NOZZLE HEIGHT COMPARED WITH A JET EXPANDING IN FREE AIR

59

SYMBOL	h_e/d_e	NOTATION	REF.
△	2	Experiment	1
○	1	Experiment	1
—·—·—	2		
— — —	1	Theory	7
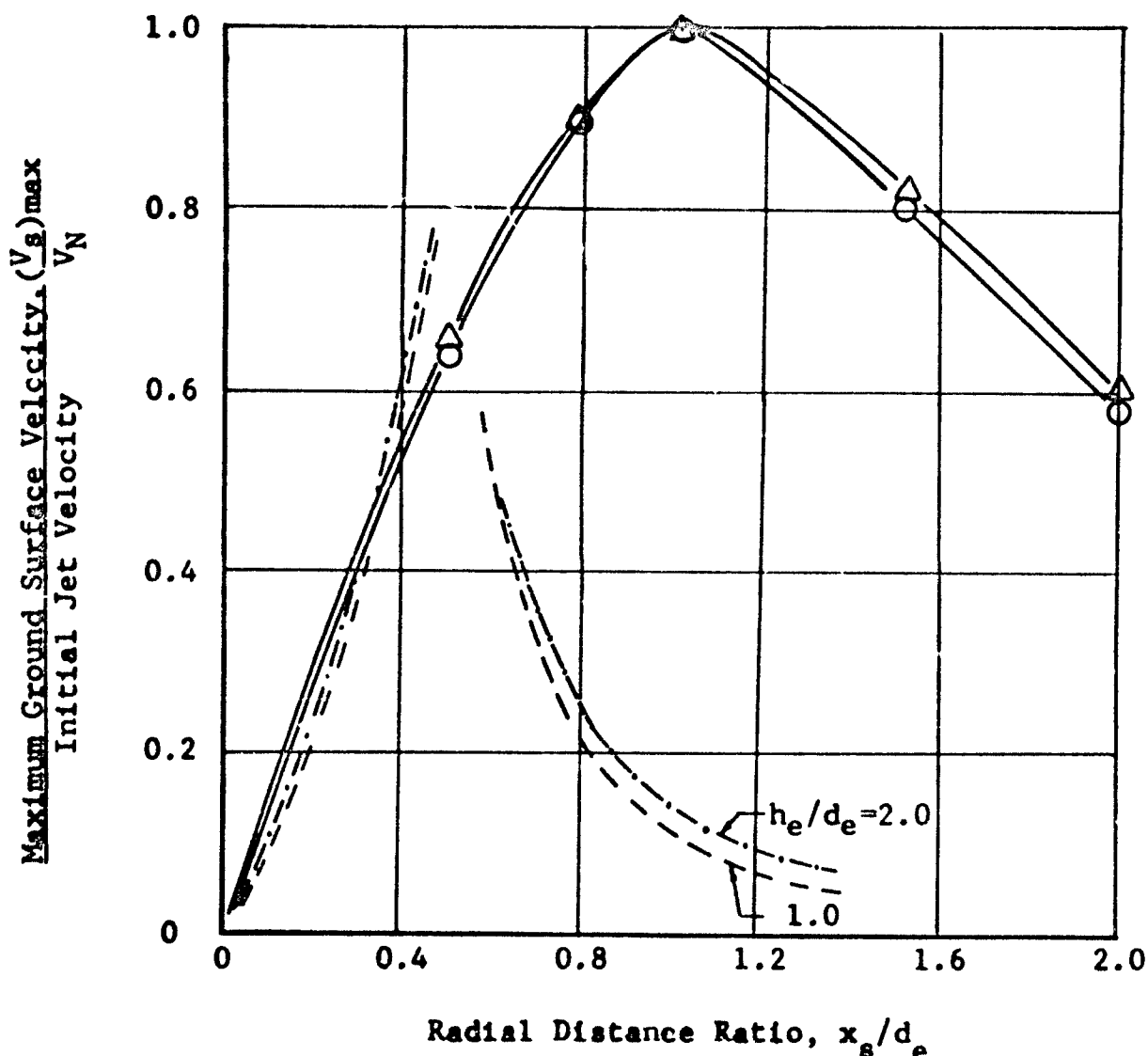
FIGURE 9: COMPARISON OF THEORETICAL AND EXPERIMENTAL
INVISCID GROUND VELOCITY DISTRIBUTIONS FOR
IMPINGING JETS
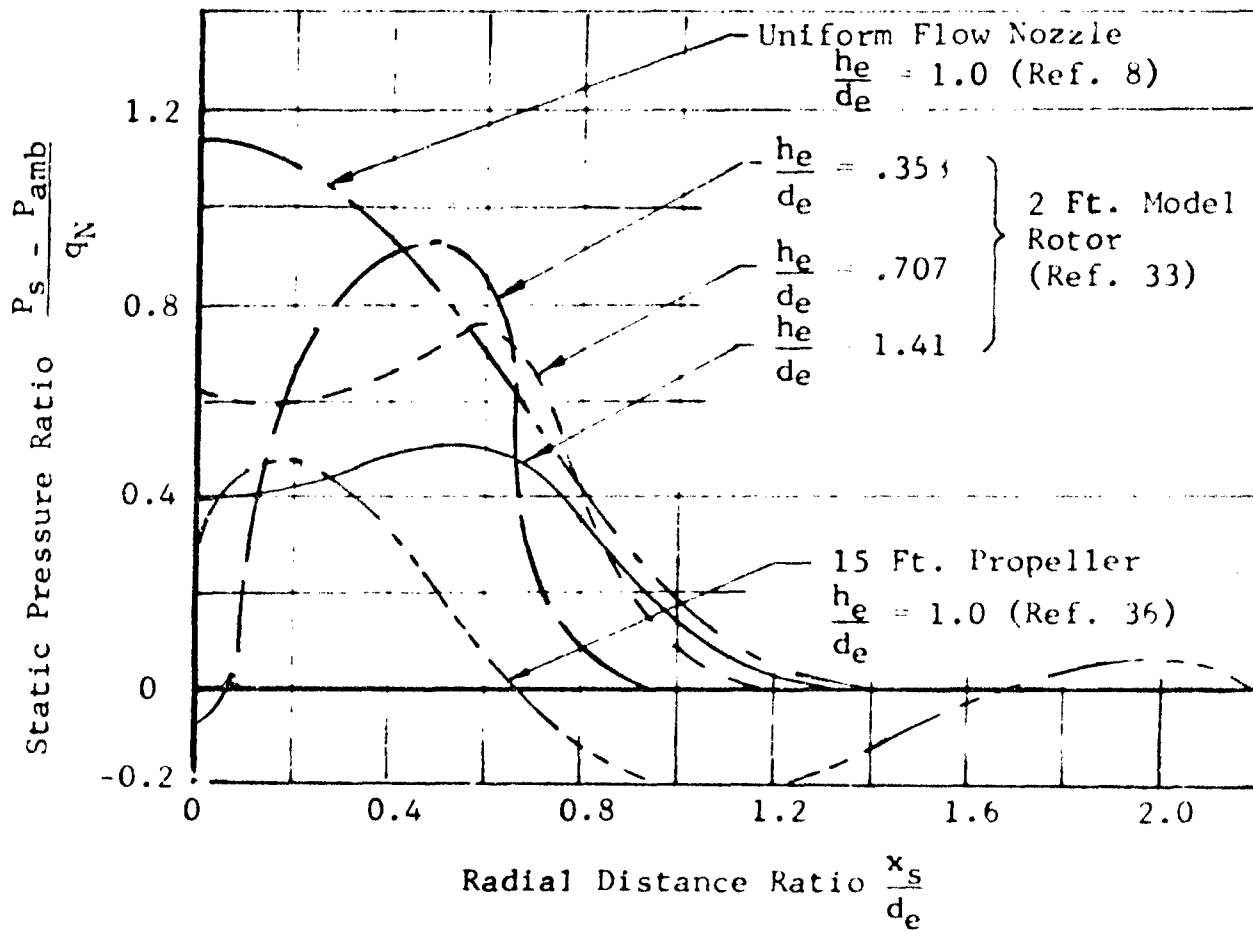
FIGURE 10: STATIC PRESSURES ON GROUND PLANE DUE TO IMPINGING JETS

61

SYMBOL	q_N
⊙	4
△	7.5
⊡	15
◇	30
◺	50

$$\frac{h_e}{d_e} = 3.0$$

Undisturbed
Water Level

Water Level, h_w

Radial Distance Ratio, $\frac{x_s}{d_e}$
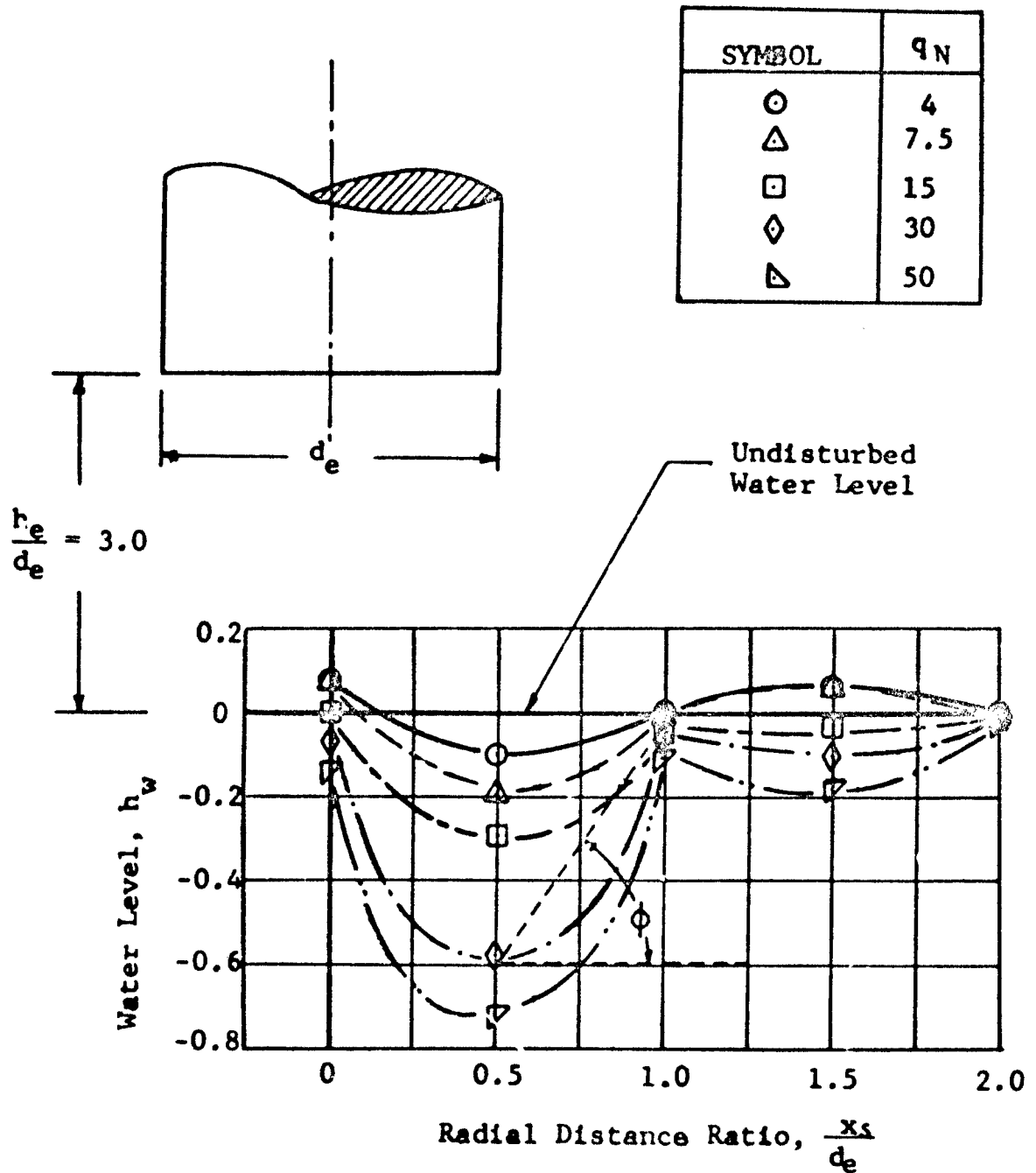
FIGURE 11: WATER SURFACE DEFLECTION FOR VARIOUS DYNAMIC
PRESSURES AS A FUNCTION OF RADIAL DISTANCE
(Reference 9)
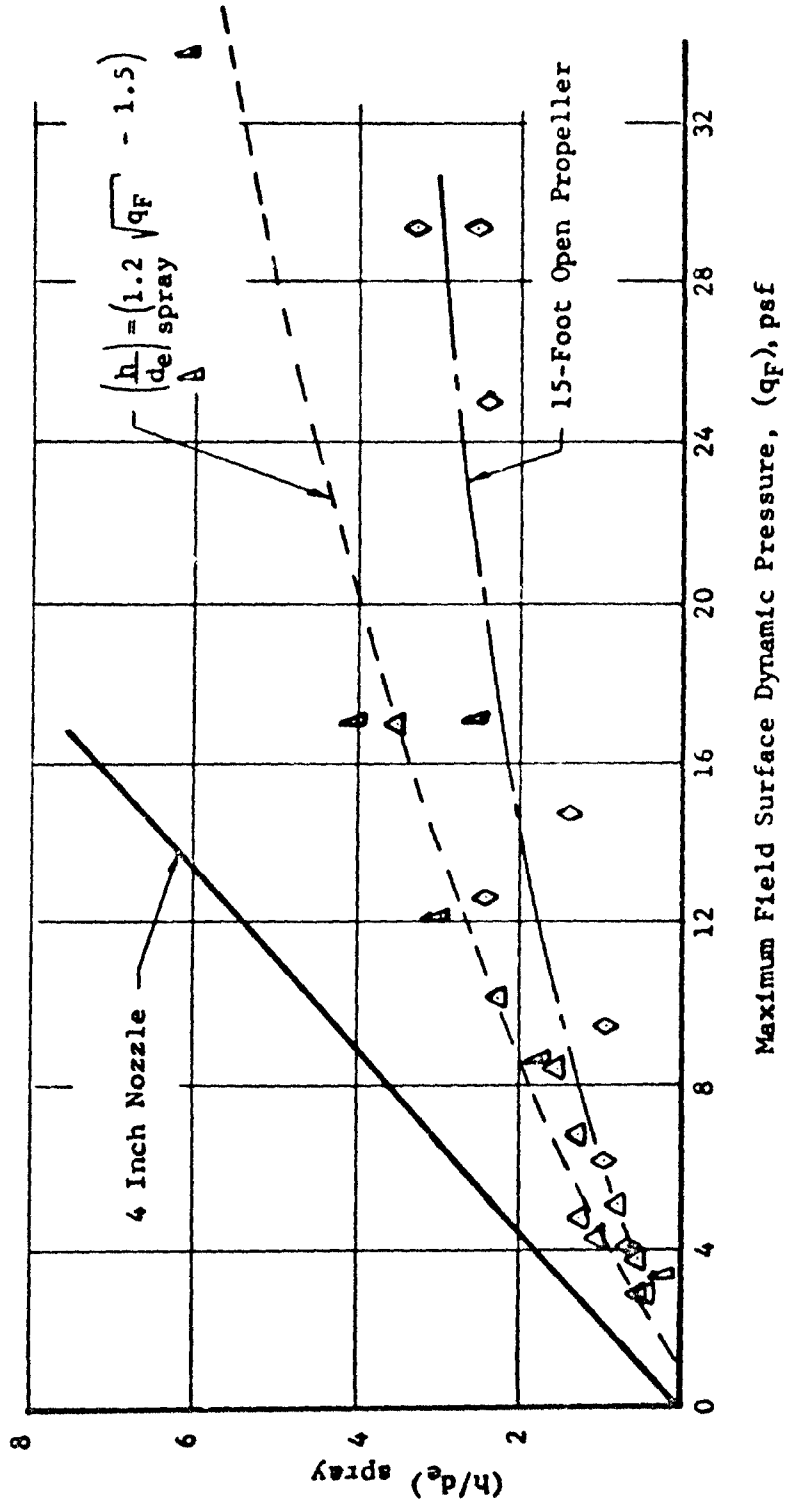
FIGURE 12:   HEIGHT AT WHICH WATER SPRAY WAS OBSERVED FOR VARIOUS DYNAMIC
PRESSURES

63
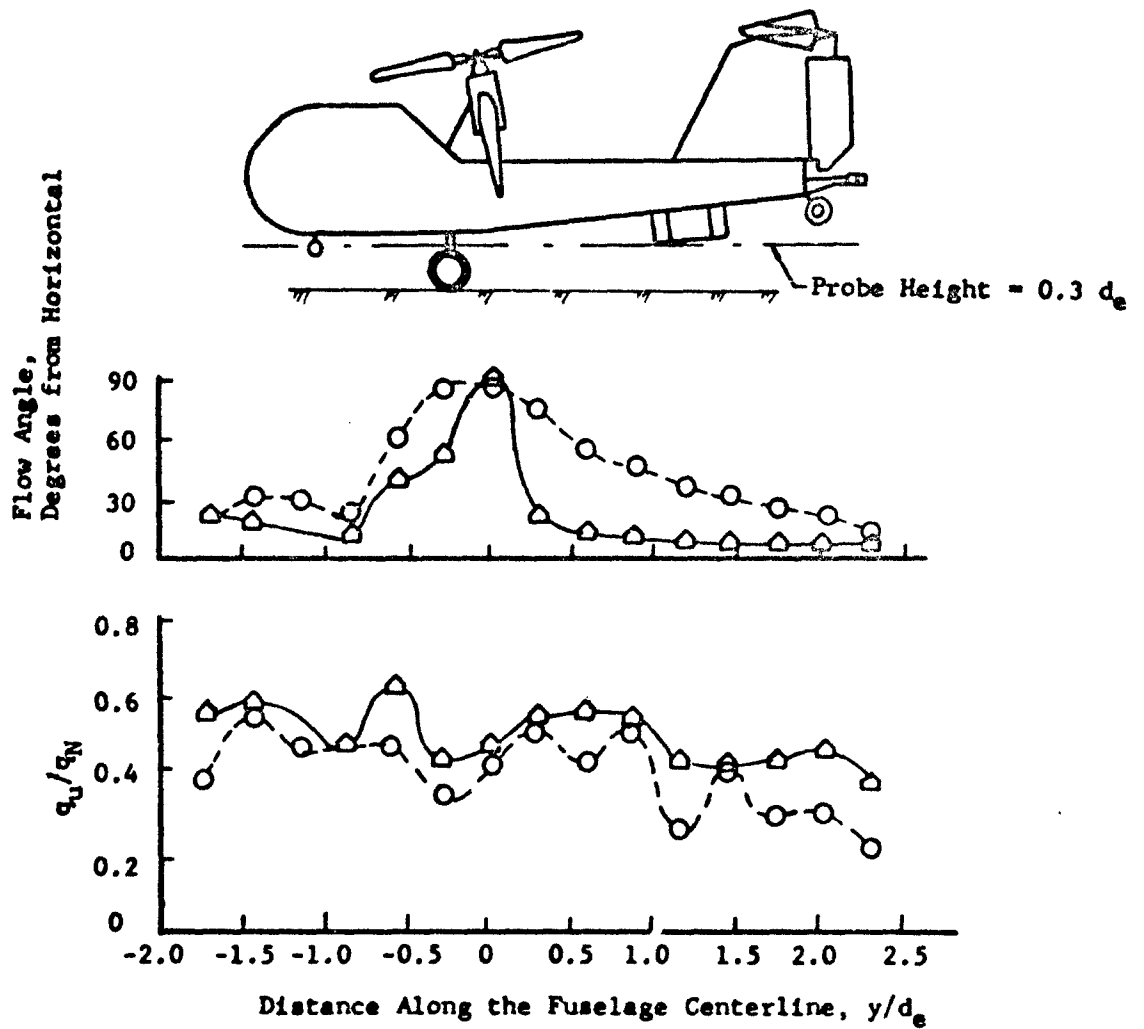
FIGURE 13: DYNAMIC PRESSURE AND ANGLE OF FLOW NEAR THE
BOTTOM OF THE FUSELAGE OF THE VZ-2 MODEL AT
THE PLANE OF SYMMETRY

64
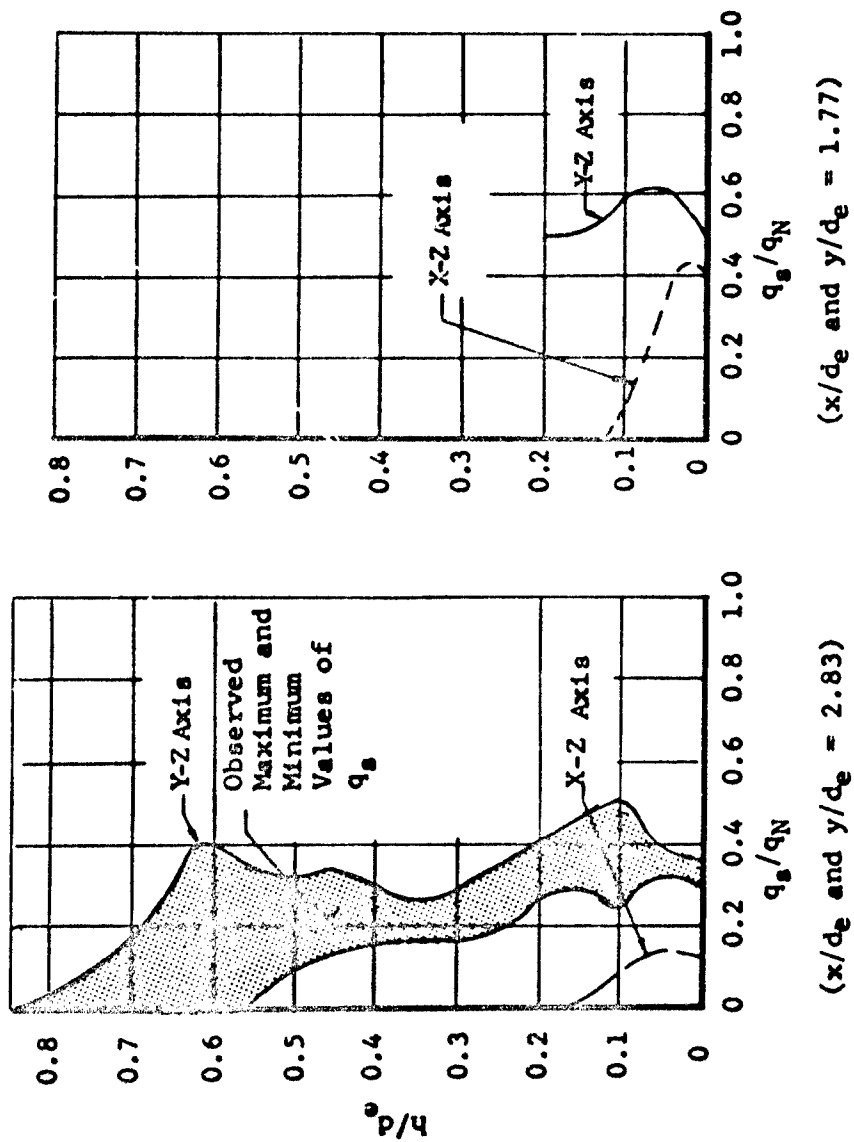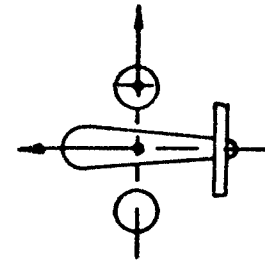
FIGURE 14: EFFECT OF MULTIPLE SLIPSTREAM INTERACTION ON THE GROUND DYNAMIC PRESSURE PROFILE (Reference 5)
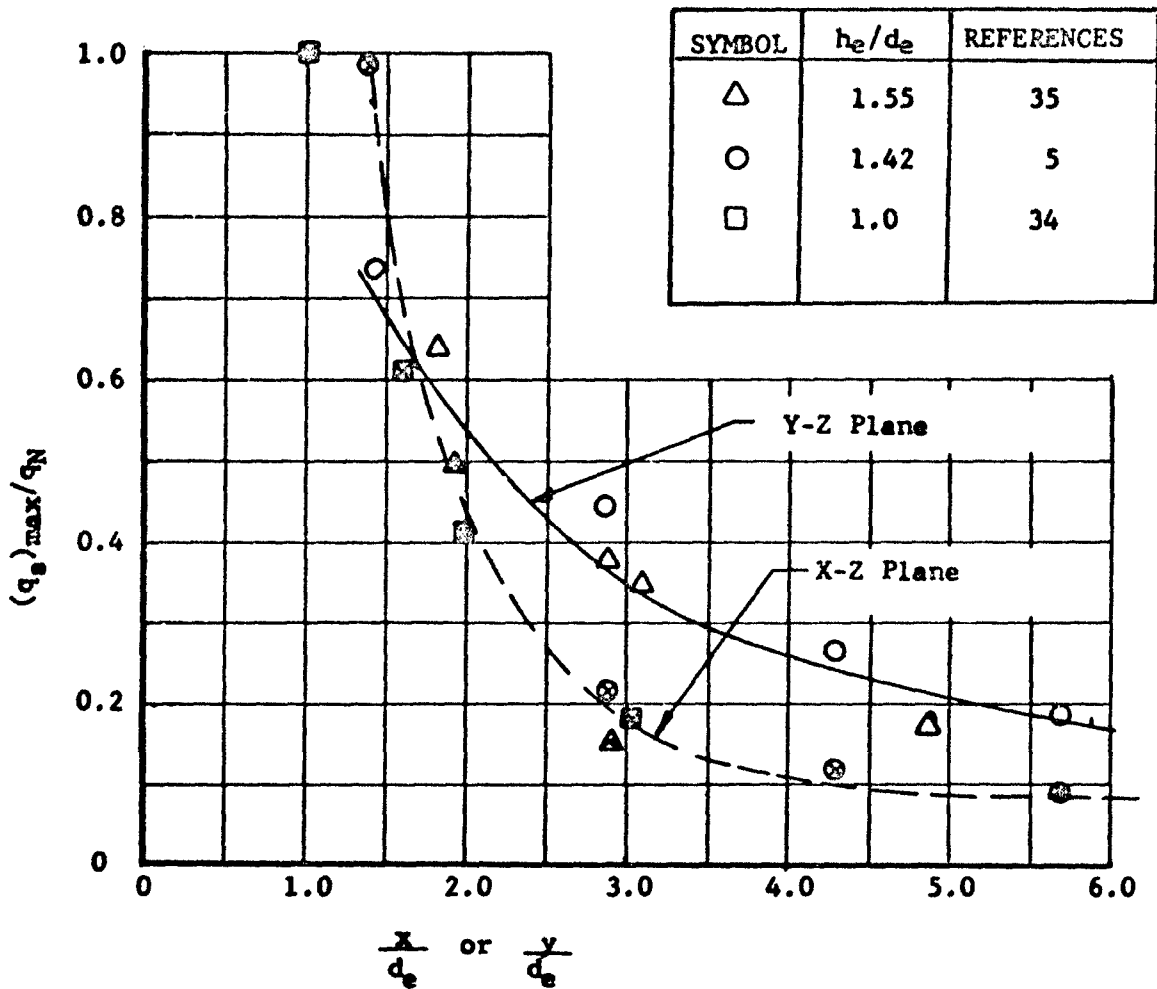
FIGURE 15: VARIATION OF MAXIMUM SURFACE DYNAMIC PRESSURE ALONG X-Z AND Y-Z PLANES FOR DUAL-LIFT-DEVICE CONFIGURATIONS
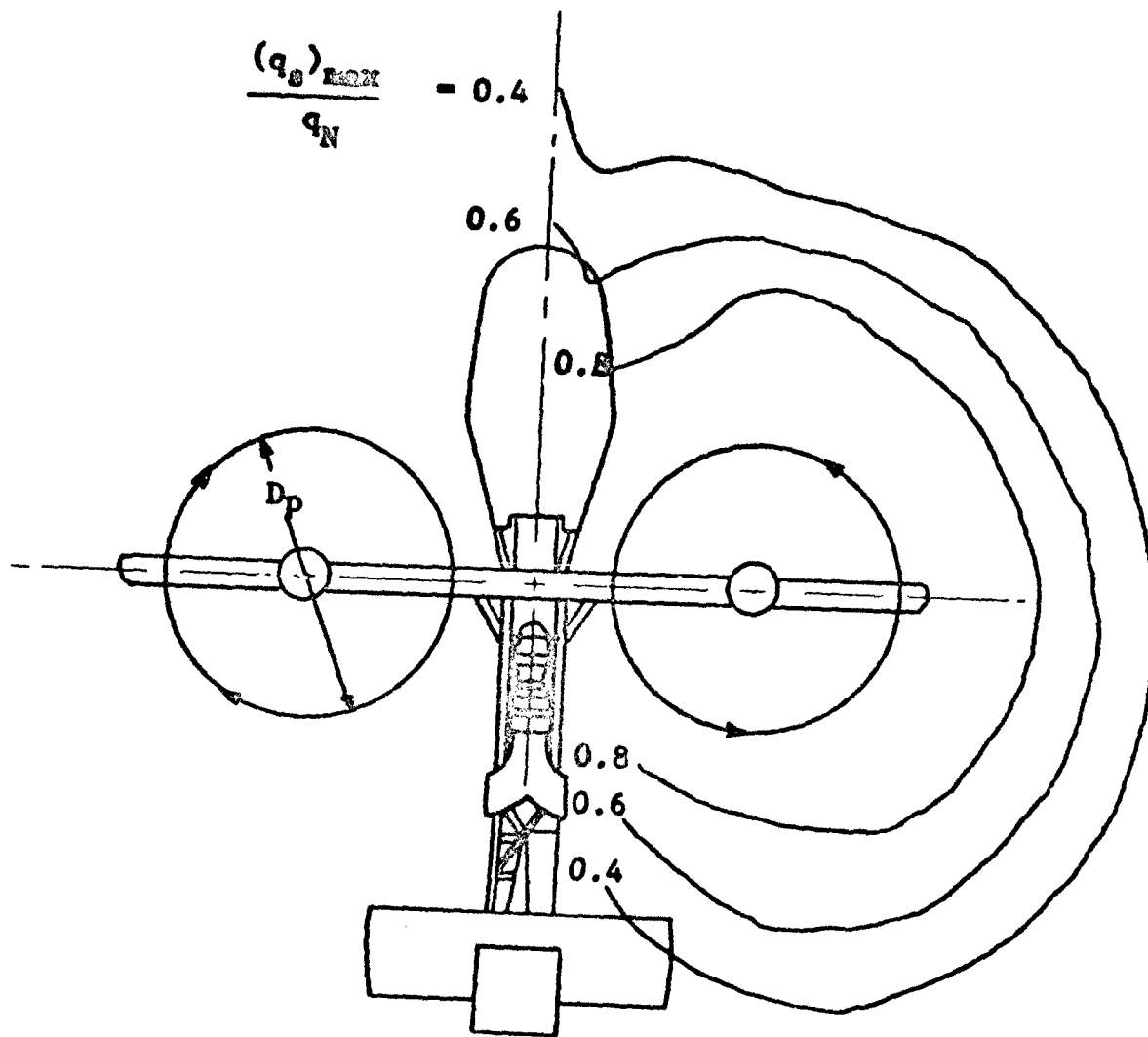
FIGURE 16: DYNAMIC PRESSURE CONTOURS OF VZ-2 MODEL, $\frac{h_e}{d_e} = 1.45$ (Reference 35)

67
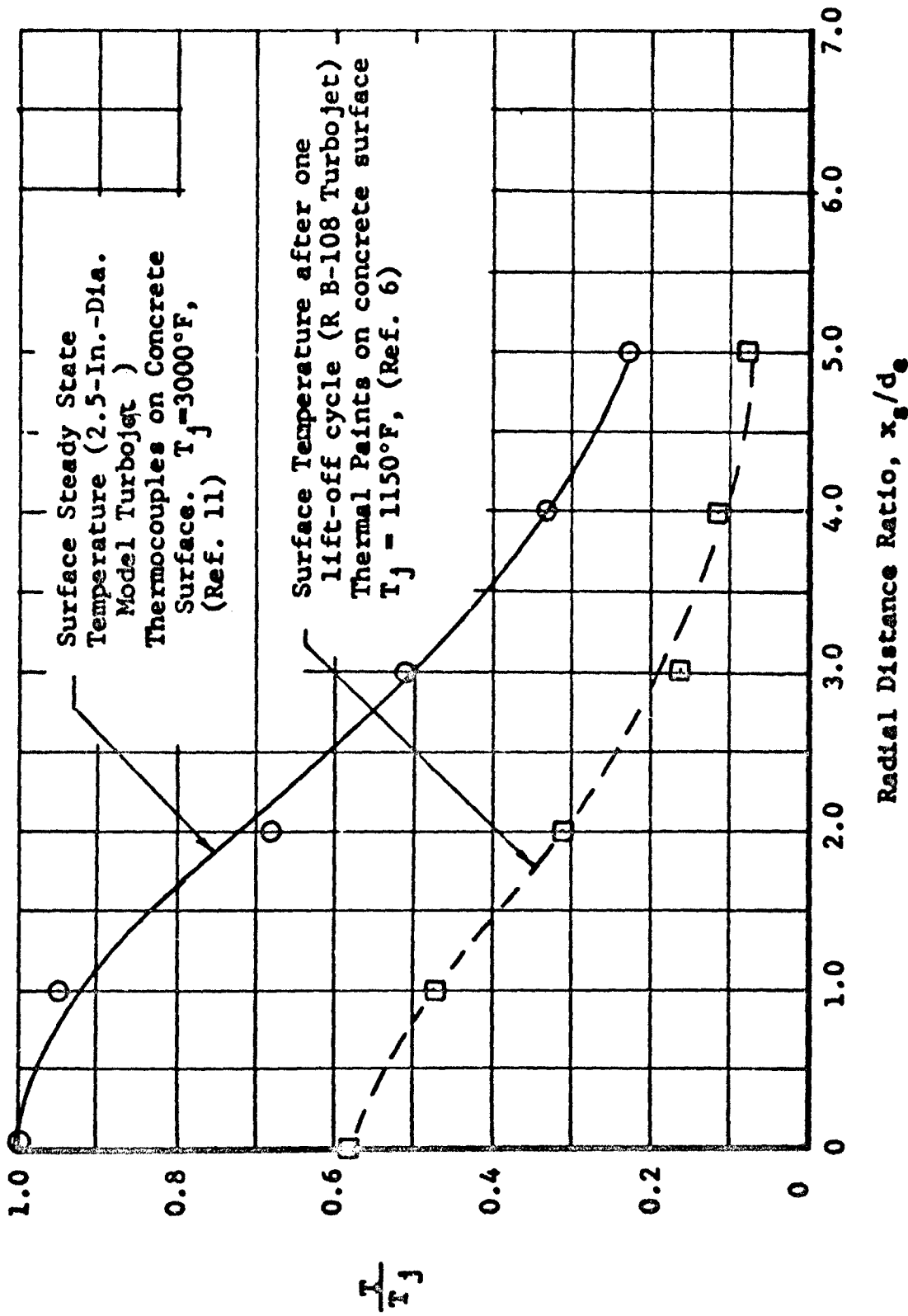
FIGURE 17: TEMPERATURE PROFILE VARIATION ALONG THE GROUND WITH RADIAL DISTANCE FROM CENTERLINE OF JET NOZZLE ($h_e/d_e = 3.0$)
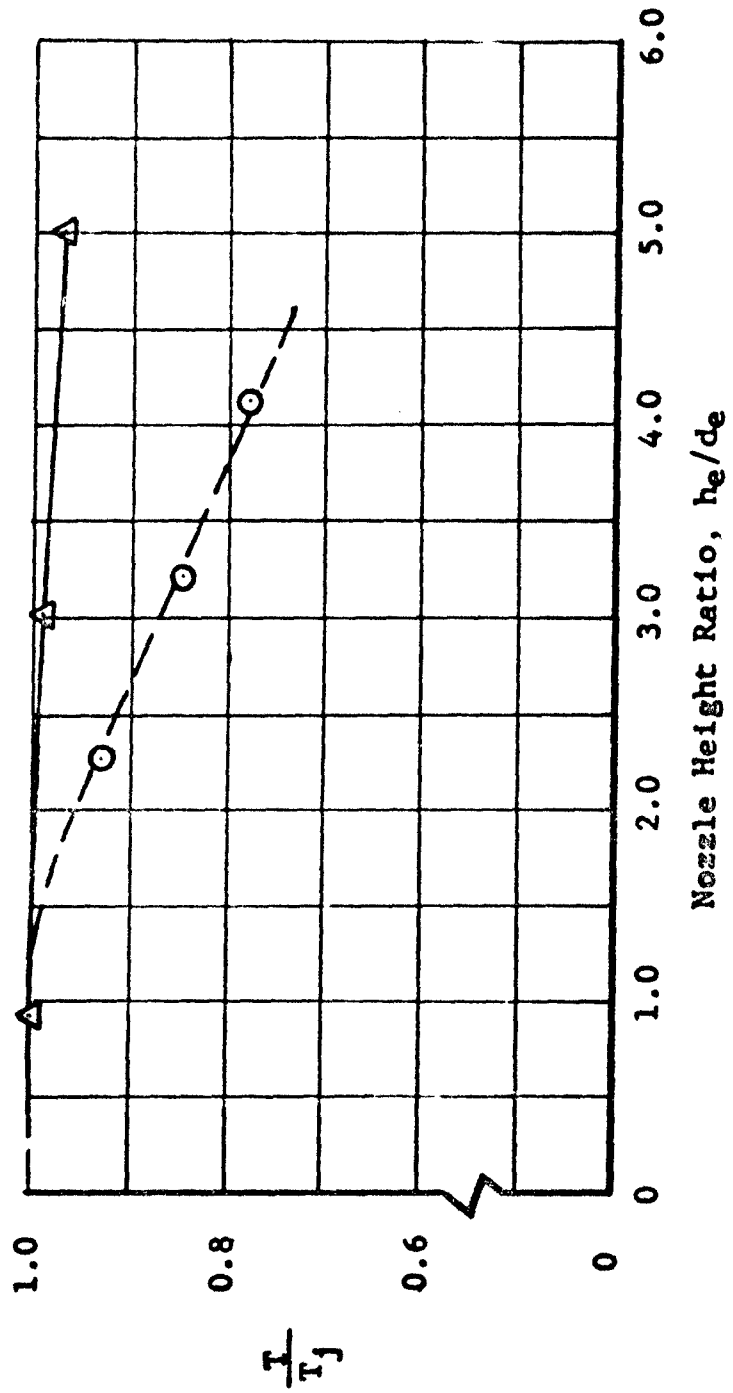
FIGURE 18: EFFECT OF NOZZLE HEIGHT ON MAXIMUM TEMPERATURE ON THE GROUND
SURFACE

69
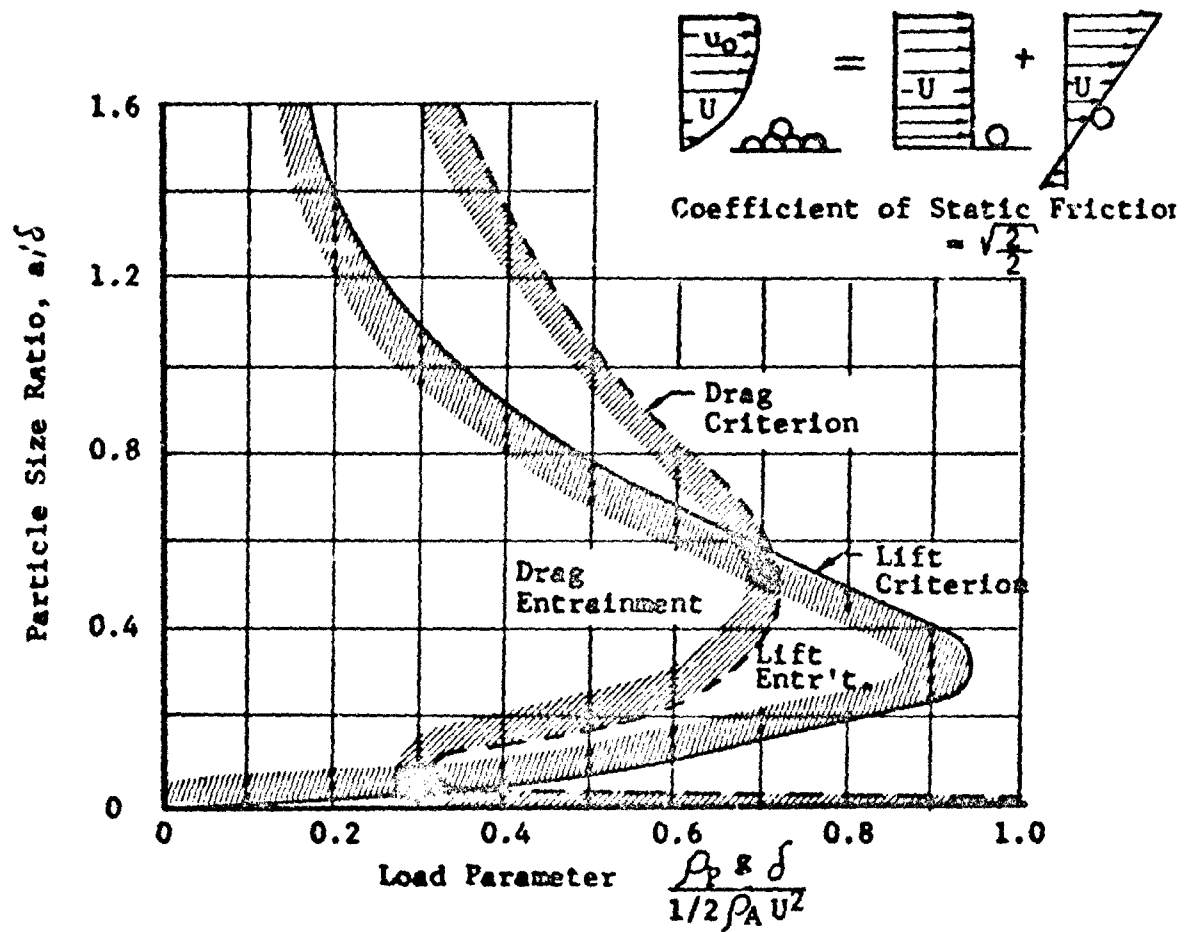
FIGURE 19: CRITERIA FOR PARTICLE ENTRAINMENT IN AXISYMMETRIC STAGNATION FLOW, FROM REFERENCE 7

70
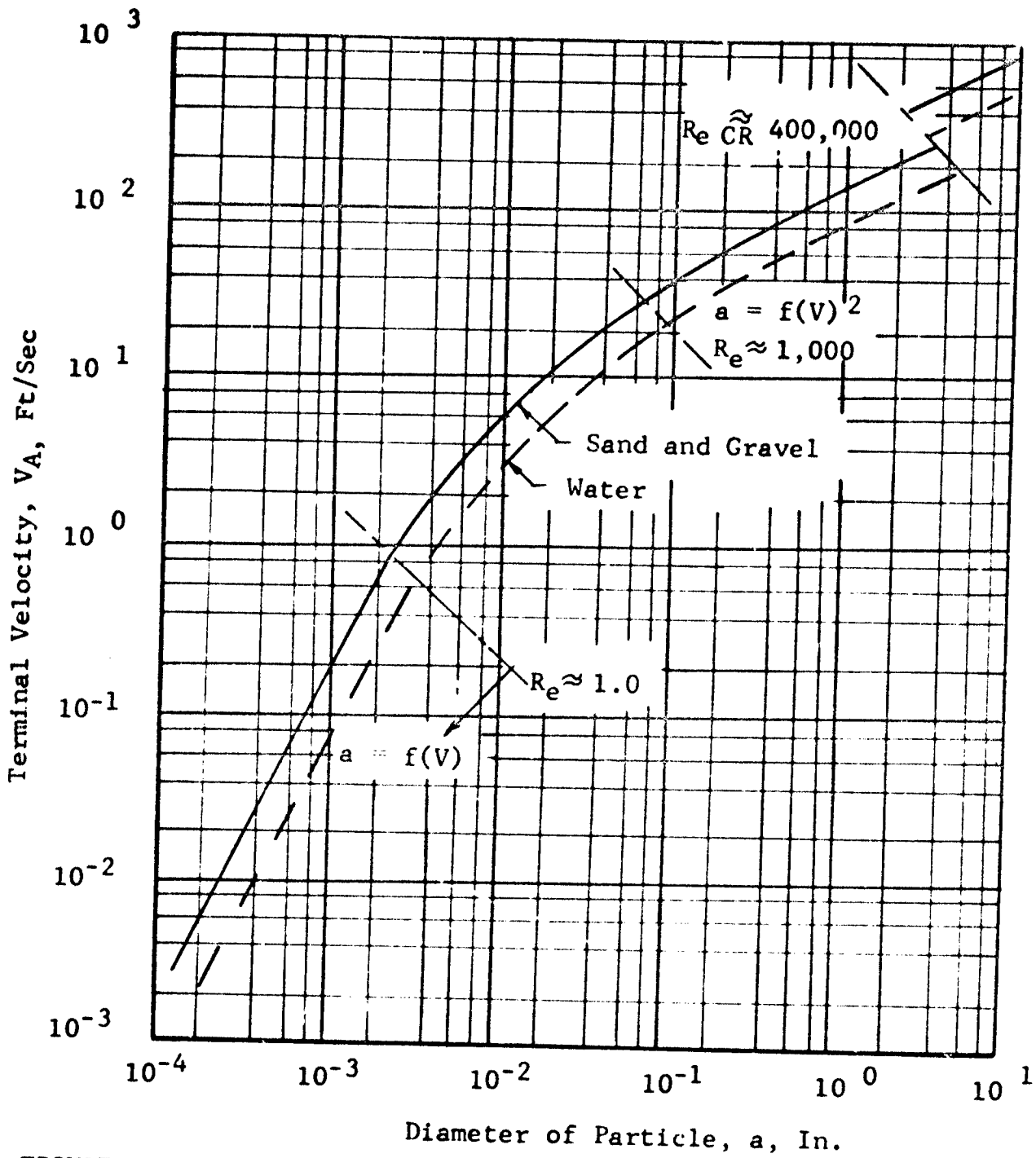
FIGURE 20: VARIATION OF TERMINAL VELOCITY OF PARTICLES WITH PARTICLE DIAMETER (Reference 1)

71

SYMBOL	x_s/d_e
⬡	3.0
◊	4.5
◯	6.0

$$V_\gamma = \sqrt{\frac{\text{Particle Weight}}{1/2\,\rho_A C_D \pi/4(a/12)^2}}$$
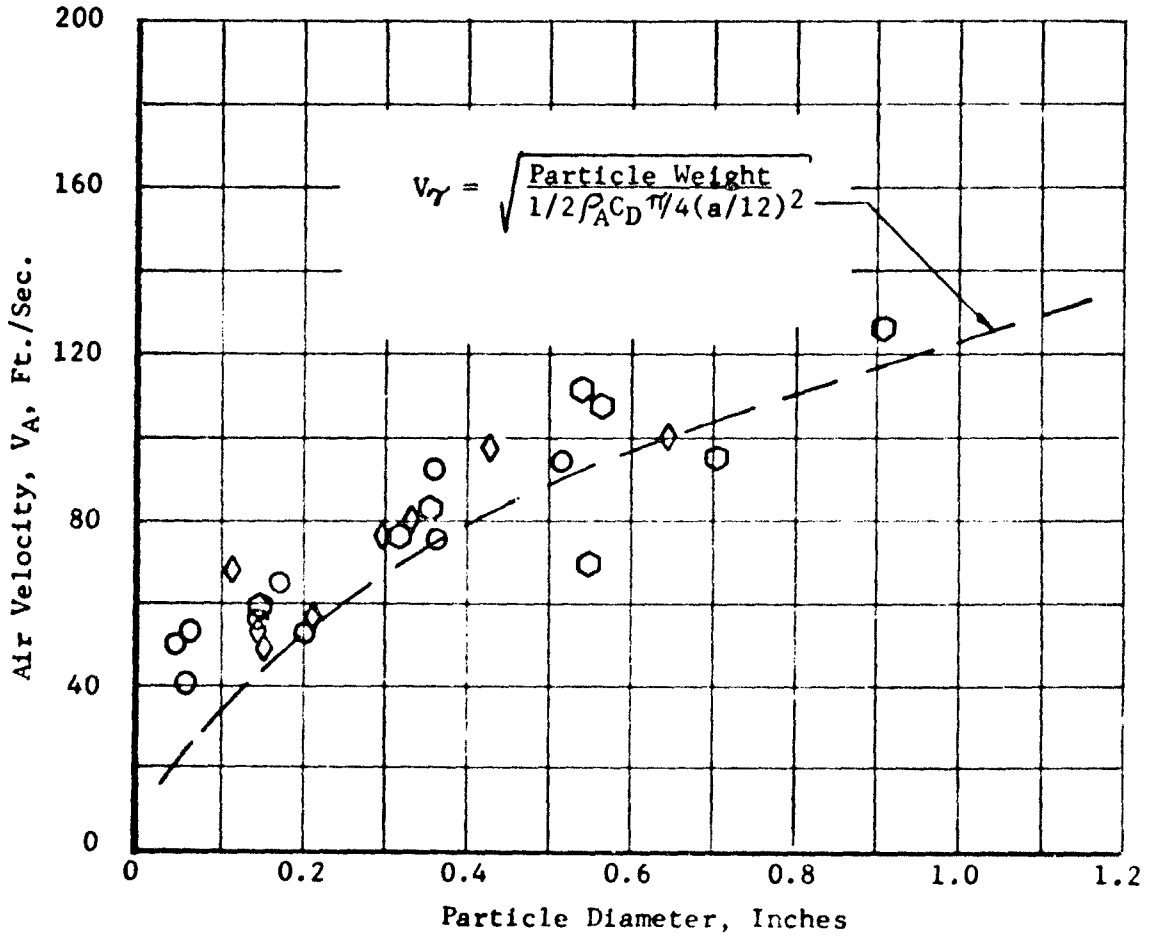
FIGURE 21: VARIATION OF PARTICLE SIZE WITH AIR VELOCITY BASED ON THE AVERAGE OF LOCAL AND MAXIMUM SURFACE VELOCITIES

72
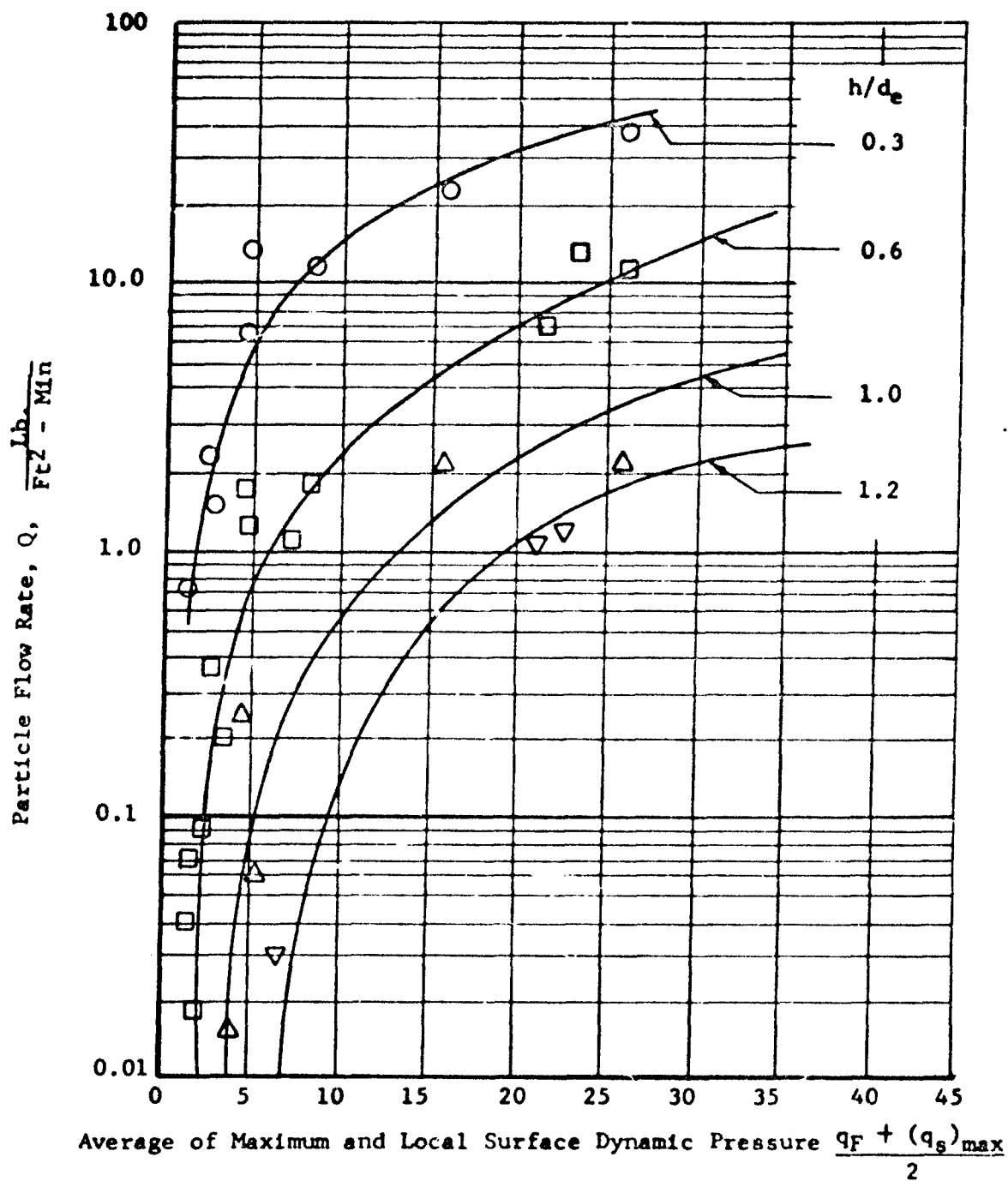
FIGURE 22:   VARIATION OF PARTICLE FLOW RATE AVERAGE
SURFACE DYNAMIC PRESSURE AS A FUNCTION OF
PARTICLE TRAP HEIGHT (Reference 9)

73
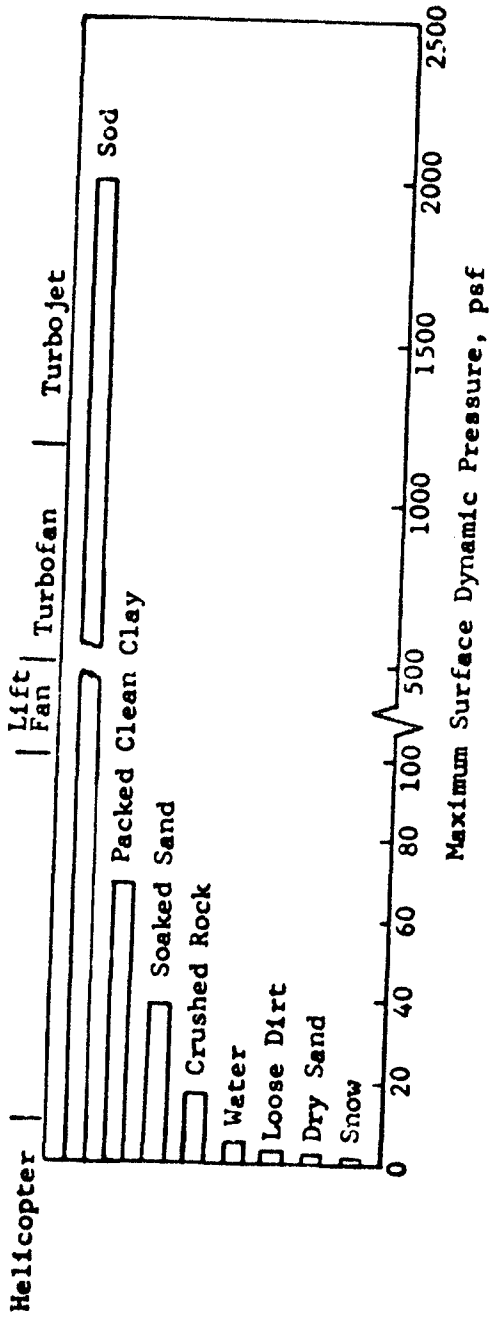
a. Incipient Erosion
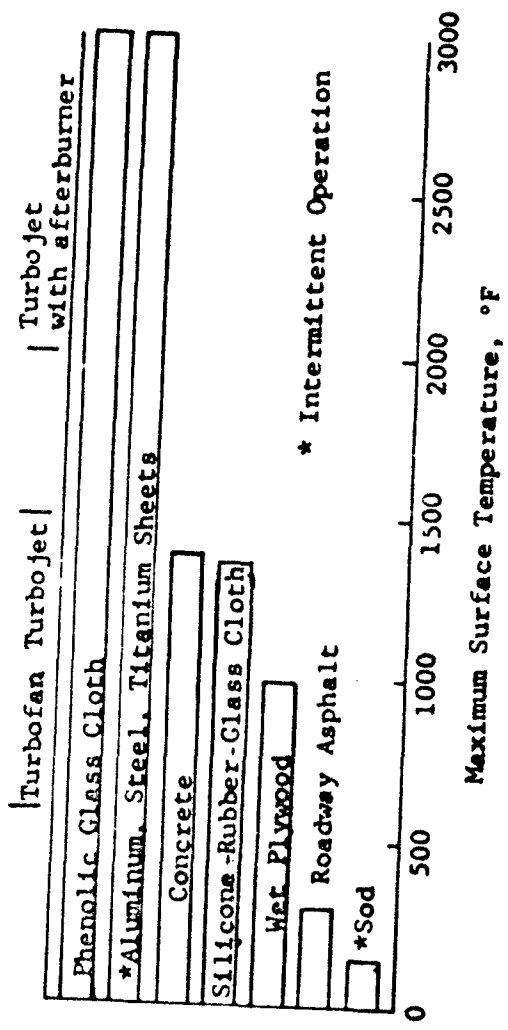
b. Temperature Limitations

FIGURE 23: DOWNWASH TERRAIN LIMITATIONS

74

$$(k_t)_W = \frac{\rho_P \, g \, a}{62.4 \times 0.10}$$
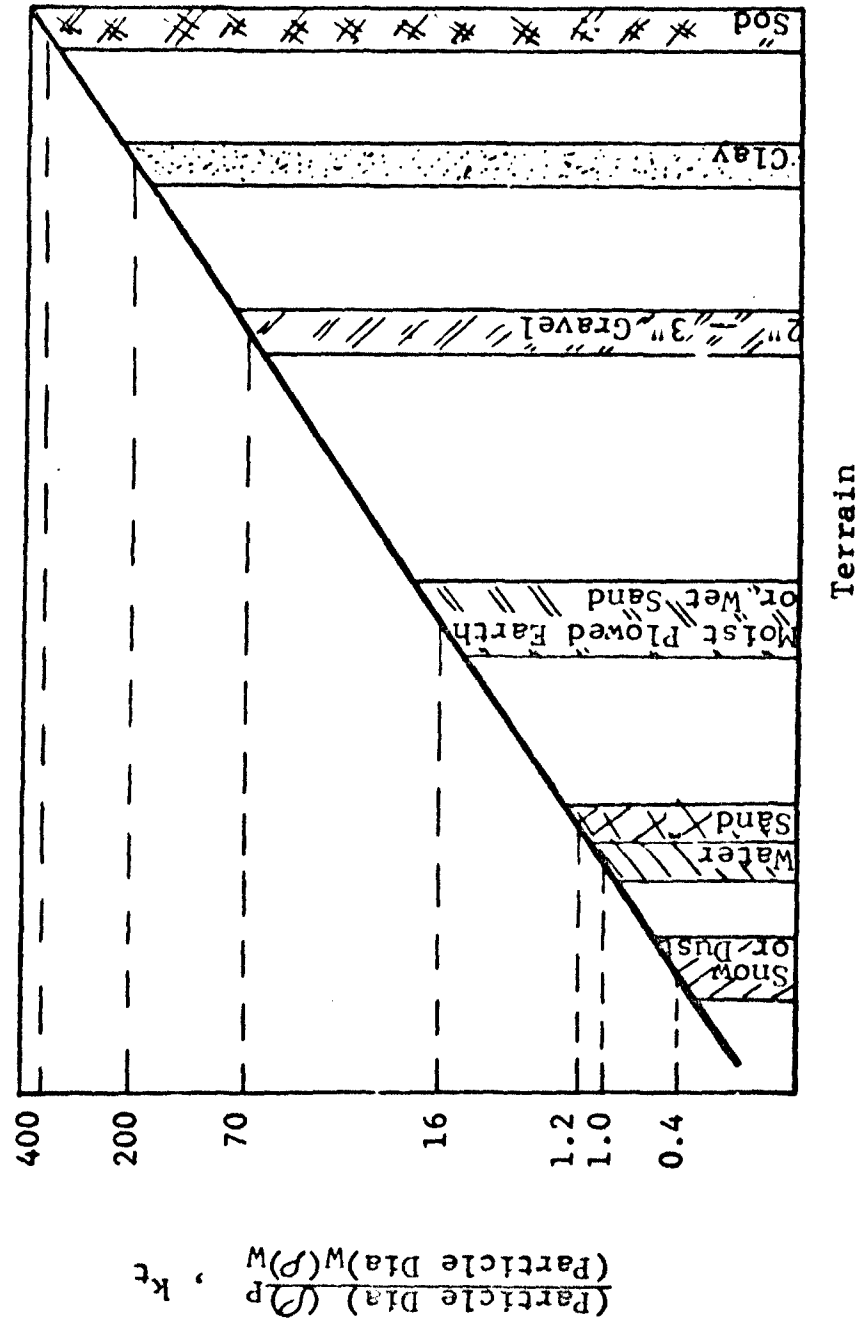
FIGURE 24: TERRAIN CHARACTERISTICS

75
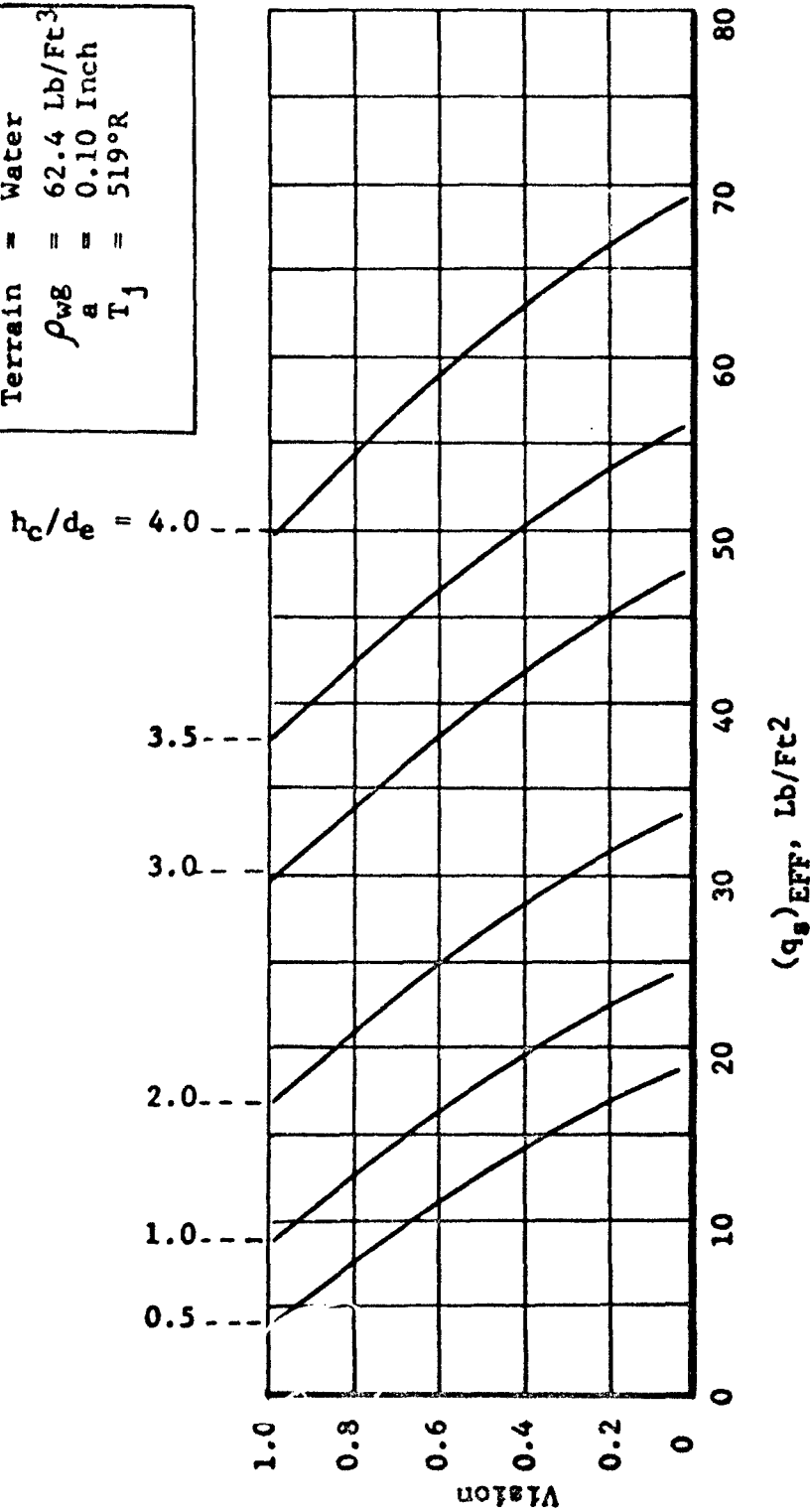
FIGURE 25: VISIBILITY AS A FUNCTION OF $(q_s)_{EFF}$ AND CLOUD HEIGHT
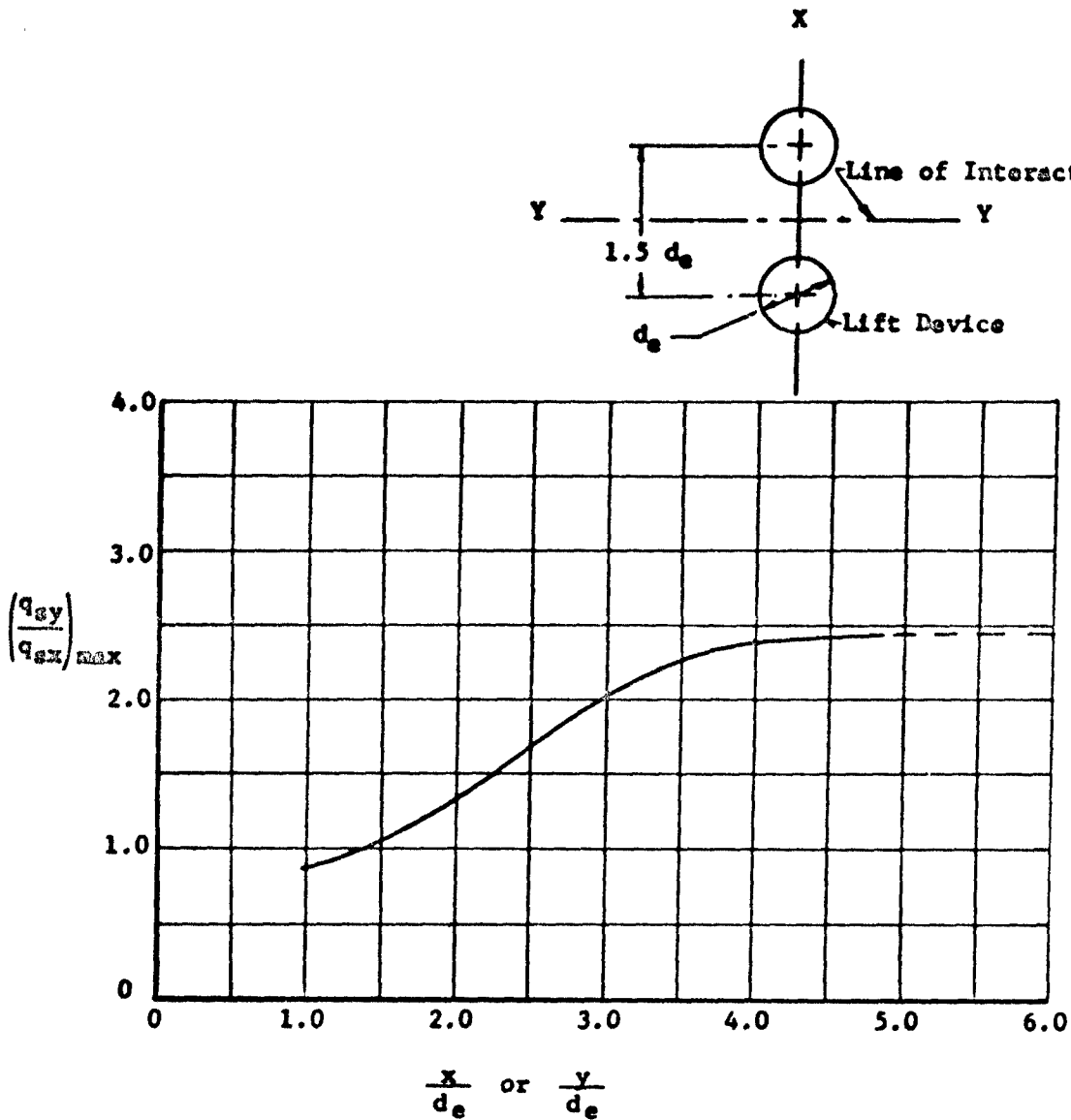
FIGURE 26:   INCREASE IN MAXIMUM SURFACE DYNAMIC PRESSURE
ALONG THE LINE OF INTERACTION BETWEEN TWO
LIFT DEVICES

77

MATERIAL	A_T(ft/sec)	MATERIAL	A_T(ft/sec)
Lead	3,900	181 Epoxy Resin	14,700
Ash	4,600	Aluminum	16,400
Lucite	5,800	Steel	17,000
Copper	12,500		
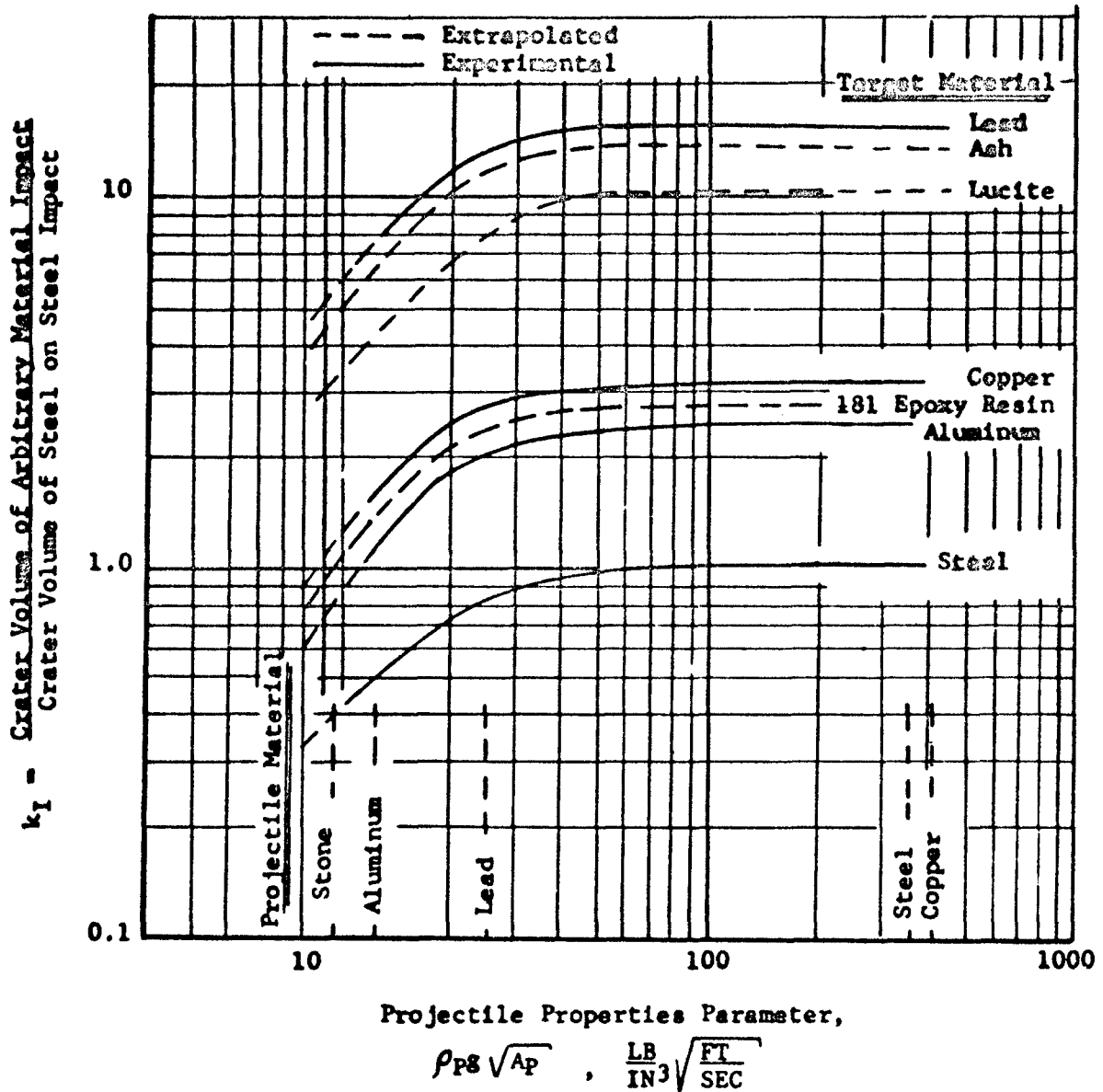
FIGURE 27: IMPACT FACTOR AS A FUNCTION OF PROJECTILE
MATERIAL, DENSITY, ACOUSTIC VELOCITY, AND
TARGET ACOUSTIC VELOCITY

SYMBOL	NOTATION
△	Test Data-0.093" Dia. Steel Ball

$$P/a = 2.28 \left(\frac{\rho_P}{\rho_T}\right)^{2/3} \left(\frac{V_P}{A_T}\right)^{2/3}$$

$$E = TA_I \left[\frac{Y}{2} + \frac{\rho_T}{4} \left(\frac{\pi}{2} V_P\right)^2\right]$$

Minimum Projectile Kinetic Energy, Ft.-Lb.
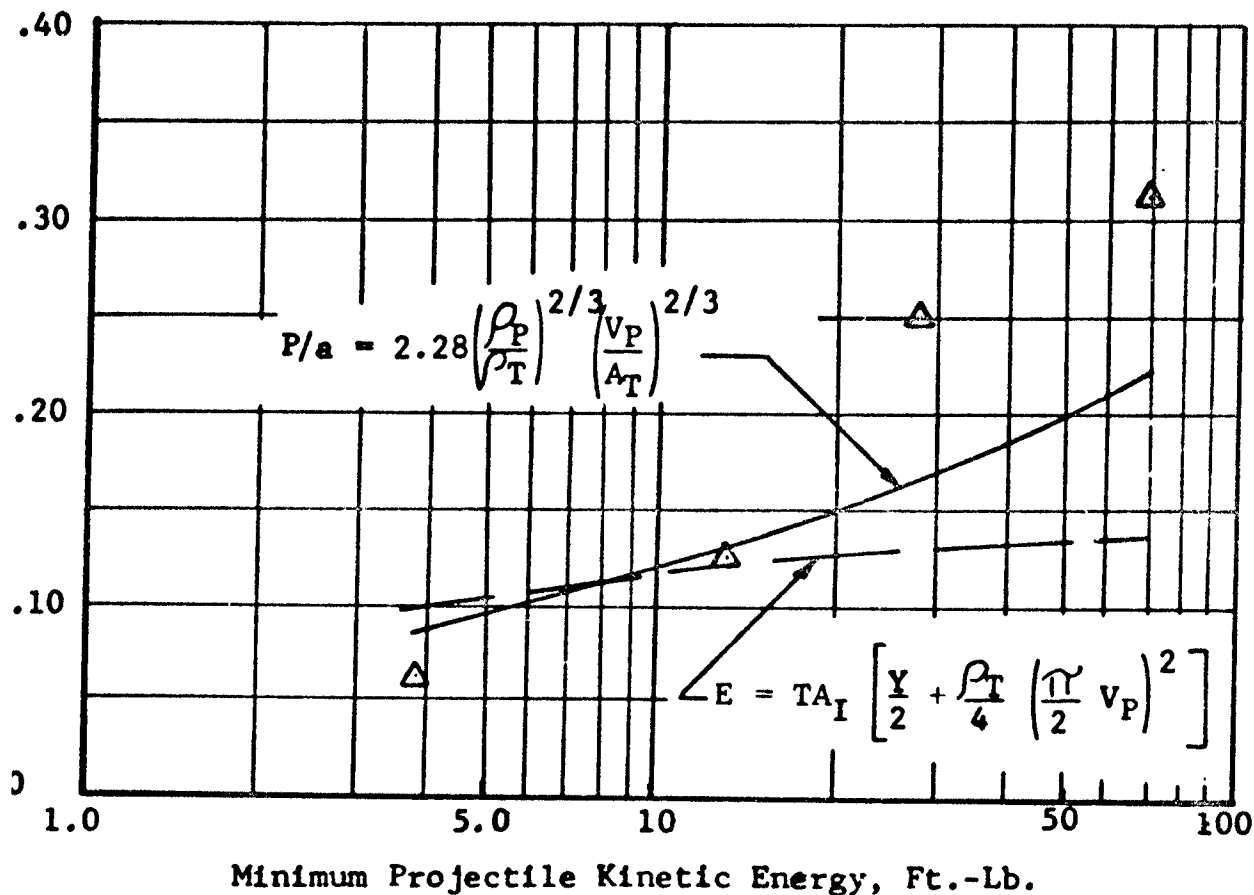
FIGURE 28: COMPARISON OF THEORETICAL AND EMPIRICAL PREDICTION METHODS WITH EXPERIMENTAL DATA FOR THE MINIMUM PROJECTILE KINETIC ENERGY REQUIRED FOR PERFORATION OF ALUMINUM TARGETS

79

$$\beta = \frac{3 d_e c_D \rho_A A_F}{m_p}$$

$$\frac{V_P}{\sqrt{q_F / \rho_A}} = 1 - \frac{1}{\sqrt{\beta} + 1}$$

Particle Velocity Ratio, $\dfrac{V_p}{\sqrt{q_F / \rho_A}}$
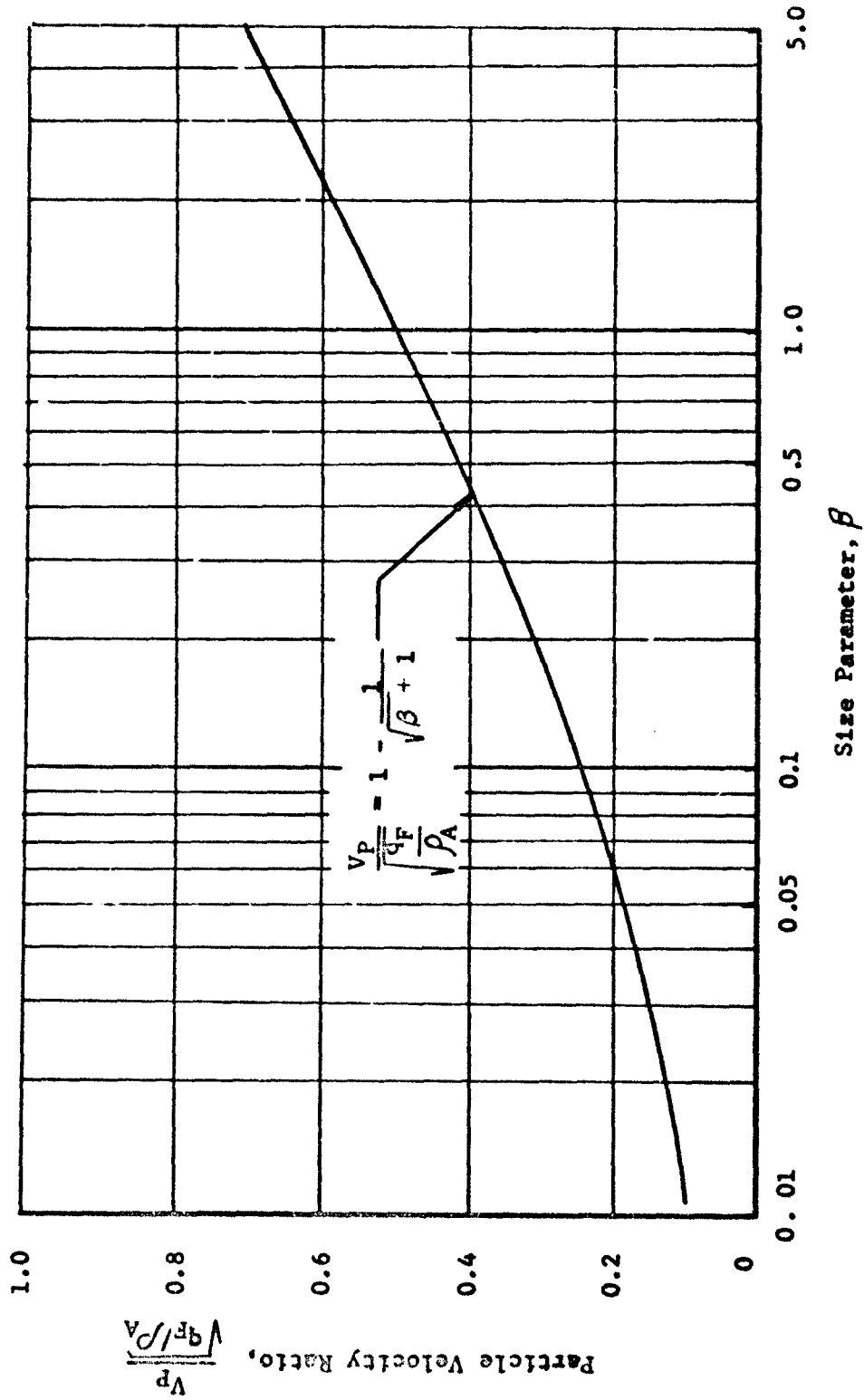
Size Parameter, β

FIGURE 29: ENTRAINED PARTICLE VELOCITY RATIO AS A FUNCTION OF SIZE PARAMETER, β
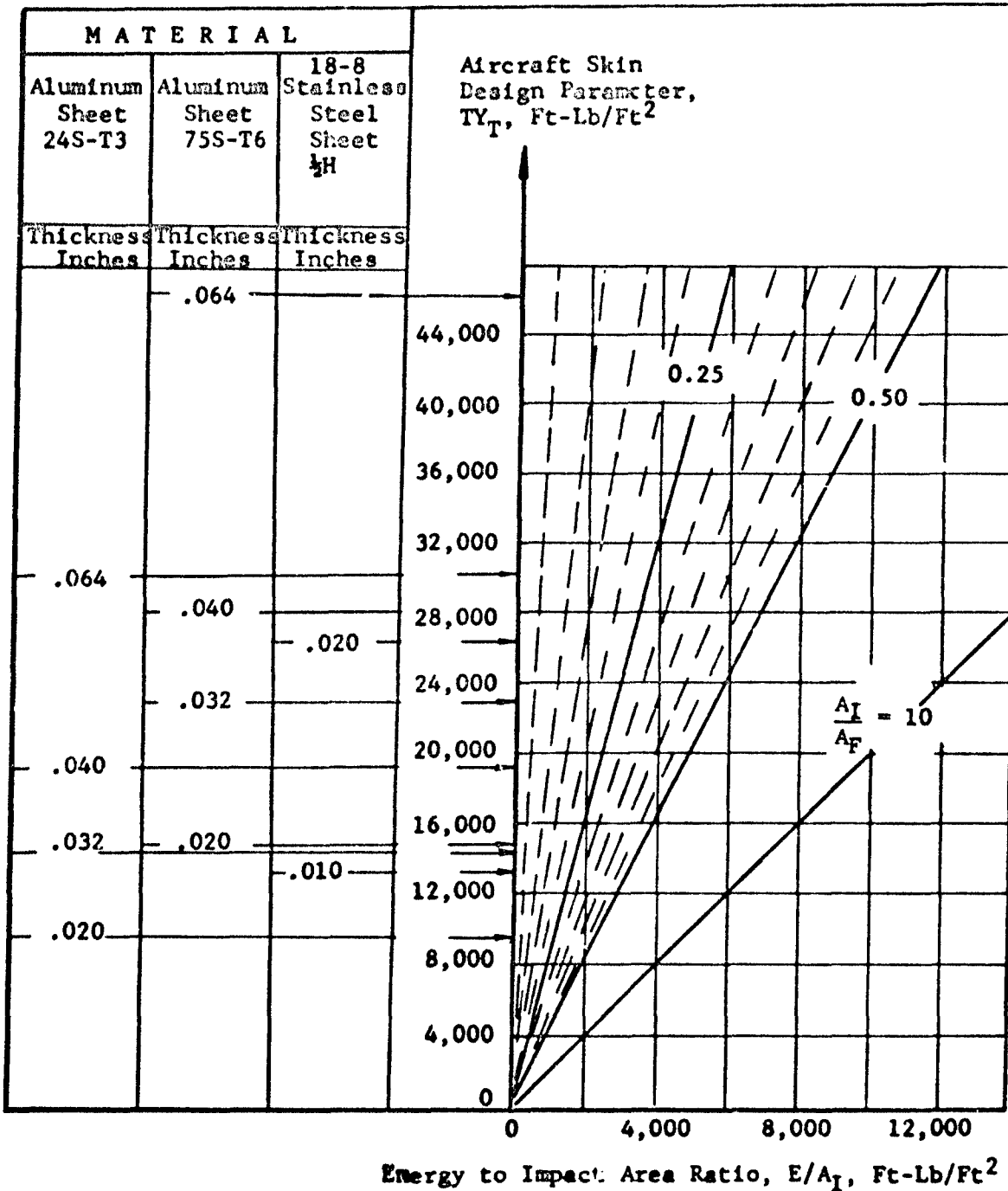
FIGURE 30: MINIMUM PARTICLE ENERGY REQUIRED FOR
PENETRATION THROUGH AIRCRAFT SKIN

81
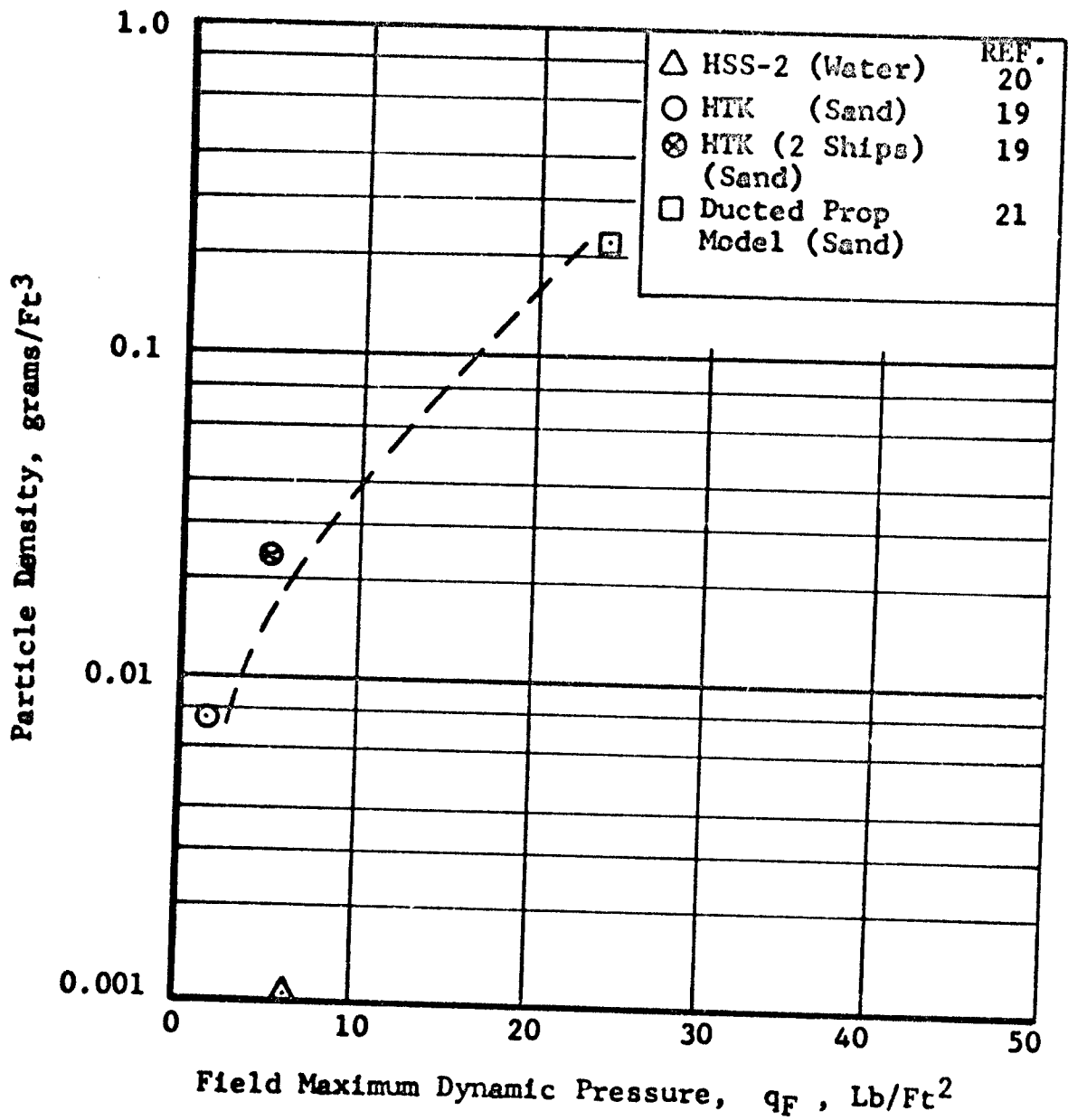
FIGURE 31: ENTRAINED PARTICLE DENSITY IN AIR AS A
FUNCTION OF MAXIMUM FIELD DYNAMIC PRESSURE

82
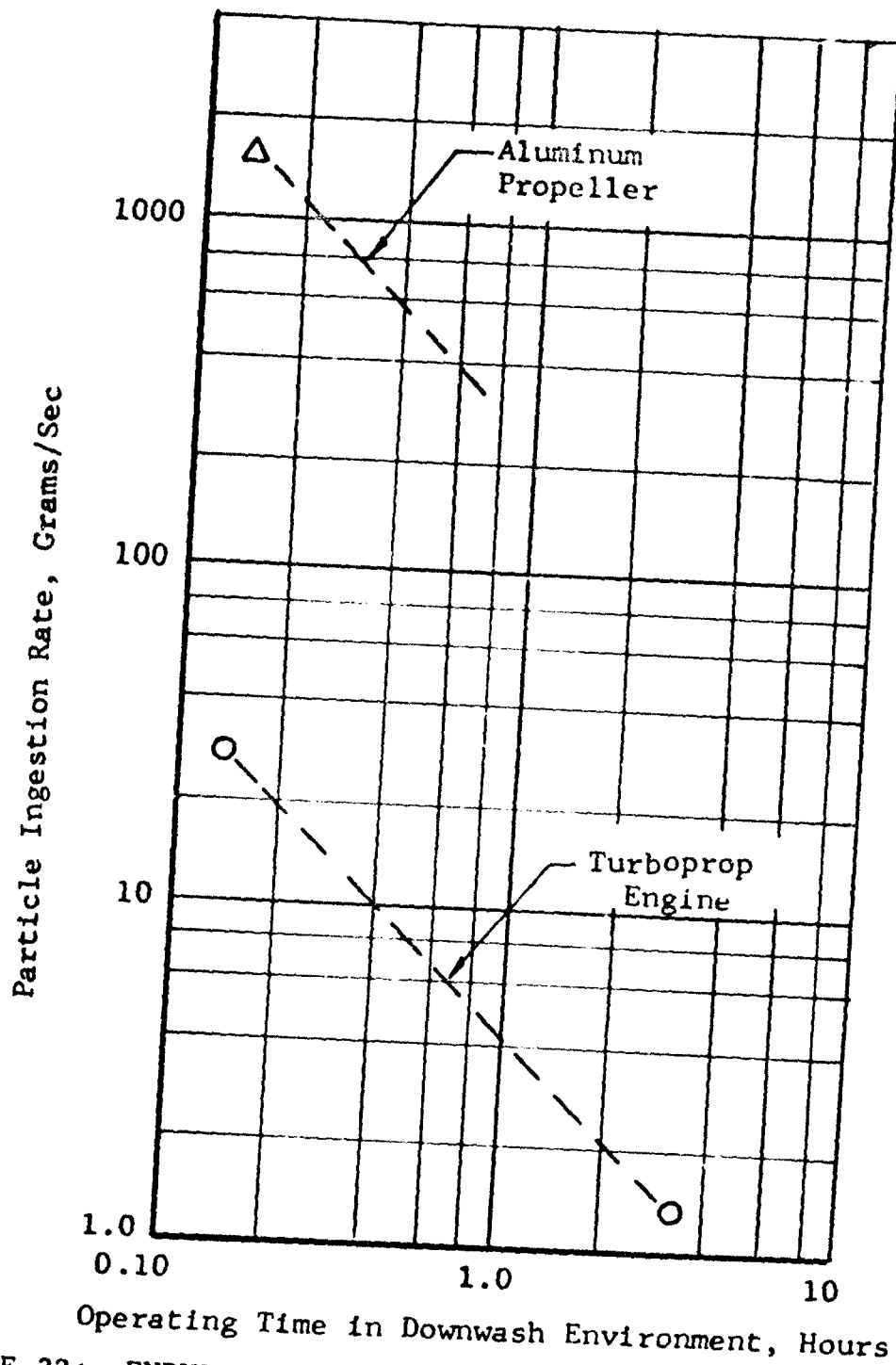
FIGURE 32: ENDURANCE LIMITS FOR LIFT DEVICES OPERATING IN SAND ENVIRONMENT

83

Percent of Initial Horsepower

Hover Time

30-Foot Hover

15-Foot Hover
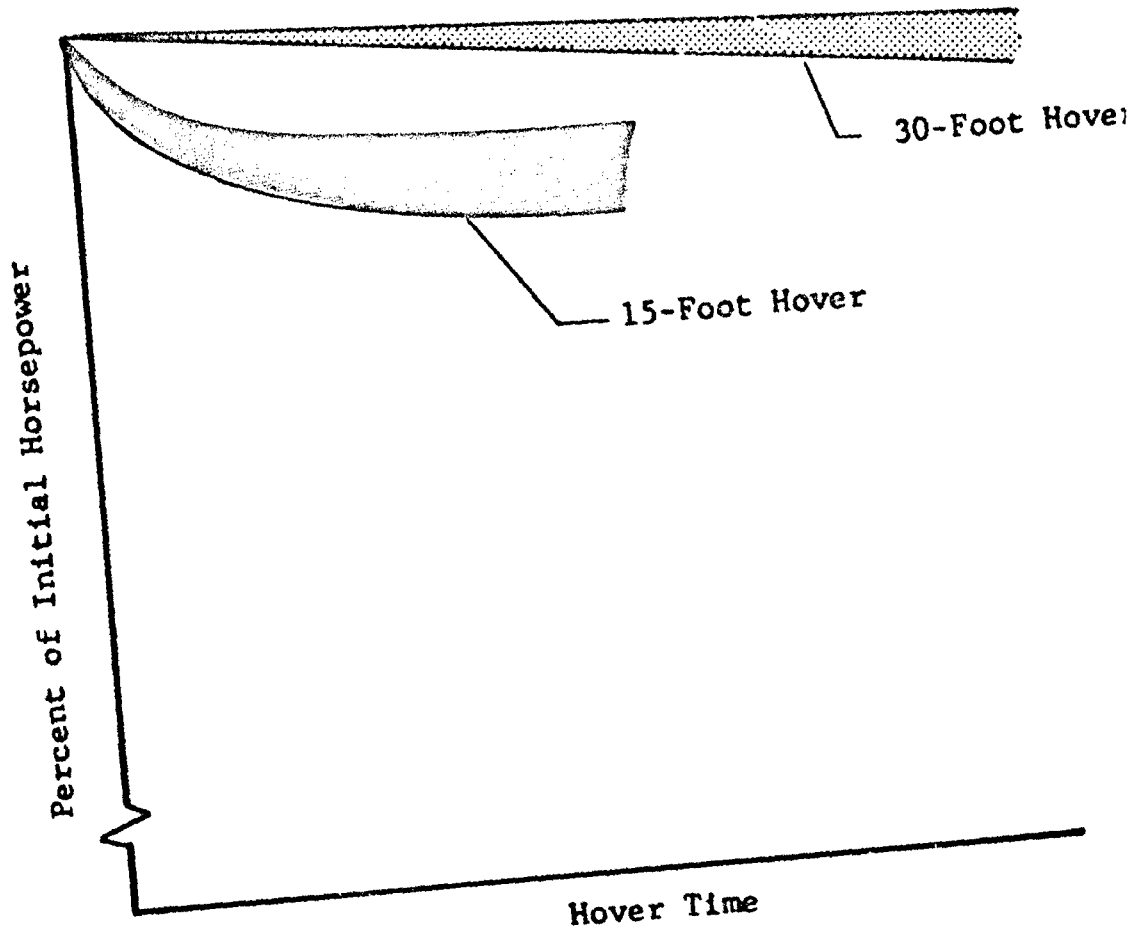
FIGURE 33: PERFORMANCE LOSS DUE TO SALT-WATER INGESTION AS A FUNCTION OF HOVER TIME AND HEIGHT FOR THE H-SS-2 HELICOPTER (Reference 20)
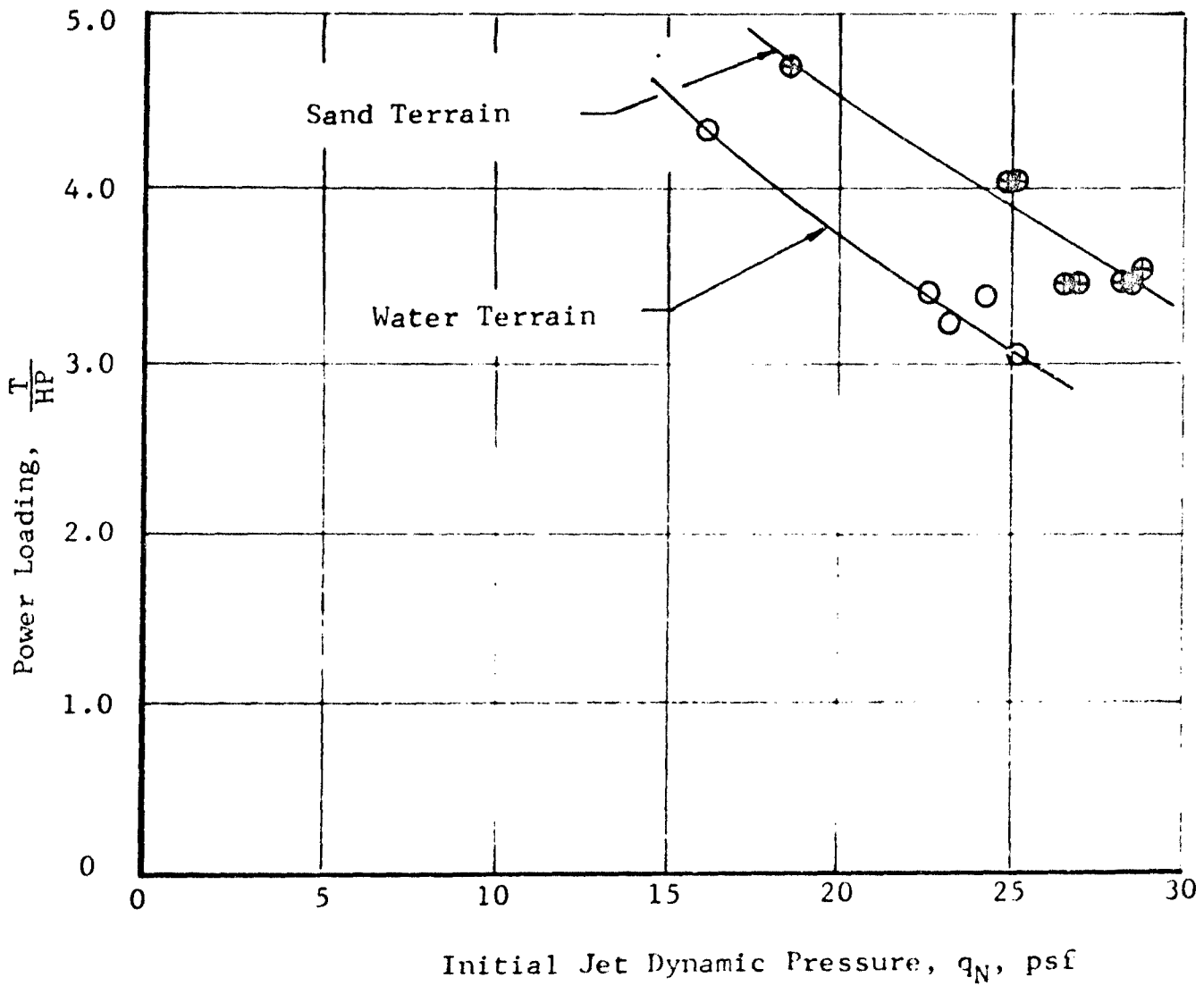
FIGURE 34:   EFFECT OF TERRAIN ON POWER LOADING OF A DUCTED
TURBOPROP VTOL MODEL AIRCRAFT (Reference 21)
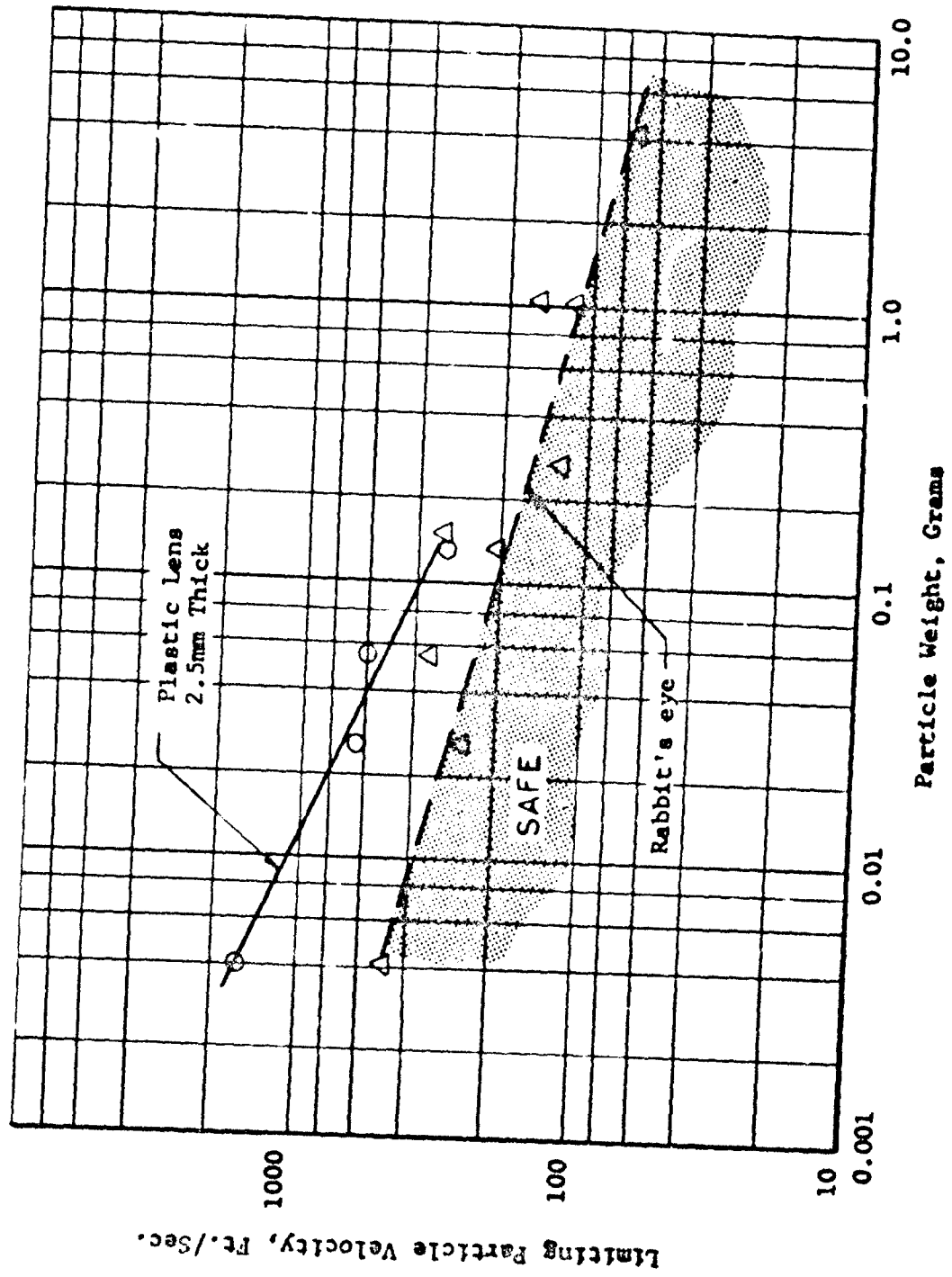
FIGURE 35: MAXIMUM PARTICLE VELOCITY AND WEIGHT LIMITS FOR EYE PENETRATION
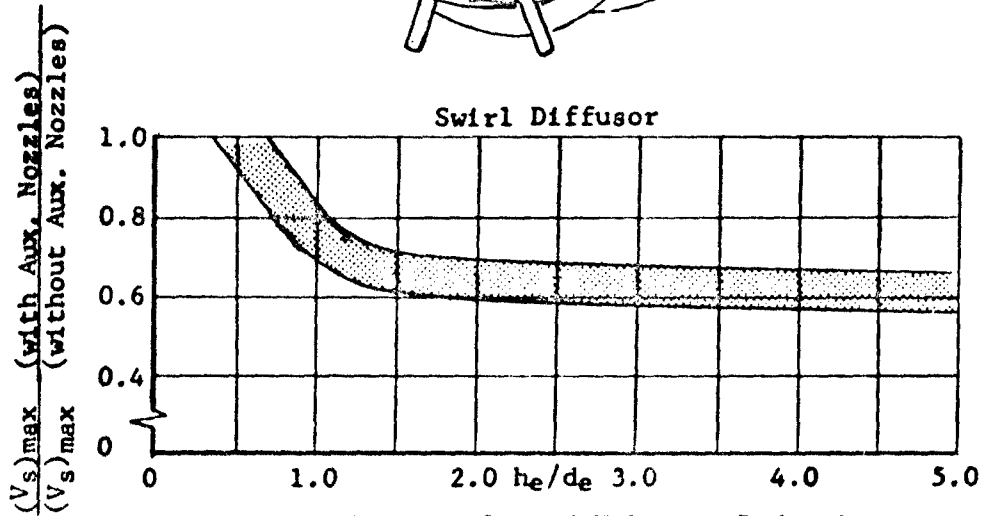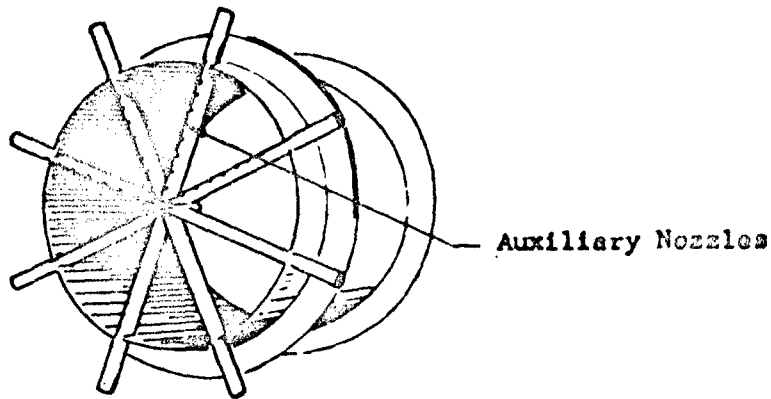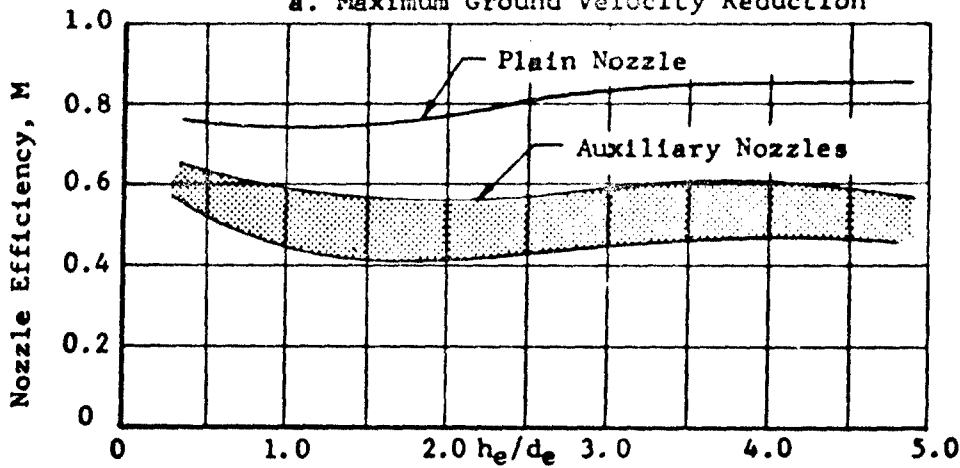
FIGURE 36: OVERALL EFFECTIVENESS OF DIFFUSORS IN REDUCING
MAXIMUM GROUND VELOCITY AS A FUNCTION OF NOZZLE
HEIGHT (Reference 28)

ANNULAR FENCE
STORAGE COMPARTMENT

RETRACTABLE ANNULAR FENCE
(Fine Mesh Wire Screen)

GUIDE WIRES
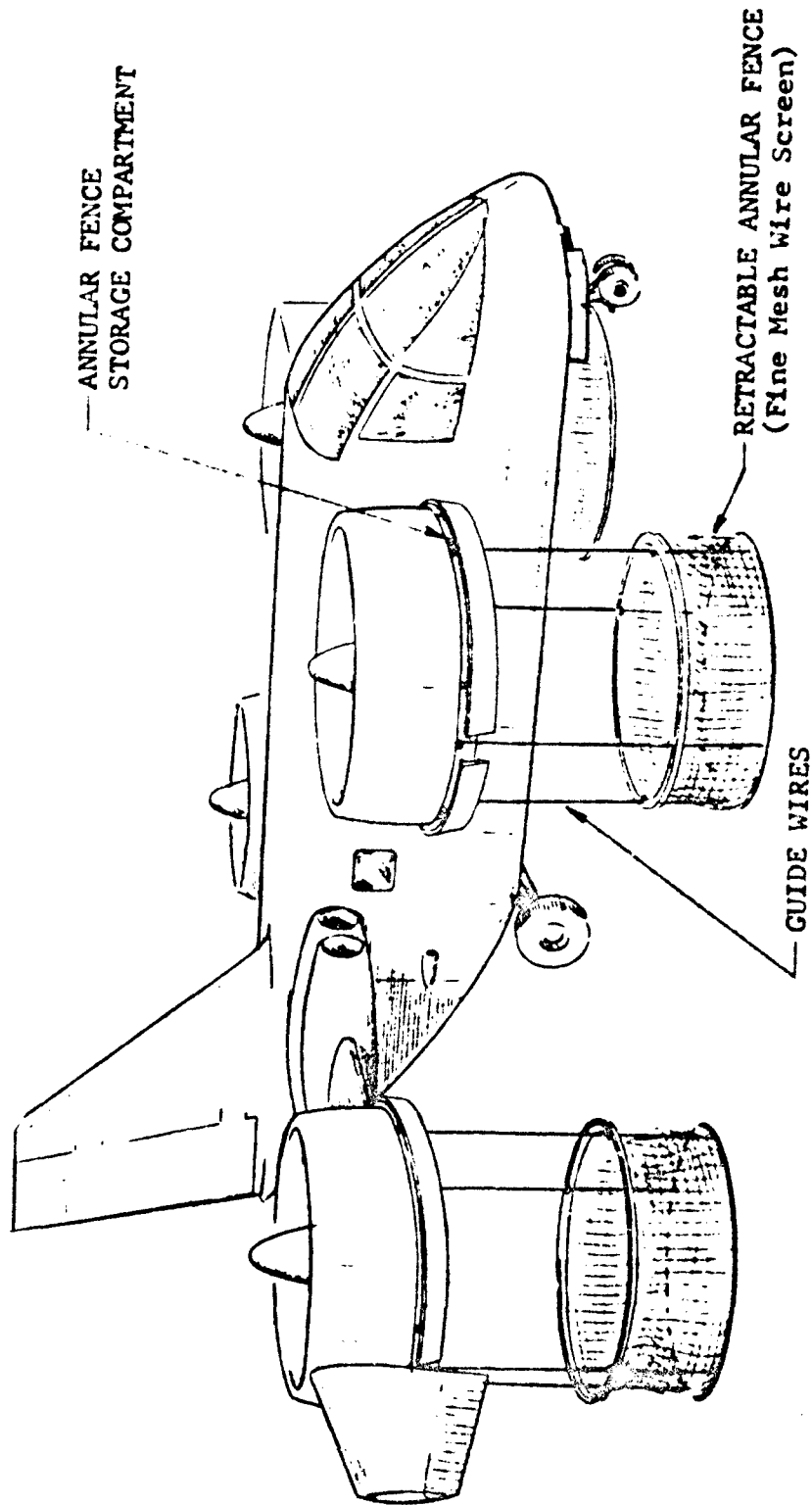
FIGURE 37: ARTIST'S CONCEPTION OF AIRBORNE ANNULAR FENCE INSTALLED ON A
DUCTED VTOL AIRCRAFT

88
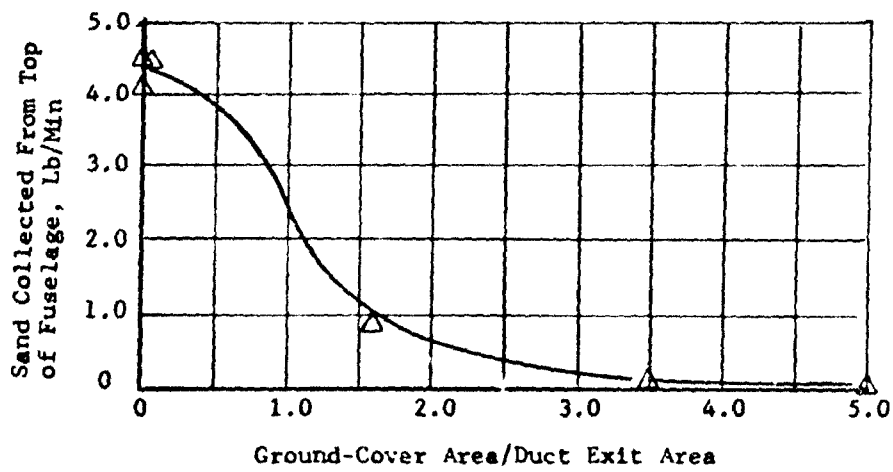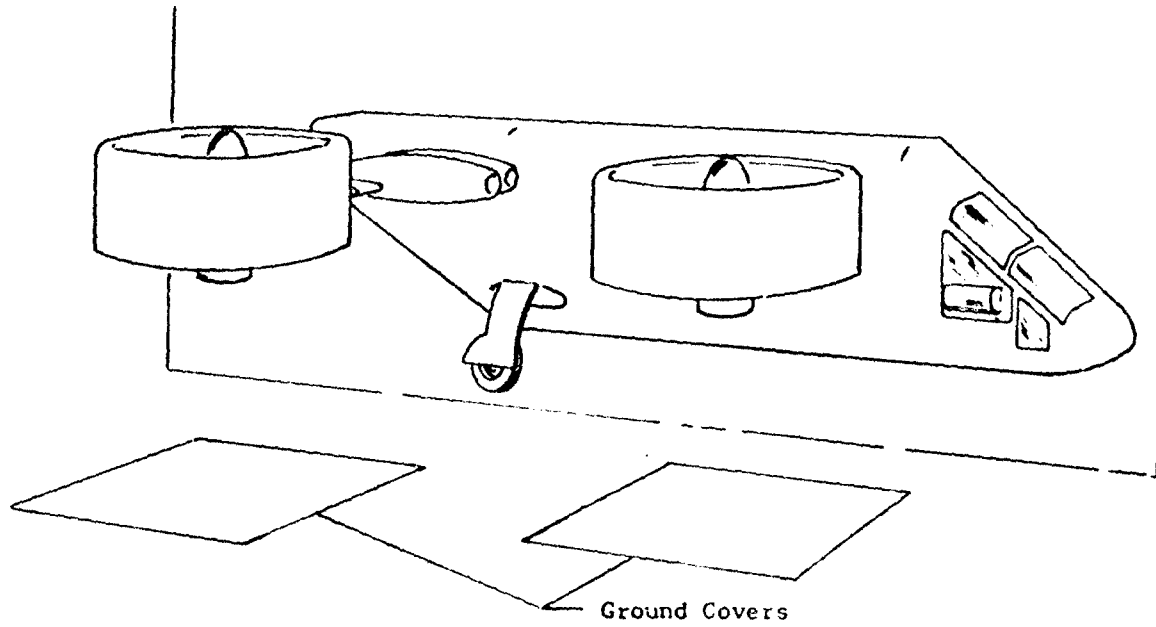
Ground Covers

FIGURE 38: GROUND COVER EFFECTIVENESS IN REDUCING
PARTICLE CIRCULATION (Reference 21)
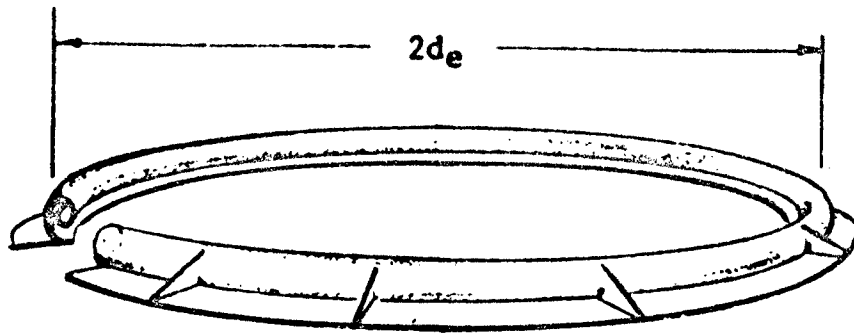
PARTICLE TRAPS
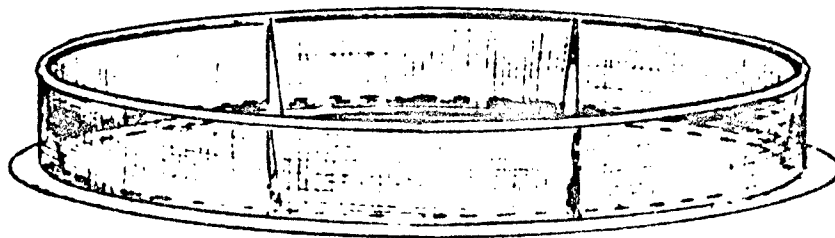
ANNULAR FENCE
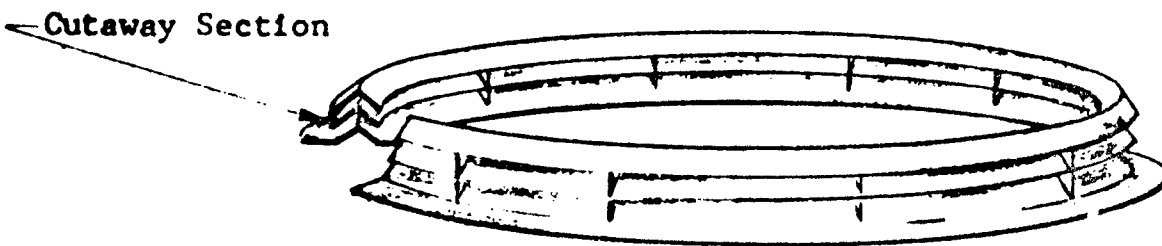
ANNULAR CHANNELS

FIGURE 39:   GROUND FLOW AND PARTICLE DIVERTERS

APPENDIX I

SAMPLE CALCULATION OF ENVIRONMENTAL CONDITIONS

FOR A TYPICAL VTOL AIRCRAFT CONFIGURATION

OPERATING IN GROUND PROXIMITY

The purpose of this appendix is to present the VTOL aircraft designer with a step-by-step example of the use of the downwash impingement criteria developed in the body of this report. Described is the procedure for estimating visibility conditions, concealment problems (cloud heights), aircraft damage and personnel injury that would accompany typical VTOL operations in ground proximity.

A hypothetical VTOL aircraft of the open-propeller type incorporating two lift devices, one on each side of the fuselage, is selected for the example calculations. A disc loading of 50 pounds per square foot and a propeller diameter, D_p, of 14 feet are assumed. Such an aircraft has an average slipstream dynamic pressure, q_N, equal to the disc loading and a fully developed slipstream diameter, d_e, equal to 0.707 D_p. It should be noted that for a ducted propeller, q_N would be one-half the disc loading and d_e would be equal to the duct exit diameter.

The sample calculation of cloud height and visibility is made for the above aircraft operating over sand terrain at an $h_e/d_e = 1.5$. Results are also shown for a calculation for $h_e/d_e = 3.0$ over sand.

The aircraft damage and personnel injury calculation is made for both mixed sand and gravel and debris-covered terrain.

It should be noted that the general procedure presented is not restricted to the terrains or aircraft type assumed above but applies to a wide range of terrain conditions and VTOL types.

91

CLOUD HEIGHT AND VISIBILITY

The estimation of cloud height and visibility requires the use of Table 1 and Figures 40, 41, 42, and 43. A column-by-column explanation of the use of Table 1 follows:

Columns 1 and 2: Select values of x/d or y/d; the values shown in this example are generally adequate for most computations.

Column 3: For x/d_e or $y/d_e < 4.0$, read the $h/d_e = 1.5$ curve of Figure 40 for $(q_s)_{max}/q_N$. For x/d_e or $y/d_e > 4.0$, $q_s/q_N = 1.4/(x/d_e)^2$.

Column 4: The surface dynamic pressure, q_s , is obtained by multiplying column 3 by q_N .

Column 5: The terrain constant k_t from Figure 41 for sand is equal to 1.2.

Column 6: Multiplying column 4 by $1/\sqrt{k_t}$ gives the $(q_s)_{eff}$ for sand.

Column 7: Since there is no ground flow interaction along the x/d_e plane, $(q_{sx})_{eff}$ is equal to $(q_s)_{eff}$ (column 7).

Columns 8 and 9: $(q_{sx})_{eff}$ being known (column 7), the particle cloud height h_e/d_e for zero and 100 percent visibility is read from Figure 42.

Column 10: Due to the arrangement of the lift devices, flow interaction exists along the Y-Z plane. This is compensated for with the interaction term from Figure 43

Column 11: $(q_{sy})_{eff}$ is then obtained by multiplying $(q_{sx})_{eff}$ (column 7) by the interaction term, q_{sy}/q_{sx} , (column 10).

Columns 12 and 13: Having $(q_{sy})_{eff}$, the particle cloud height along the y/d_e axis for zero and 100 percent visibility is read from Figure 42.

Columns 8, 9, 12, and 13 are plotted on Figure 44. The zero and 100 percent visibility for locations other than along the X-Y and Y-Z planes are then faired in as also shown in Figure 44. From this figure, both the visibility within the cloud and the overall cloud pattern generated by a VTOL aircraft can be evaluated. To illustrate the effect of increasing h_e/d_e . the above method was repeated for $h_e/d_e = 3.0$; the resulting cloud pattern is presented in Figure 45.

AIRCRAFT DAMAGE

As was discussed in the design criteria section aircraft damage due to impacts from entrained particles is primarily a function of the particle and the aircraft material being impacted. An example computation of the damage that may be sustained by the hypothetical VTOL aircraft, described previously in this appendix, is presented below.

Airframe Damage

The airframe damage will be evaluated by assuming the following terrain and geometry conditions:

$$h_e/d_e = 1.0$$

$$q_N = 50 \text{ pounds per square foot}$$

Terrain Particles: Sand - 80 to 3000 microns

Gravel - Maximum 4.0-inch diameter

40-pound empty barrel-2-foot diameter x 3-foot height

93

Aircraft Skin: 0.064-inch 24 ST aluminum sheet
                 at bottom of fuselage.
                 0.032-inch 24 ST aluminum sheet
                 for top, sides, wings, and tail
                 surfaces.

Landing Gear Struts: 6-inch diameter by 48-inch-
                       long .ain gear.

Particle Size

The maximum average radial velocity, V_A , generated
by the hypothetical aircraft, occurring at $x/d_e \approx 1.0$ is
obtained by

$$V_A = \sqrt{\frac{2q_F}{\rho_A}}$$

where q_F is obtained from Figure 40.   For this example

$$V_A = \sqrt{\frac{2(50)}{0.00238}}$$

$$V_A = 204 \text{ ft/sec.}$$

It is assumed that the maximum size of particle which can
be transported along the ground by V_A is obtained by equating
the maximum drag of the particle to its weight.   From Figure
46, maximum gravel size is 3.0 inches.

Airframe Skin Design Limitations

The resistance of the aircraft skin to penetrations
due to impacts from entrained particles will be determined
using Table 2 in conjunction with Figures 47 and 48.   A
column-by-column explanation of the use of Table 2 follows:

94

Columns 1, 2, and 3: Tabulate particle or debris characteristics.

Column 4: Calculate maximum drag area, A_F .

Column 5: Calculate impact area, A_I .

Column 6: Calculate particle mass, m_p .

Column 7: Obtain the size parameter, β , from

$$\beta = \frac{3 d_e C_D \rho_A A_F}{m_p} \quad .$$

For stone spheres, β reduces to

$$\beta = 0.001 \, d_e / a \quad .$$

Column 8: Values of $\dfrac{V_p}{\sqrt{q_F / \rho_A}}$ are obtained from

Figure 47 or calculated using

$$\frac{V_p}{\sqrt{q_F / \rho_A}} = 1 - \frac{1}{\sqrt{\beta} + 1} \quad .$$

Column 9: $\sqrt{q_F / \rho_A}$ is calculated using q_F from the section on particle size (page 94).

Column 10: Column 9 is multiplied by Column 8 to obtain particle velocity, V_p .

Column 11: Particle energy, E_p, is obtained using $E_p = 1/2 m_p V_p^2$.

95

Column 12: Divide the particle impact area, A_I , (Column 5)
by the maximum drag area, A_F (Column 4).

Column 13: The ratio E_P/A_I is obtained by dividing Column 11
by Column 6.

Column 14: Values of TY_T for each particle are read from
Figure 48.

Referring to Figure 48, it is seen that for the
particles considered, the aircraft skin design parameter,
TY_T , is less than the value required to penetrate 0.032-
inch aluminum sheet. It should be noted, however, that
penetration by the barrel is based on a large impact area.
If, however, the barrel were to strike the aircraft on
edge, A_I would be greatly reduced; hence, much higher values
of TY_T would occur. In this manner the skin could be
punctured or severely dented by the barrel.

Landing Gear Impacts

A simplified analysis of landing gear stresses de-
veloped from rolling debris impacts will be presented be-
low for the hypothetical VTOL aircraft. Although landing
gear design is far more complex, a simple cantilever tubular
beam struck by the entrained barrel will be assumed, merely
to indicate the method to be used.

The landing gear, as specified previously, is assumed
to consist of a 6-inch-diameter aluminum tube, with ½-inch
wall thickness, mounted cantilever to the airframe. The
fully extended gear length is 48 inches. The maximum static
stress, σ , developed by the barrel weight is

$$\sigma = \frac{Mc}{I}$$

$$\sigma = \frac{40.0 \times 48 \times 3.0}{0.491(6^4 - 5^4)} = 17.5 \text{ psi} .$$

The maximum static deflection, ϵ, is

$$\epsilon = \frac{40 \times 48^3}{3 \times 10^7 \times 0.491(6^4-5^4)} = 4.45 \times 10^{-4} \text{ inch}$$

$$\epsilon = 3.71 \times 10^{-5} \text{ ft.}$$

Using Equation 28,

$$\sigma_I/\sigma = \sqrt{V_P^2/g\epsilon}$$

$$= \sqrt{\frac{53.4^2}{32.2 \times 3.71 \times 10^{-5}}}$$

$$\sigma_I/\sigma = 1545.$$

The impact stress σ_I is

$$\sigma_I = 1545 \times 17.5$$

$$\sigma_I = 27,100 \text{ . psi.}$$

Material to be used must have allowable yield stress greater than 27,100 pounds per square inch. Alternately, the design may be modified to reduce the stress level. Furthermore, wherever possible, antenna or other appendages should be mounted at the highest possible location to avoid rolling debris.

It must again be emphasized, however, that the above relationship is based on the following assumptions:

1. Perfect elasticity of the beam.
2. Rigidity of the moving body.
3. Simultaneous contact of the moving body with the end of the beam.

97

Such conditions, however, are practically unattainable.

The dampening of the initial stress wave by elastic hysteresis in the beam and the diminution of the intensity of that stress wave by cushioning effect of the actually nonrigid moving body would serve to make the actual maximum stress less than the theoretical value.

Rotating Components

As was pointed out in the text, no data exist at present which will indicate the density of particles existing at the propeller plane or turbine intakes of the hypothetical aircraft. As a first-order approximation, however, the density will be assumed to be equal to that reported in the full-scale ducted model tests of Reference 21.

$$\text{Sand density} = 0.213 \text{ gr/ft}^3 \text{ (from Figure 49)}$$

$$\text{Propeller volume flow} = V_N A_e$$
$$= (204)(78.5)$$
$$= 16,000 \text{ ft}^3/\text{sec}$$

$$\begin{aligned}\text{Quantity of sand}\\\text{ingested}\end{aligned} = 0.213(16,000) = 3410 \text{ gr/sec}.$$

The particle ingestion rate is greater than the limits indicated in Figure 50. Since the possibility exists that large debris located in the plane of interaction may be lifted as high as the propeller plane, operations of the hypothetical aircraft over the terrain defined previously would be extremely hazardous.

PERSONNEL INJURY

From Table 2, the energy of entrained sand and gravel particles is not greater than 12.5 foot-pounds. Debris such as barrels may develop energies as high as 1775 foot-pounds. Using the criterion of 58 foot-pounds it may be concluded that ground personnel, when wearing protective clothing, will not be injured by entrained small particles but may be incapacitated if struck by large debris.

TABLE 1

VISIBILITY AND CLOUD HEIGHT FOR A VTOL AIRCRAFT, TWO OPEN-
PROPELLER LIFT DEVICES, HOVERING AT h/d_e - 1.5 OVER SANDY TERRAIN

① x/d_e	② y/d_e (Selected)	③ $\left(\dfrac{q_s}{q_N}\right)_{max}$ Fig. 40	④ q_s q_N ③	⑤ k_t Fig. 41	⑥ (q_s) eff ④×⑤$^{-\frac{1}{2}}$	⑦ (q_{sx}) eff ⑥	⑧ h_c/d_e at x/d_e vision 0 Fig. 42	⑨ h_c/d_e at x/d_e vision 100% Fig. 42	⑩ q_{sy}/q_{sx} Fig. 43	⑪ (q_{sy}) eff ⑦×⑩	⑫ h_c/d_e at vision 0 Fig. 42	⑬ y/d_e vision 100% Fig. 42
0	0	0	0	1.2	0	0	--	--	--	0	--	--
1.0	1.0	0.88	44.0		40.1	40.1	2.5	3.6	0.85	34.1	2.0	3.20
1.4	1.5	0.69	34.5		31.5	31.5	1.7	3.07	1.05	33.0	1.7	3.06
2.0	2.0	0.37	18.5		16.9	16.9	.40	2.30	1.32	22.3	0.8	2.30
3.0	3.3	0.16	7.8		7.1	7.1	--	0.8	2.05	14.6	0.1	1.29
4.0	4.0	0.13	6.5*		5.9	5.9	--	0.7	2.35	13.9	0.05	1.45
5.0	5.0	0.06	2.8	1.2	2.6	2.6	--	0.3	2.40	6.22	--	0.75
6.0	6.0	0.04	2.0		1.8	1.8	--	0.1		4.31	--	0.40
--	10.0	0.01	0.70		0.6	0.6	--	--		1.44	--	0

* When x/d_e or $y/d_e > 4.0$, q_s/q_N $\dfrac{1.4}{\left(x/d_e\right)^2}$

99

TABLE 2: AIRCRAFT SKIN DESIGN LIMITATIONS

(1) Particle	(2) Dia. a Ft.	(3) Length Ft.	(4) A_F Ft.^{2}	(5) A_I Ft.^{2}	(6) m_P Slugs	(7) β	(8) $\frac{V_P}{\sqrt{\frac{\sigma_F}{\rho_A}}}$ Fig. 47	(9) $\sqrt{\frac{\sigma_F}{\rho_A}}$	(10) V_P (8)×(9) ft/sec	(11) E_P ×10^2	(12) $\frac{A_I}{A_F}$ (5)÷(4)	(13) $\frac{E_P}{A_I}$ (11)÷(5)	(14) TY_T Fig. 48
Sand	2.6×10^{-4}	--	5.4×10^{-8}	5.4×10^{-8}	5.0×10^{-11}	38.2	0.861	144	124.0	3.8×10^{-7}	1.0	7.04	0
Sand	0.0099	--	7.6×10^{-5}	7.6×10^{-5}	2.65×10^{-6}	1.015	0.50	→	72.0	6.9×10^{-3}	1.0	90.8	400
Gravel	0.25	--	4.9×10^{-2}	4.9×10^{-2}	4.33×10^{-2}	0.04	0.167	→	24.1	12.55	1.0	256	1000
Empty Barrel	2.0	2.83	5.66	3.14	1.24	0.324	0.37	→	53.3	1775	0.565	566	2500
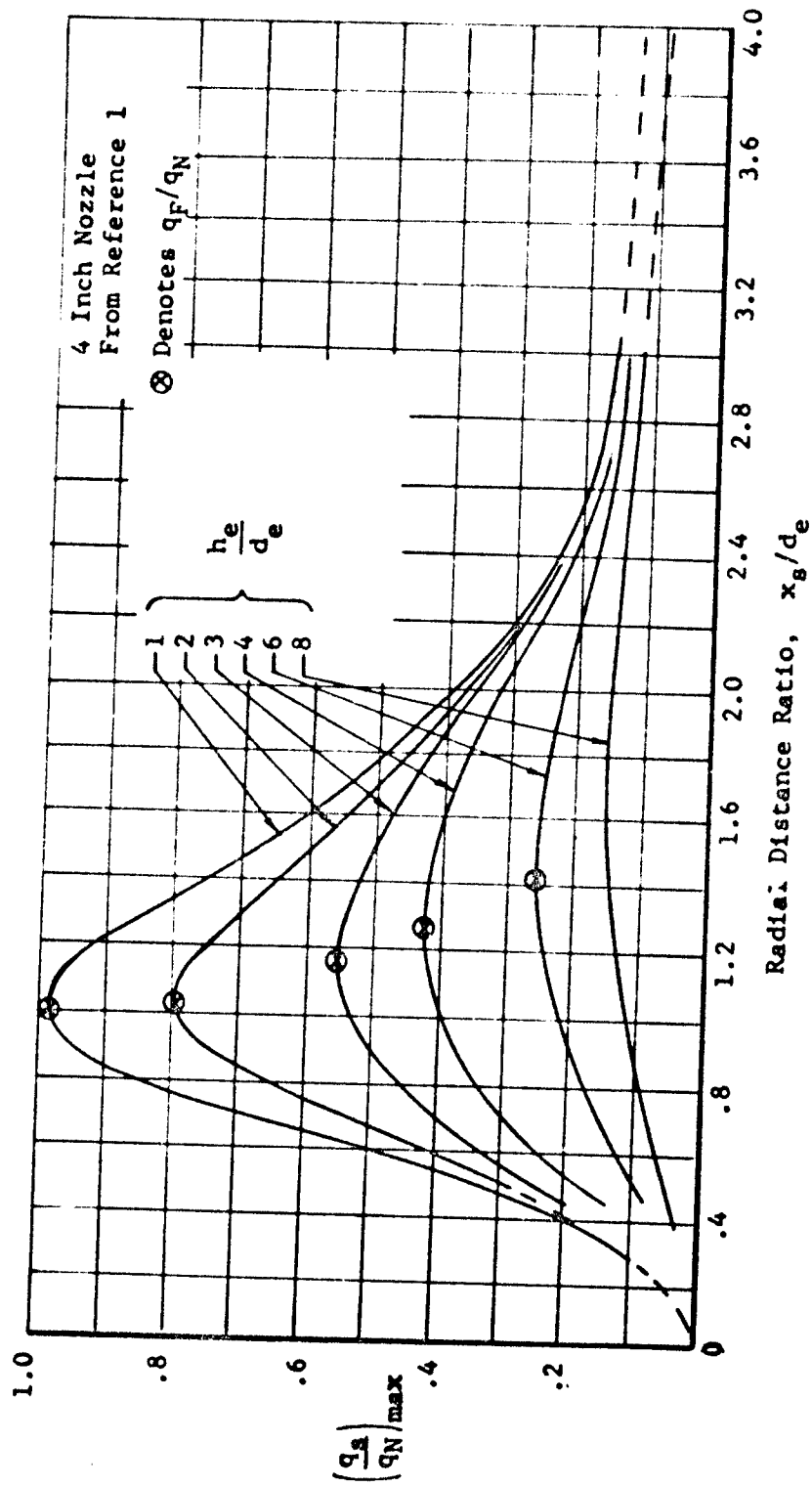
FIGURE 40: MAXIMUM SURFACE DYNAMIC PRESSURE AS A FUNCTION OF
NOZZLE HEIGHT AND RADIAL DISTANCE ALONG THE GROUND

$$(k_t)_W = \frac{\rho_P g\, a}{62.4 \times 0.10}$$

$$\frac{(\text{Particle Dia})(\rho)_P}{(\text{Particle Dia})_W(\rho)_W}, \ k_t$$
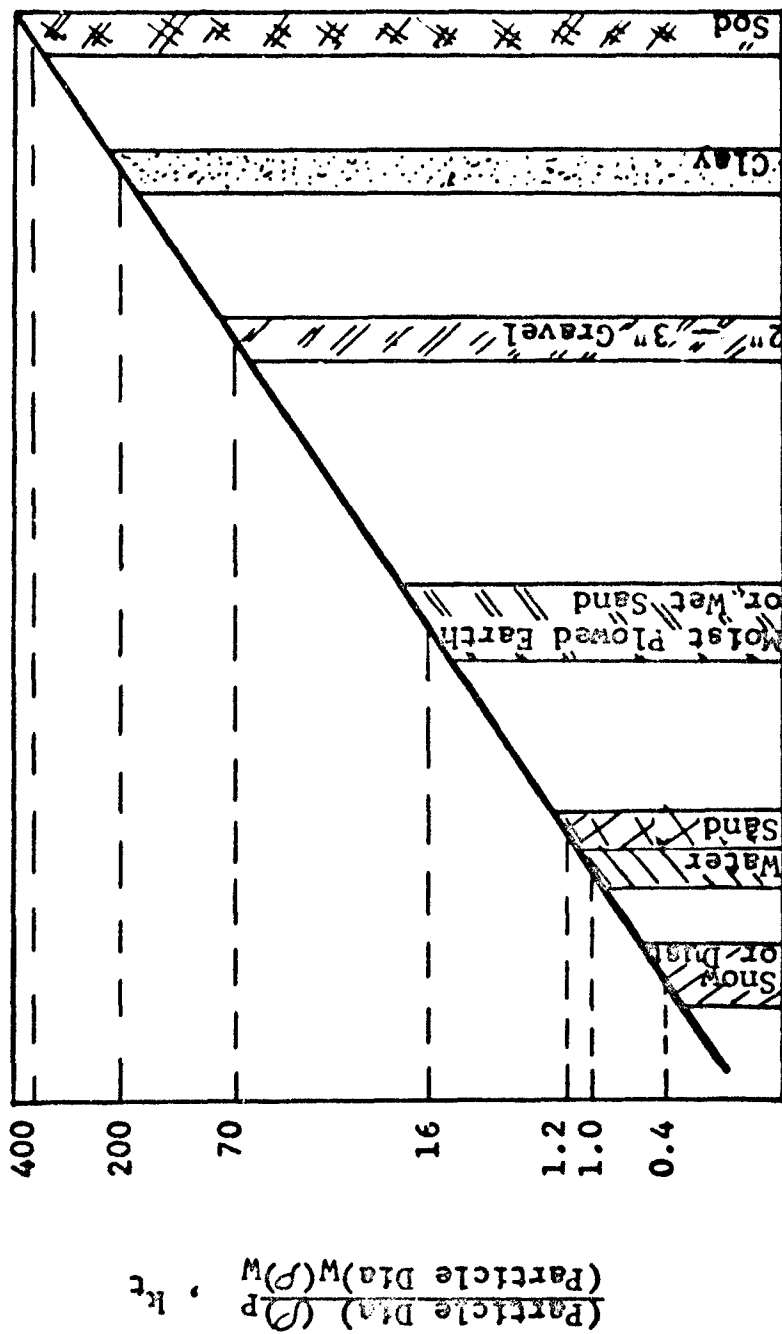
Terrain

FIGURE 41: TERRAIN CHARACTERISTICS
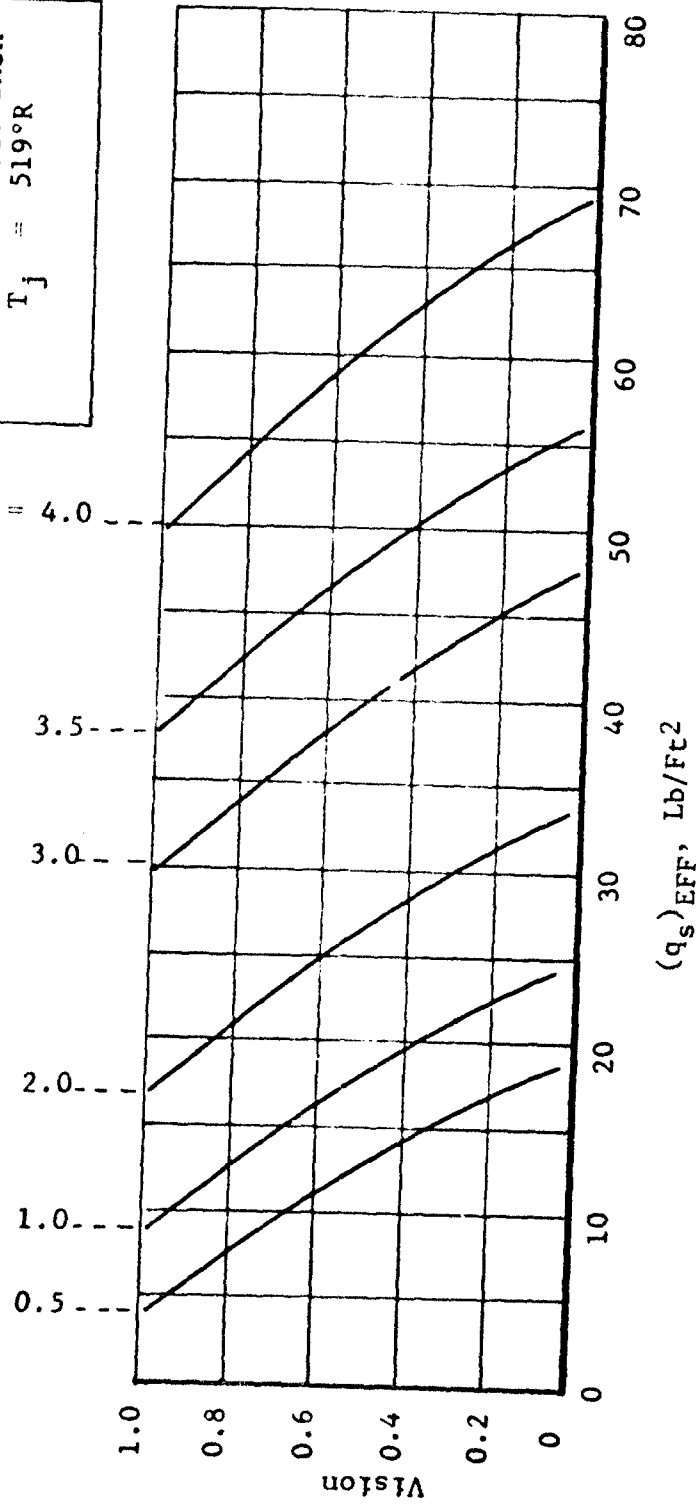
FIGURE 42: VISIBILITY AS A FUNCTION OF $(q_s)_{EFF}$ AND CLOUD HEIGHT
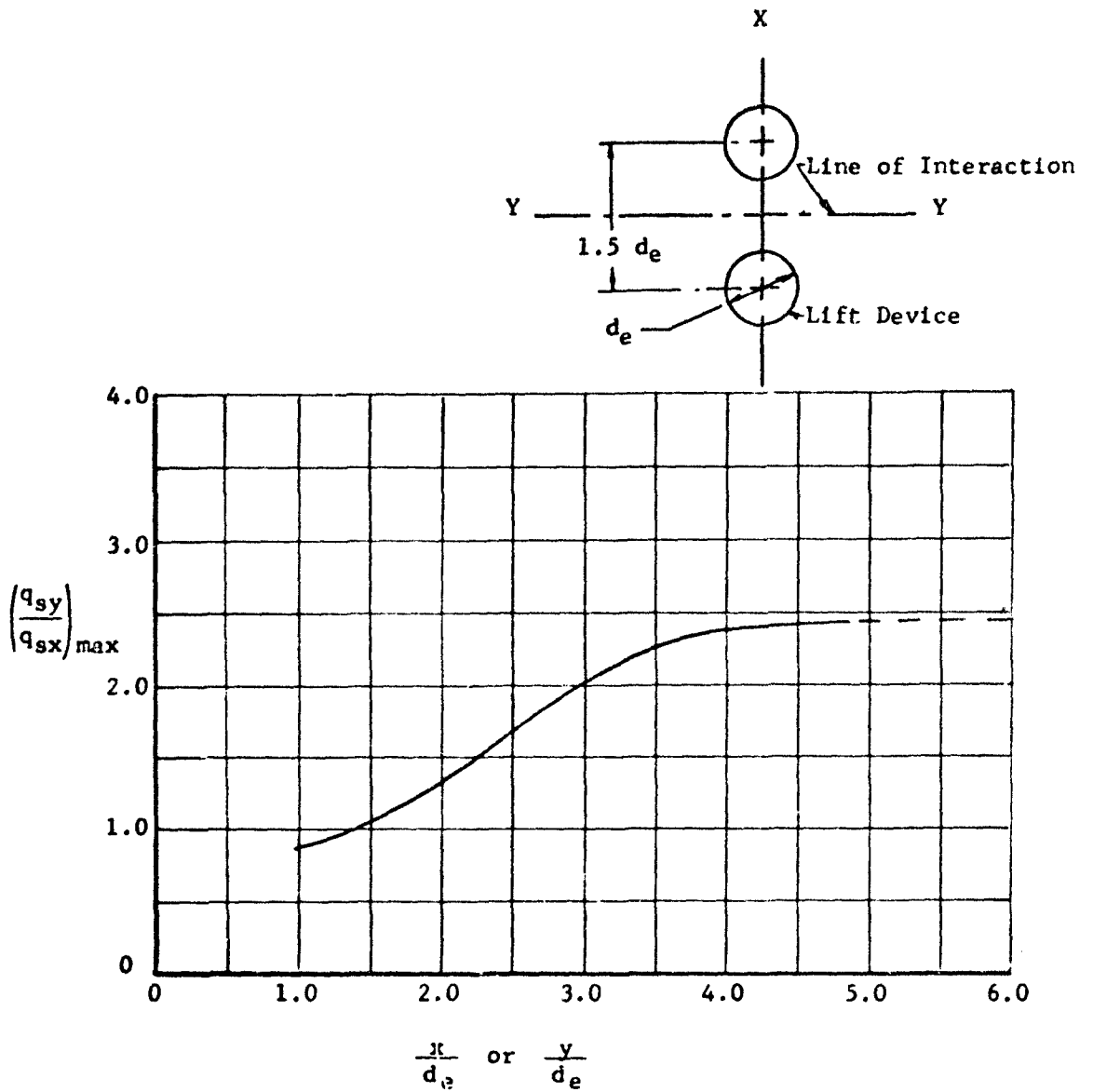
FIGURE 43:   INCREASE IN MAXIMUM SURFACE DYNAMIC PRESSURE
ALONG THE LINE OF INTERACTION BETWEEN TWO
LIFT DEVICES

104
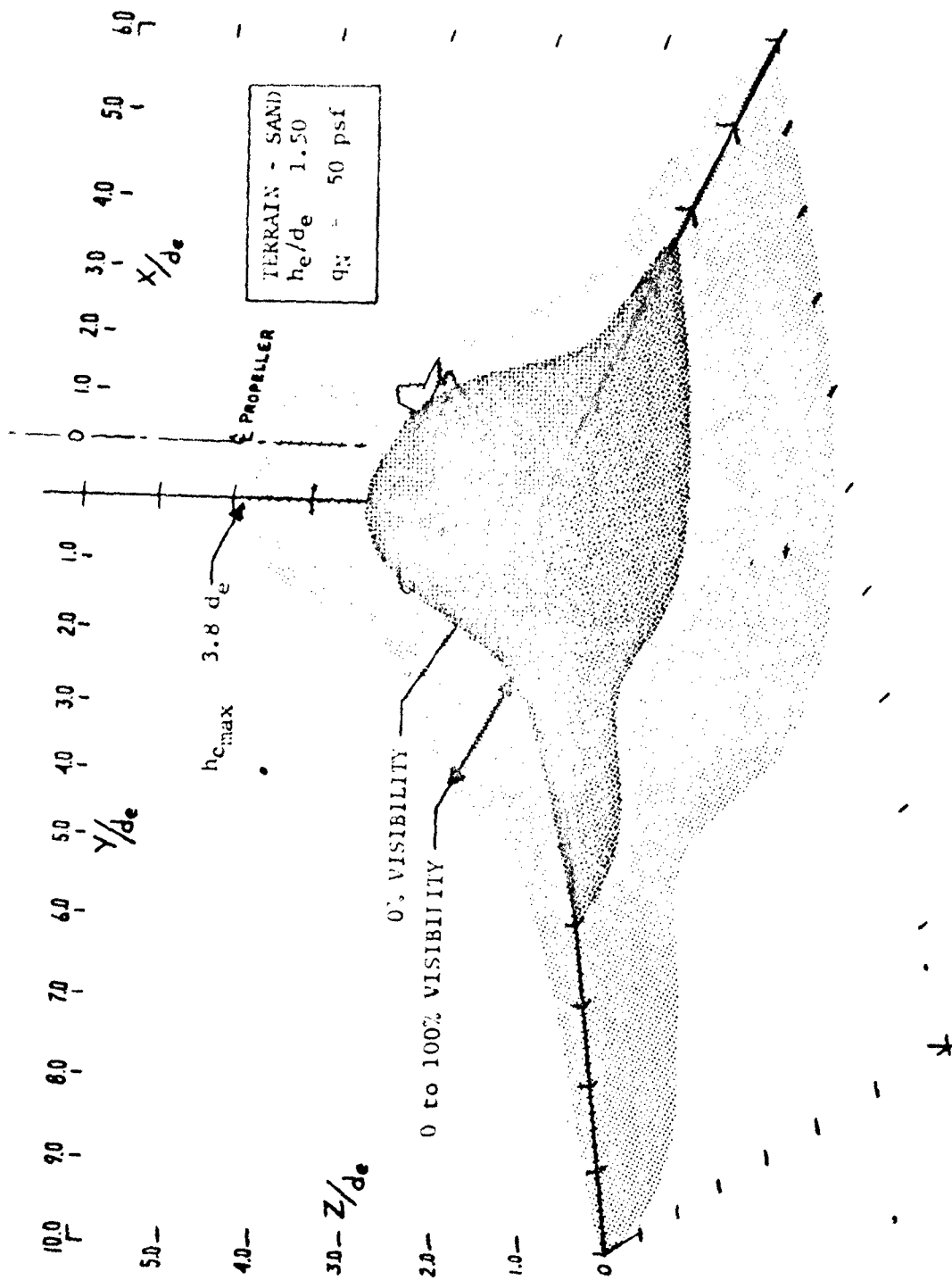
FIGURE 44:   THREE-DIMENSIONAL PLOT OF PARTICLE CLOUD HEIGHT, h_e/d_e = 1.5

105
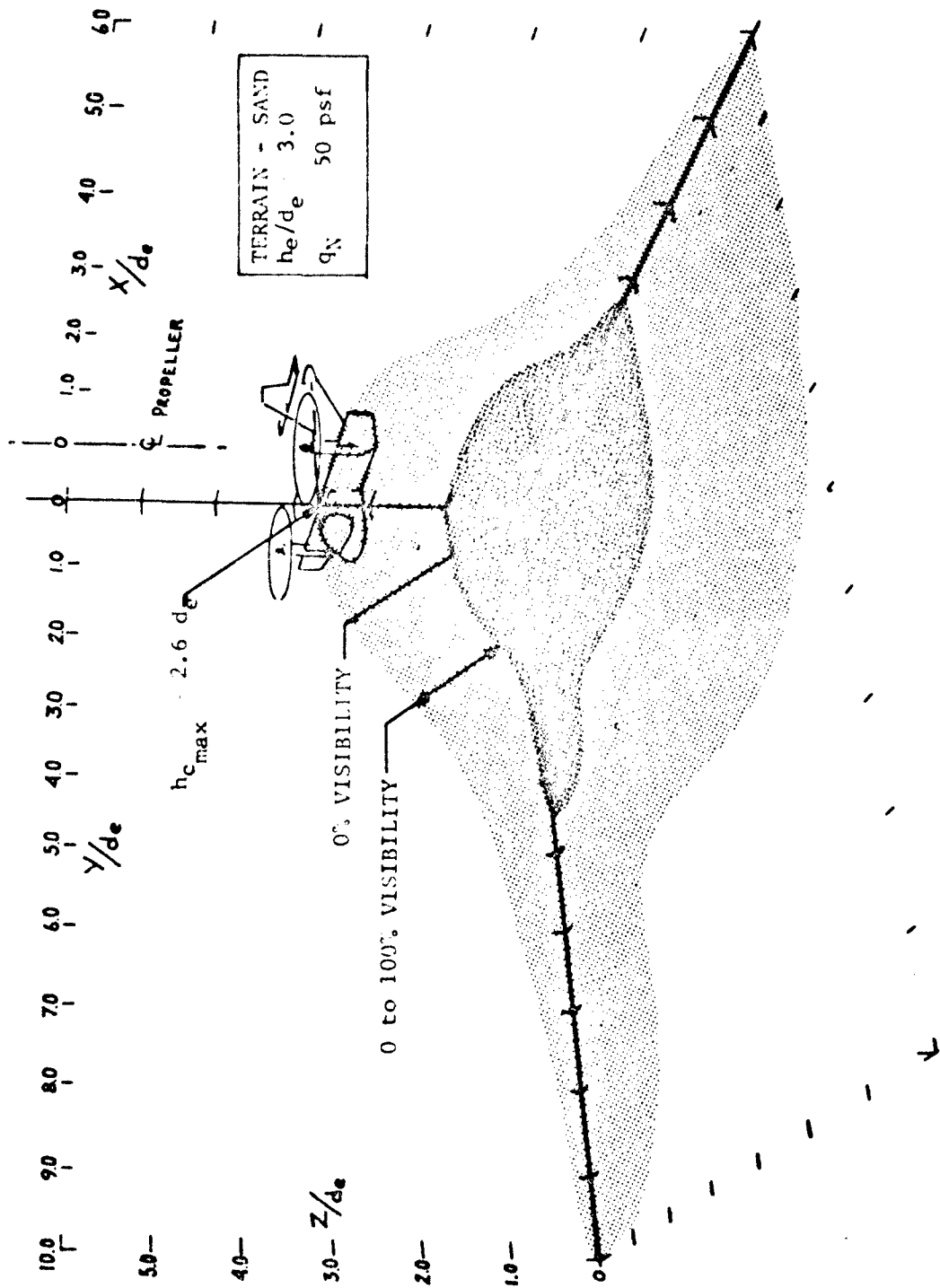
FIGURE 45: THREE-DIMENSIONAL PLOT OF PARTICLE CLOUD HEIGHT, $h_e/d_e = 3.0$

106
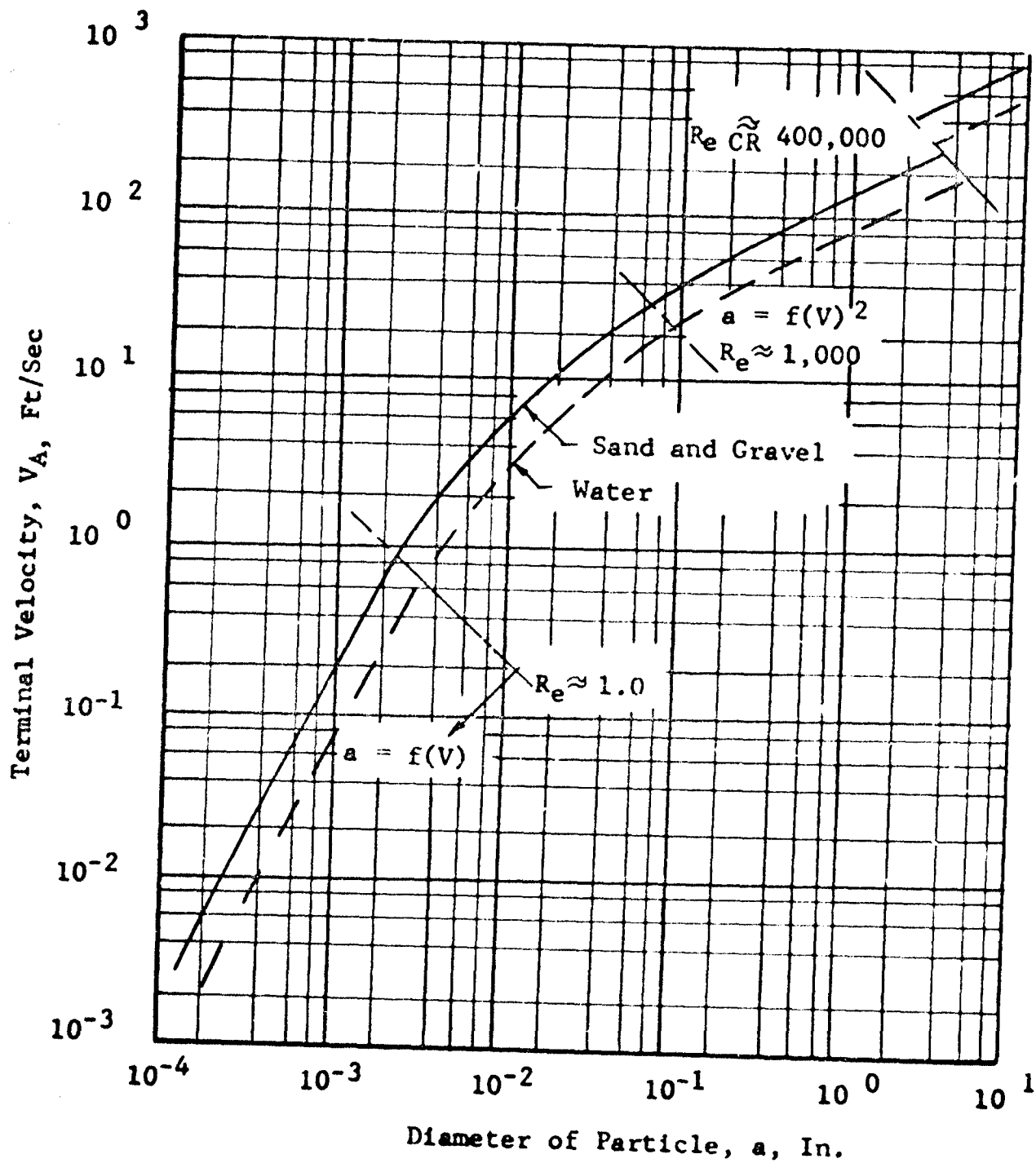
FIGURE 46: VARIATION OF TERMINAL VELOCITY OF PARTICLES
WITH PARTICLE DIAMETER (Reference 1)

107
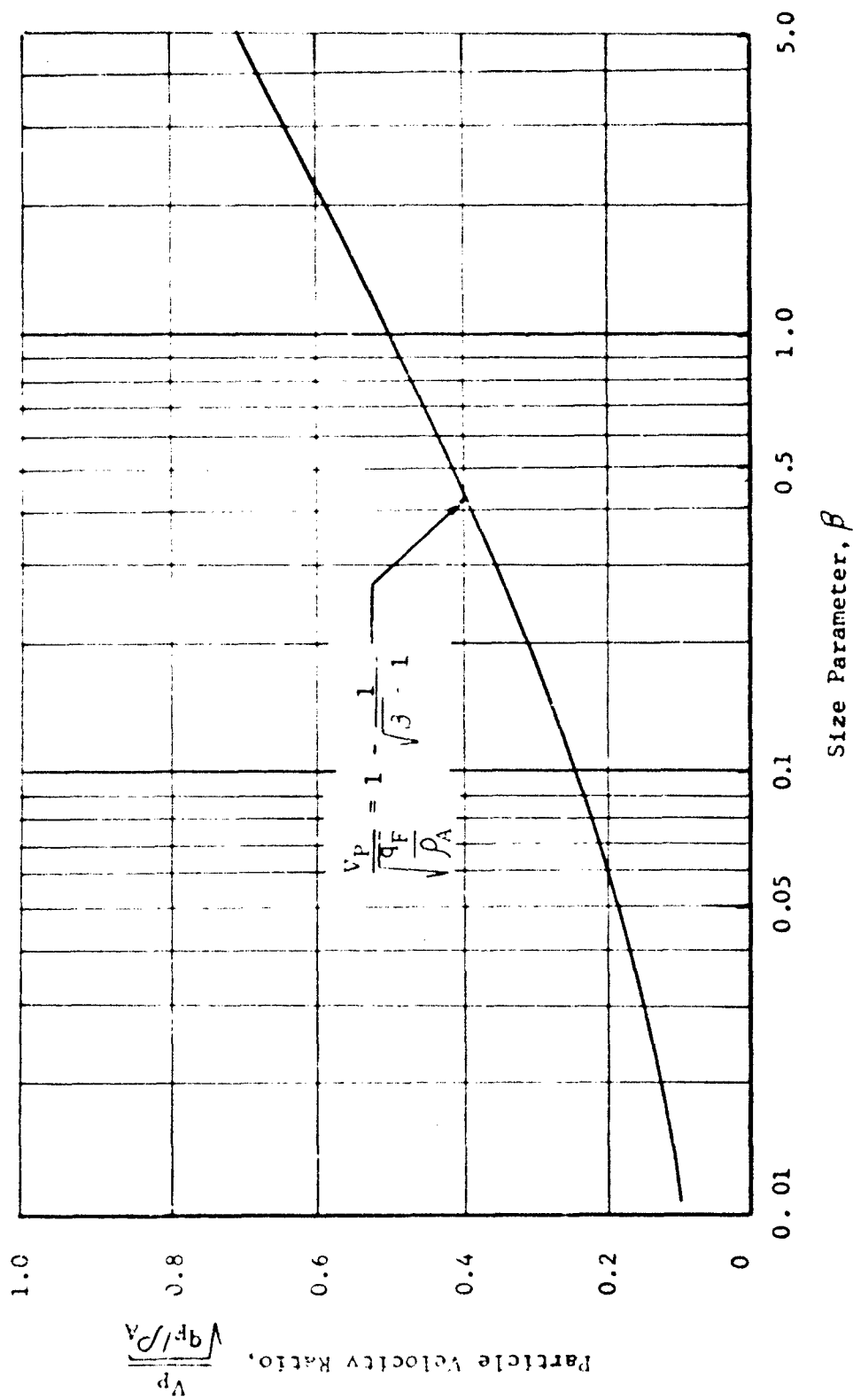
FIGURE 47: ENTRAINED PARTICLE VELOCITY RATIO AS A FUNCTION OF SIZE PARAMETER, β

M A T E R I A L		
Aluminum Sheet 24S-T3	Aluminum Sheet 75S-T6	18-8 Stainless Steel Sheet ½H
Thickness Inches	Thickness Inches	Thickness Inches

Aircraft Skin Design Parameter, TY_T, Ft-Lb/Ft^2

.064

44,000

0.25

40,000   0.50

36,000

32,000

.064

.040   28,000

.020   26,000

24,000

.032   22,000

20,000 $\frac{A_I}{A_F} = 10$

.040   16,000

.032   .020   14,000

.010   12,000

8,000

.020   4,000

0

0   4,000   8,000   12,000

Energy to Impact Area Ratio, E/A_I, Ft-Lb/Ft^2
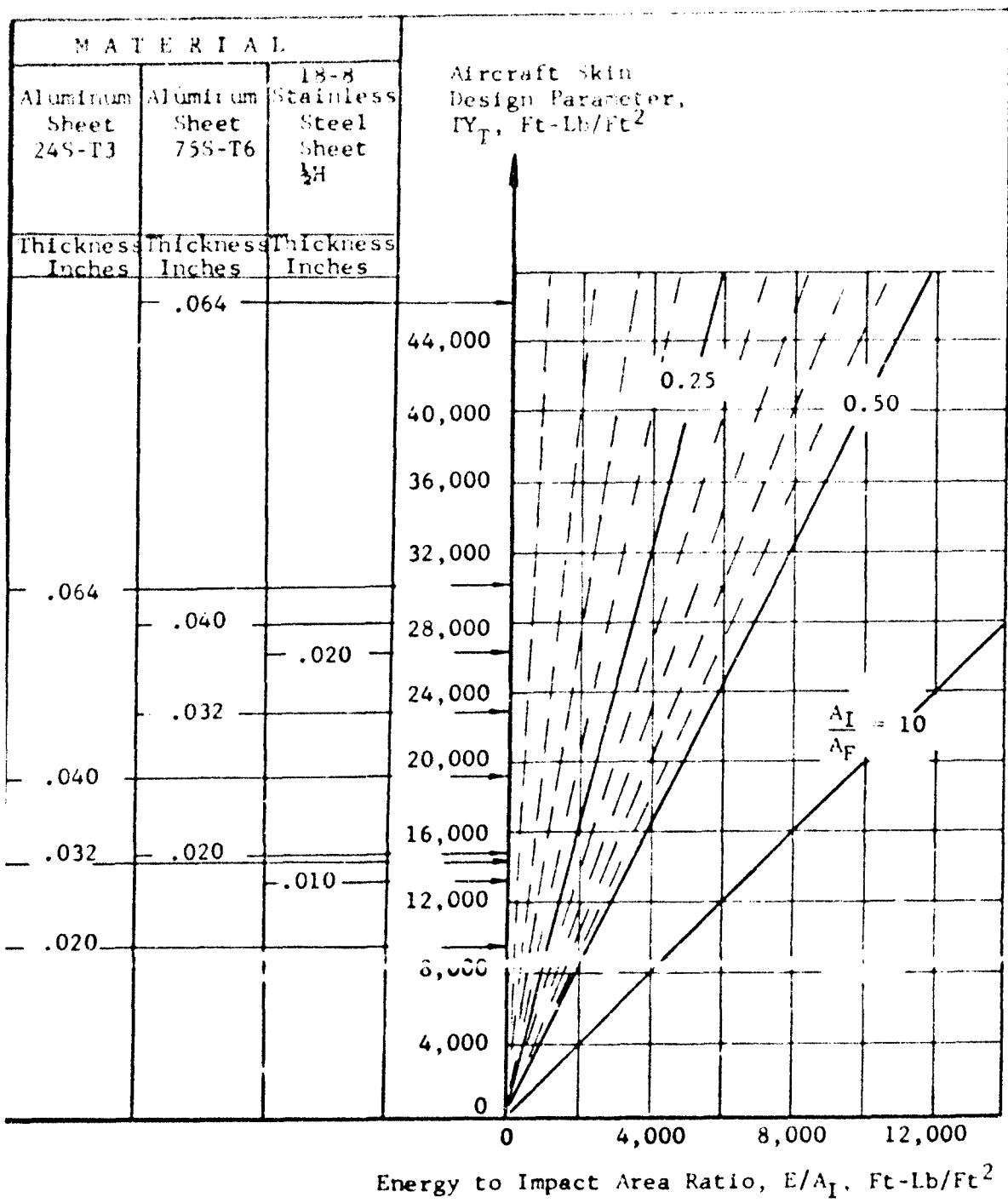
FIGURE 48:   MINIMUM PARTICLE ENERGY REQUIRED FOR
             PENETRATION THROUGH AIRCRAFT SKIN
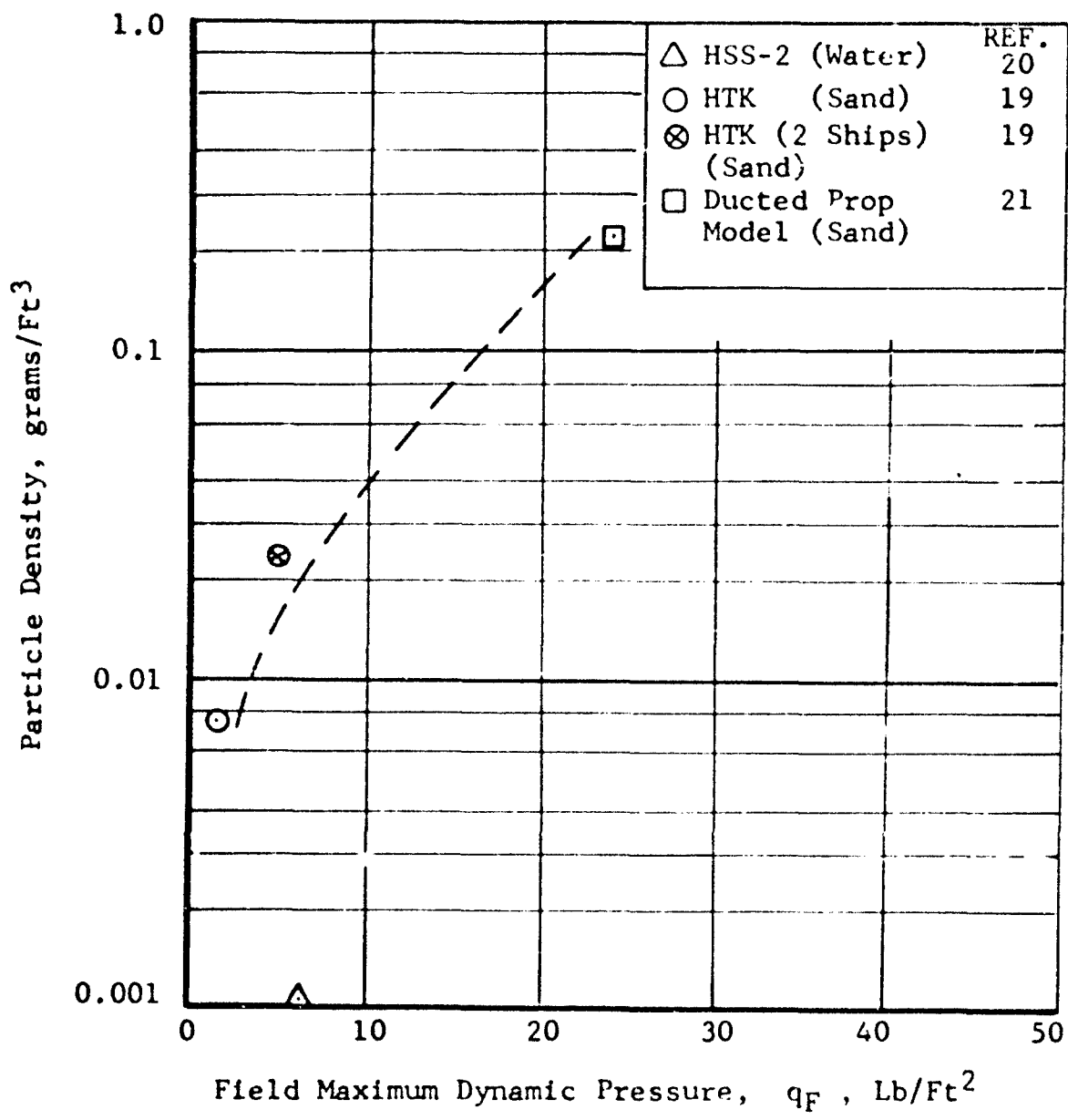
FIGURE 49: ENTRAINED PARTICLE DENSITY IN AIR AS A
FUNCTION OF MAXIMUM FIELD DYNAMIC PRESSURE

110
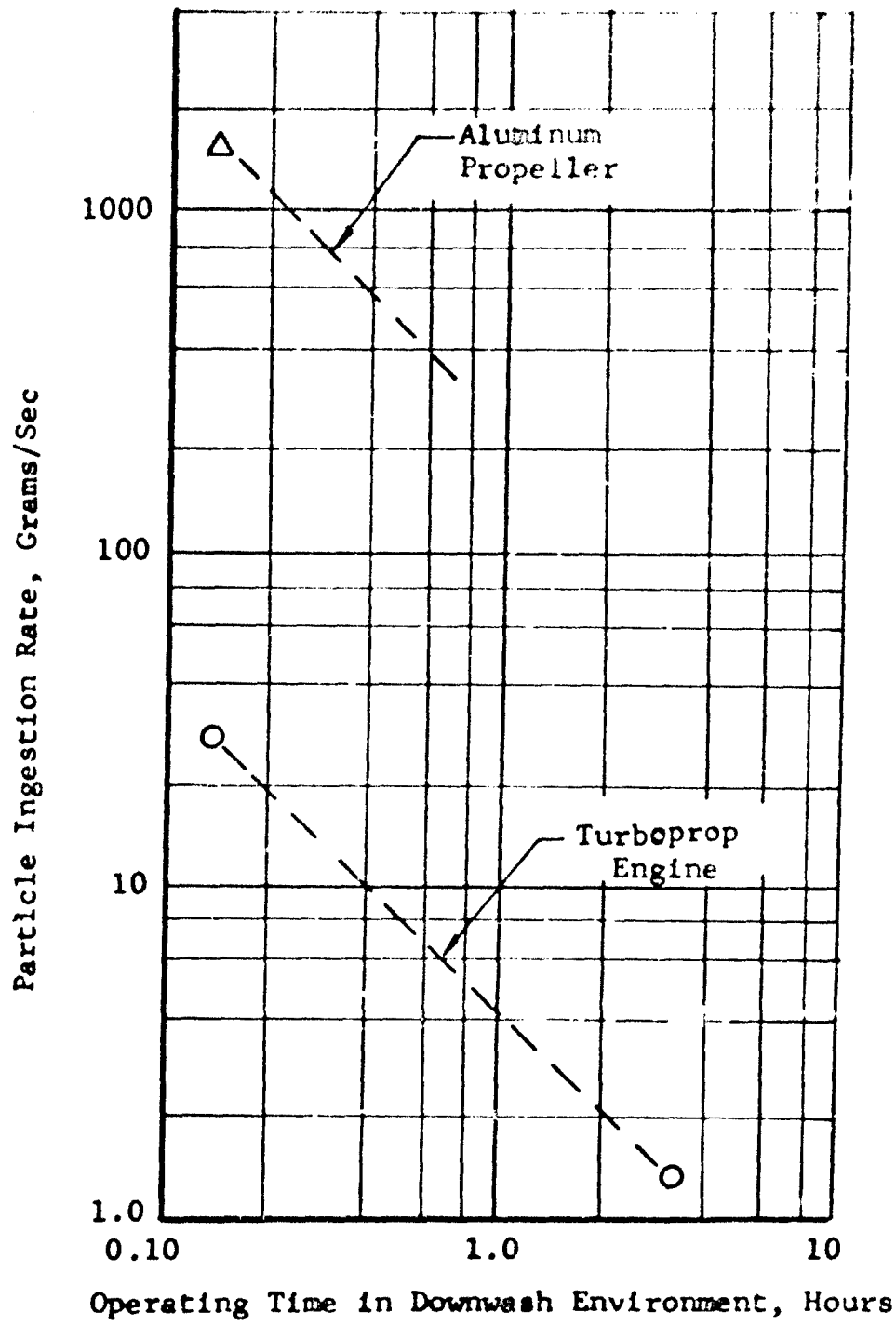
FIGURE 50:   ENDURANCE LIMITS FOR LIFT DEVICES OPERATING
             IN SAND ENVIRONMENT

111

APPENDIX II

BIBLIOGRAPHY OF DOWNWASH IMPINGEMENT

1.   White, R. P., and Vidal, R. J., "Study of the VTOL Downwash Impingement Problem," TREC Technical Report 60-70, 1960.

2.   Keith-Lucas, D., "The Role of the Jet Lift", _Journal of the Royal Aeronautical Society_, May 1962.

3.   Vidal, R. J., "Factors Influencing Ground Particle Entrainment," VTOL Aircraft Downwash Impingement Symposium, TREC Technical Report 61-1, December 1960.

4.   O'Bryan, T. C., "Considerations of the Effect of VTOL Downwash on the Ground Environment", NASA Conference on V/STOL Aircraft, Nov. 1960.

5.   Schade, R. O., "Ground Interference Effects", NASA TN D-727, 1961.

6.   Williams, J., "Some British Research on the Basic Aerodynamics of Powered Lift Systems", _Journal of the Royal Aeronautical Society_, July 1960.

7.   Newson, W. A., Jr., "Effect of Ground Proximity on the Aerodynamic Characteristics of a Four Engine Vertical Take-Off and Landing Transport Airplane Model with Tilting Wings and Propellers", NACA TN 4124, 1957.

8.   Tosti, L. P., "Force Test Investigation of the Stability and Control Characteristics of a 1/8 Scale Model of a Tilt Wing Vertical Take-Off-and-Landing Airplane", NASA TN D-44, 1960.

9.   Davenport, E. E., and Spreeman, K. P., "Thrust Characteristics of Multiple Lifting Jets in Ground Proximity", NASA TN D-513, 1960.

10. Spreeman, K. P., and Sherman, I. R., "Effects of Ground Proximity on the Thrust of a Simple Downward Directed Jet Beneath a Flat Surface", NACA TN 4407, 1958.

11. Pegg, R. J., "Summary of Flight-Test Results of the VZ-2 Tilt-Wing Aircraft", NASA TN D-989, 1962.

12. Morse, A., and Newhouse, H., "VTOL Downwash Impingement Study, Duct Adapter Test Program", TREC Technical Report 61-34, 1961.

13. Goland, L., "Kellett Full-Scale Downwash Impingement Experimental Investigation", VTOL Aircraft Downwash Impingement Symposium, TREC Technical Report 61-1, Dec. 1960.

14. Campbell, J. P., "NASA Research on Downwash Impingement", VTOL Aircraft Downwash Impingement Symposium, TREC Technical Report 61-1, Dec. 1960.

15. Heyson, H. H., "An Evaluation of Linearized Vortex Theory as Applied to Single and Multiple Rotors Hovering In and Out of Ground Effect", NASA TN D-43, 1959.

16. Morse, A., "Particle Movement and Velocity Survey Tests Conducted by Hiller Aircraft With Various VTOL and GEM Propulsion Devices", VTOL Aircraft Downwash Impingement Symposium, TREC Technical Report 61-1, Dec. 1960.

17. Sutton, J. F., "Model and Full-Scale Test of Ground Impingement of a Jet VTOL", VTOL Aircraft Downwash Impingement Symposium, TREC Technical Report 61-1, Dec. 1960.

18. Michel, P. L., "Downwash: Some Experimental Results and Operational Experiences", VTOL Aircraft Downwash Impingement Symposium, TREC Technical Report 61-1, Dec. 1960.

19. Hansen, G. A., "Simulated VTOL Exhaust Impingement on Ground Surfaces", VTOL Aircraft Downwash Impingement Symposium, TREC Technical Report 61-1, Dec. 1960.

20. Shields, R. T., "Some Notes on United Kingdom Experience in Testing of VTOL Aircraft", AGARD Report 318, 1961.

21.   Mitchell, W. H., "Downwash and Recirculation Studies",
        VTOL Aircraft Downwash Impingement Symposium, TREC
        Technical Report 61-1, Dec. 1960.

22.   Pegg, R. J., "Damage Incurred on a Tilt-Wing Multi-
        Propeller VTOL/STOL Aircraft Operating Over a Level
        Gravel-Covered Surface", NASA TN D-535, 1960.

23.   Kuhn, R. E., "Review of Basic Principles of V/STOL
        Aerodynamics", NASA TN D-733, March 1961.

24.   Kuhn, R. E., and Hayes, W. C., Jr., "Wind Tunnel
        Investigation of Longitudinal Aerodynamic Characteris-
        tics of Three Propeller-Driven VTOL Configurations in
        the Transition Speed Range, Including Effects of
        Ground Proximity", NASA TN D-55, 1960.

25.   Newson, W. A., Jr., "Effect of Ground Proximity on
        Aerodynamic Characteristics of Two Horizontal Attitude
        Jet Vertical-Take-Off-and-Landing Airplane Models",
        NASA TN D-419, 1960.

26.   Grunwald, K. J., "Investigation of Longitudinal and
        Lateral Stability Characteristics of a Six-Propeller
        Deflected-Slipstream VTOL Model with Boundary-Layer
        Control Including Effects of Ground Proximity", NASA
        TN D-445, 1961.

27.   Parlett, L. P. "Experimental Investigation of Some
        of the Parameters Related to the Stability and Control
        of Aerial Vehicles Supported by Ducted Fans", NASA
        TN D-616, 1961.

28.   Reeder, J. P., "Handling Qualities Experience With
        Several VTOL Research Aircraft", NASA TN D-735, 1961.

29.   Grunwald, K. J., "Aerodynamic Characteristics of a
        Four-Propeller Tilt-Wing VTOL Model With Twin Vertical
        Tails, Including Effects of Ground Proximity", NASA TN
        D-901, 1961.

30.   Spreeman, K. P., "Investigation of Interference of a
        Deflected Jet With Free Stream and Ground on Aerodynamic
        Characteristics of a Semispan Delta-Wing VTOL Model",
        NASA TN D-915, 1961.

114

DISTRIBUTION

U. S. Army Materiel Command	3
U. S. Army Mobility Command	2
U. S. Army Aviation Materiel Command	4
Chief of R&D, D/A	1
U. S. Army Transportation Research Command	70
U. S. Army Research and Development Group (Europe)	1
U. S. Army Engineer Research and Development Laboratories	3
Army Research Office-Durham	2
U. S. Army Test and Evaluation Command	1
U. S. Army Engineer Waterways Experiment Station	1
U. S. Army Combat Developments Command Aviation Agency	1
U. S. Army War College	1
U. S. Army Command and General Staff College	1
U. S. Army Aviation School	1
U. S. Army Infantry Center	2
U. S. Army Aviation Test Board	1
Air Force Systems Command, Wright-Patterson AFB	1
Air Force Flight Test Center, Edwards AFB	1
Bureau of Naval Weapons	4
U. S. Naval Postgraduate School	1
Naval Air Test Center	1
David Taylor Model Basin	1
Ames Research Center, NASA	1
NASA-LRC, Langley Station	1
Lewis Research Center, NASA	1
Manned Spacecraft Center, NASA	1
NASA Representative, Scientific and Technical Information Facility	2
Research Analysis Corporation	1
National Aviation Facilities Experimental Center	1
U. S. Army Standardization Group, Canada	1
Canadian Liaison Officer, U. S. Army Transportation School	1
British Army Staff, British Embassy	1
U. S. Army Standardization Group, U. K.	1
Defense Documentation Center	10

Dynasciences Corporation, Fort
Washington, Pennsylvania,
DOWNWASH IMPINGEMENT DESIGN
CRITERIA FOR VTOL AIRCRAFT,
George, M. M., Perlmutter, A.A.,
and Butler, L. J., TCREC
Technical Report 64-48, August
1964, 114 pp. (Contract DA 44-
177-AMC-65(T))USATRECOM Task
1D121401A14129.

Unclassified Report

Design criteria for VTOL air-
craft are presented to aid in
the establishment of aircraft

1. VTOL Downwash
   Impingement

2. Contract No.
   DA 44-177-
   AMC-65(T)

Dynasciences Corporation, Fort
Washington, Pennsylvania,
DOWNWASH IMPINGEMENT DESIGN
CRITERIA FOR VTOL AIRCRAFT,
George, M. M., Perlmutter, A.A.,
and Butler, L. J., TCREC
Technical Report 64-48, August
1964, 114 pp. (Contract DA 44-
177-AMC-65(T))USATRECOM Task
1D121401A14129.

Unclassified Report

Design criteria for VTOL air-
craft are presented to aid in
the establishment of aircraft

1. VTOL Downwash
   Impingement

2. Contract No.
   DA 44-177-
   AMC-65(T)

Dynasciences Corporation, Fort
Washington, Pennsylvania,
DOWNWASH IMPINGEMENT DESIGN
CRITERIA FOR VTOL AIRCRAFT,
George, M.M., Perlmutter, A. A.,
and Butler, L. J., TCREC
Technical Report 64-48, August
1964, 114 pp. (Contract DA 44-
177-AMC-65(T))USATRECOM Task
1D121401A14129.

Unclassified Report

Design criteria for VTOL air-
craft are presented to aid in
the establishment of aircraft

1. VTOL Downwash
   Impingement

2. Contract No.
   DA 44-177-
   AMC-65(T)

Dynasciences Corporation, Fort
Washington, Pennsylvania,
DOWNWASH IMPINGEMENT DESIGN
CRITERIA FOR VTOL AIRCRAFT;
George, M. M., Perlmutter,A.A.,
and Butler, L. J., TCREC
Technical Report 64-48, August
1964, 114 pp. (Contract DA 44-
177-AMC-65(T)) USATRECOM Task
1D121401A14129.

Unclassified Report

Design criteria for VTOL air-
craft are presented to aid in
the establishment of aircraft

1. VTOL Downwash
   Impingement

2. Contract No.
   DA 44-177-
   AMC-65(T)